8-2011

Application of microfabrication in electrochemical sensing.

Susan Carroll
University of Louisville

APPLICATION OF MICROFABRICATON IN ELECTROCHEMICAL SENSING

By

Susan Carroll
B.S., Kansas State University, 2004
M.S., University of Louisville, 2009

A Dissertation
Submitted to the Faculty of the
Graduate School of the University of Louisville
in Partial Fulfillment of the Requirements
for the Degree of

Doctor of Philosophy

Department of Chemistry
University of Louisville
Louisville, Kentucky

August, 2011

APPLICATION OF MICROFABRICATON IN ELECTROCHEMICAL SENSING

By

Susan Carroll
B.S., Kansas State University, 2004
M.S., University of Louisville, 2009

A Dissertation Approved on

August 5, 2011

Advisor: Dr. Richard P. Baldwin

Dr. Cecilia M. Yappert

Dr. Francis P. Zamborini

Dr. Craig A. Grapperhaus

Dr. Kevin M. Walsh

DEDICATION

This dissertation is dedicated to my daughter Johanna,

to my husband Harry, and parents Edith and Hans-Georg,

and to all of my friends and family.

ACKNOWLEDGEMENTS

I would like to thank my advisor, Dr. Richard P. Baldwin, for being my mentor over the course of my graduate career, and for instructing me that all problems are learning experiences. His guidance and experience have been invaluable tools in my progress as a graduate student and a scientist.

I would also like to thank my committee members Dr. Yappert, Dr. Grapperhaus, Dr. Zamborini, and Dr. Walsh for their unconditional assistance and countless discussions involving scientific, professional and sometimes personal challenges.

I offer my thanks to several other faculty, staff members and students who assisted and supported me in my endeavors. Tommy Rousell played a pivotal role on the coulometric project where he relentlessly redesigned flow cells, performed computer simulations, created a home build potentiostat, and wrote programs for data analysis. Thanks also to Douglas Jackson for consultations about instrumentation and fabrication of custom electrical connections. I also received often useful advice for microfabrication techniques from Mark Crain, Julia Aebersold, and Michael Martin.

Finally, an acknowledgment to a number of my fellow graduate students who were of great support as friends and colleagues throughout my graduate studies: Amy Hay, Jessy Koehler, Marty O'Toole, Rick Woofter, Edd Miracco, Radika Dasari, and Mohammed Marei.

ABSTRACT

APPLICATION OF MICROFABRICATON IN ELECTROCHEMICAL SENSING

Susan Carroll, B.S., Kansas State University

Chair Advisory Committee: Dr. Richard P. Baldwin

August 5, 2011

In this work, microfabrication techniques are explored not only to simplify the production of complex lab on-a-chip devices (LOC), but also microfabrication will be utilized to create intelligent design features that will enhance an electrochemical sensor's capabilities. First, a low temperature adhesive bonding procedure for LOC glass devices was evaluated for capillary electrophoresis (CE) applications. This low temperature method utilizes UV adhesive to bond the glass microchips under the assistance of a mask aligner. The bonding process was carried out at room temperature in < 30 minutes, and provided a near 100% success rate. Microchips exhibited similar electroosmotic flow, separation characteristics, stable long-term performance, excellent chip-to-chip reproducibility, as their thermally bonded counter parts. This bonding approach required new but easily implemented structural features.

In addition to cost effective and reliable fabrication techniques, microchips designed for long-term unattended electrochemical sensing have been evaluated. Specific advantages of the microfabrication approach include the capability to create an intelligent

design containing features such as redundant sensing electrodes, on-chip reference and auxiliary electrodes, and *in situ* electrode regeneration/calibration.

One system targeted involves continuous pH monitoring in drinking water at solid-state iridium oxide electrodes. Microchips utilized consist of a flow-through silicon platform containing patterned gold electrodes onto which iridium oxide was deposited electrochemically. To simulate drinking water detection scenarios, sensors were integrated into a flow system. Elven equivalent pH electrodes where evaluated for electrode-to-electrode reproducibility, long-term drift, and response to expected interfering agents. With on-chip voltage treatment, absolute potentials measured for an electrode array are within ± 4 mV, with identical (±1 mV/pH unit) calibration slopes. This performance level is sustainable over weeks.

Sensors for exhaustive coulometry were designed, fabricated and evaluated. Microchips contained thin-film gold working and Ag/AgCl pseudo-reference electrodes. A custom flow cell containing a counter electrode chamber was constructed to integrate the sensor and to create an electrolysis chamber with a fixed volume. Different chip designs were evaluated for reproducibility and longevity using $Fe(CN)_6^{3-/4-}$ as model analytes. The relative standard deviation (RSD) for a chip (over 42 days) was 5.5% whereas the sensor-to-sensor reproducibility was within 6.3%. A more practical application for utilizing exhaustive coulometry by the determination of free chlorine in drinking water is briefly evaluated. Initially studies will outline the challenges involved by analyzing hypochlorite.

TABLE OF CONTENTS

LIST OF FIGURES

LIST OF TABLES

CHAPTER I

INTRODUCTION

Microfabrication techniques, developed primarily for the electronics and computer industries, have been employed for the past 15-20 years for the miniaturization of diverse analytical instrumentation. The most obvious characteristic of such microfabricated devices, their greatly diminished physical size, carries with it several distinct advantages including increased speed, reduced sample/reagent consumption, and the possibility of decreased costs through mass production. However, other perhaps more important benefits result from the capability to create a diverse collection of micrometer-sized structures able to carry out complex measurement operations, integrate them seamlessly onto a single platform, and then replicate this instrument on a large scale and with essentially absolute fidelity.

Microfabrication is particularly well suited for electrochemically based sensors where the primary sensing element is a set of metallic electrodes, e.g., gold or platinum. Such materials are able to be patterned via photolithography and other conventional microfabrication techniques, and the resulting electrodes can be modified and optimized for specific applications by appropriate electrochemical post-processing operations. As a consequence, the construction of customized electrode designs for specific applications and of complex but highly reproducible electrode systems can be readily realized. Finally, literally hundreds of electrode systems have already been reported for many

important analytes. These include traditional potentiometric and voltammetric assay procedures as well as non-redox approaches involving conductimetry,[1-2] ac impedance measurements,[3-4] and the electrochemical microbalance.[5] Therefore, in many cases, completely original electrode schemes do not need to be devised but rather these already well characterized electrodes may often only need to be adapted appropriately to the microfabricated format.[6]

The perfect fit between microfabrication and electrochemistry has led to great advancement in the area of micro total analysis systems (μ-TAS). To date, most of micro total analysis systems or "lab on a chip" (LOC) work has targeted biomedical applications such as DNA sequencing and analysis and high-throughput screening; and remarkable advances in these areas have occurred as a result.[7-9]

1.1. Objective:

This dissertation will describe the application of microfabricated systems for electrochemical analysis. First, it will highlight the necessity to improve and simplify fabrication steps on the example of glass bonding lab-on-a-chip (LOC) devices in order to extend applications, reduce production cost, and possibly attract other researchers' interest due to more user-friendly manufacturing capabilities. This particular research was also performed to obtain value skill for microfabrication processes.

In addition, the necessity for better behaving sensor and sensor systems that can be potentially employed for remote environmental, industrial, security, and medical monitoring applications has recently attracted great attention. As a consequence, the major part of this research will focus on the development of microfabricated sensors for

possible remote sensing applications. The work presented here will describe how microfabrication can be utilized to construct miniaturized analytical sensing systems, but more importantly to create smart sensors for chemical analysis. I will describe, demonstrate, and discuss how various microfabricated features can be employed to enhance the sensor's capabilities and therefore make it behave more intelligently. The enhanced capabilities will be demonstrated by investigating two important drinking water parameters (pH and free chlorine).

1.2. Research interest:

1.2.1. Microfabricated devices for electroanalysis

Our group's interest focuses on the utilization of microfabricated devices for electrochemical detection of various analytes. Over the course of several LOC projects, great expertise in miniaturizing analytical systems and integrating metallic electrodes onto microchip platforms were obtained. Proficiency in fabricating glass microchips containing Pt electrodes for capillary electrophoresis with electrochemical detection was the first major accomplishment.[10-12] Following that success, a silicon-based microchip was developed for the detection of heavy metals in drinking water via anodic stripping voltammetry (ASV).[13] While both projects greatly differ from each other in chip configuration, substrate, electrode material, analytical methodology, sample introduction and detection mode, the microfabrication procedures to manufacture the devices are similar.

Utilizing microfabrication for the construction of LOC devices/sensors carries the benefit that most procedural steps are related and only details of the fabrication

parameters (e.g. etching times and adhesion material layers) need to be adjusted according to the substrate material employed. However, the number of procedural steps necessary and hence the time required completing the fabrication of devices may vary from a simple 10 to a more intricate 55-step manufacture sequence.

1.2.2. Common microfabrication steps

A chip fabrication process always begins by identifying the initial layout and construction sequence. Depending on the complexity of the desired devices, procedure steps such as oxidation, photolithography, etching, deposition, and possibly ion implantation or bonding can become parts of the fabrication process. After outlining the process steps in a sequential order and ensuring the compatibility of materials utilized during each fabrication step, photomasks are then generated for pattern transfer of the sensor design. L-Edit (Tanner, Monrovia, CA) or AutoCAD (Autodesk, CA) are software programs commonly used to create photomasks, where the latter software package offers more design flexibility to create complex structures. A laser pattern generator will then interpret the drawing features and produce patterned chrome-masks accordingly.

In general, photolithography encompasses all steps necessary to transfer a pattern from a mask to a substrate. This process always begins with a clean substrate onto which photoresist is deposited. According to the optical and composition of the photoresist, different baking and exposure times are required to ensure proper resist development (as outlined by the manufacturer). After UV exposure, the unwanted resist is stripped in a bath of liquid developer and the final pattern development can be inspected under a microscope.

Wet chemical etching, or dry plasma etching are techniques to remove substrate material not protected by photoresist. Wet etching is an isotropic process that etches equally in all directions and therefore tends to undercut the photoresist. This is only a serious problem when a feature size is smaller than the thickness of the photoresist.

Film depositions like sputtering, evaporation and chemical vapor deposition are processes used to deposit various thin film materials onto a substrate. Most metal depositions are performed via sputtering where a target is bombarded with Ar^+ knocking atoms at the surface loose which are then transported and deposit on the substrate. After depositing the metal on the substrate, unwanted material is removed by a technique known as lift off. Photoresist with the deposit metal is removed by soaking the substrate in either acetone or 1-Methyl-2-Pyrrolidinone positive photoresist stripper (NMP).

As a last step, some devices require a bonding process for the final device assembly. This is most often encountered in the production of microfluidic devices where two processed substrate materials have to be brought together to form a single device. For instance, our group utilized thermal bonding to assemble two-glass substrates containing Pt electrodes and microfluidic channels.[10-11, 14] This approach worked well when high temperature resistant materials were used for the fabrication of the CE devices. But with the introduction of temperature sensitive materials, like carbon electrodes, alternative bonding methodologies needed to be explored.

1.2.3. Low temperature adhesive bonding

Glass or quartz substrates would be the preferred choice for capillary electrophoresis microchips due to glass' hydrophilic character which allows, under the presence of an

electric field, creation of electroosmotic flow. The challenge for fabricating these devices is the bonding of the two glass substrates. In particular the smoothness of the substrates is critical for successful bonding, requiring the usage of commercially available ultraflat glass with a surface roughness of circa 1nm.[15] Additionally, rigorous cleaning is essential to remove any particles from both substrates prior bonding. The most frequently utilized glass-to-glass bonding method is thermal fusion bonding. During this approach both substrates are heated up slowly at a ramp rate of 1-2°C/min to about 600°C and higher in order to soften the glass surface. It is believed that at the fusion temperature the silanol groups (Si-OH) will be linked covalently to form siloxane bonds (Si-O-Si) under the release of water.[15] In principal, thermal bonding leads to advantageously high bonding strength.

$$\text{Si-OH} + \text{OH-Si} \rightarrow \text{Si-O-Si} + H_2 \qquad (1.1)$$

Although the bonding process seems to be straightforward, it is in fact quite challenging for trained personnel to achieve yields of > 25% successfully bonded chips, which is mainly attributed to the procedure's sensitivity to cleanliness and smoothness of the substrates. In addition, other disadvantages include the length of time required to bond both substrates (8 – 24 hours), possible distortions in channel dimensions, the incompatibility with any substrate features that are temperature sensitive, the lack of alignment control, and the non-reversibility of the glass bond.

Other attempts to circumvent high fusion temperatures included the use of hydrofluoric acid, concentrated sulfuric acid or even hot piranha solutions with a subsequent drying period of 12 to 48 hours.[16-17] Even robot-controlled bonding chambers were utilized to clean and activate the surface prior to bonding with a reactive ion etching

(RIE) oxygen radio frequency (rf) plasma and nitrogen radical microwave (MW) plasma, respectively.[18] Understandably, many shy away from the strenuous fabrication process for glass microchips and employ more user-friendly and less fragile materials like PDMS or PMMA to produce CE devices. While aware of the shortcomings of those materials (e.g. hydrophobicity of the material, absorption of hydrophobic molecules, swelling issues, feature size limitation to > 500 nm etc), polymer substrates are still the most popular materials for the microfluidic community.[19] Hence, it is important to find alternative ways to simplify, reduce time and costs for the production of glass/quartz microchips.

1.3. Smart Sensors:

The main force behind developing smart sensing devices or smart materials is to create sensors that are capable of monitoring various analytical parameters remotely. Great innovations in the area of smart materials have been reported by the usage of stimuli-sensitive polymers.[20-21] In particular, polymers like hydrogels that are able to shrink or swell in response to physical/chemical parameters such as temperature, pH and glucose concentration are being utilized to construct numerous biomedical sensing systems.[22] Even the construction of smart textiles is of interest for human biomonitoring. Kotov et al. transformed cotton threads into intelligent electronic fabric by using a polyelectrolyte-based coating with carbon nanotubes. Besides sensing humidity, he also demonstrated the detection of albumin by integrating antialbumin into the CNT-cotton yarn.[23]

The approach that we believe will make sensors smarter is the use of microfabrication techniques to include features onto a sensor platform that will extend the lifetime, and reduce or even eliminate calibration. This combination of improvements will make the sensor platform more suitable for environmental and security application where real-time, long-term, and on-site measurements are required. The smart sensor concept has already been realized in areas of traditional sensing such as accelerometers, temperature sensors, and pressure sensors. In these examples, supporting electronics (amplifiers, signal conditioning circuitry, temperature compensation, etc.) are now included with the actual sensing element, making the devices no longer passive transduction mechanisms, but rather smart sensors that are capable of much greater range and precision compared to previous generations of such devices.

There are several features that can be included to enhance a sensor's capabilities; one technique is to include redundant sets of electrodes onto the same sensing platform. Multiple copies of electrodes can for example circumvent the issue of false positive and false negative results during on-line analysis. In the past, when implementing warning systems for contamination threats, people have been overwhelmed with the amount of false positives in relation to the rare occurrence of true positives.[24-25] Proper data interpretation, which requires the minimization of false results, is vital for suitable warning systems. This can be accomplished by simply employing at least two working sensors on a single device; this way a faulty working electrode can be recognized faster or a questionable result can be confirmed.

Multiple copies of electrodes can also enhance a sensor's capabilities by affording simultaneous detection of different analytes. Various examples of thick and thin film

sensors that are capable of multi analyte analysis already exist[26-28] and their usefulness has been illustrated by for example simultaneous detection of nitric oxide and peroxynitrite,[26] molecules that control important cell functions (e.g. proliferation, apoptosis).

Frequent calibration and failure of parts that require replacement limit the practicality of typical devices employed in a sensor network. It is therefore important to develop rugged sensors which are essentially self-sustainable. Biological sensors have only limited use due to their short lifetime. Furthermore, drinking water is chlorinated, making impossible the utilization of bio-sensors based on the fact that there are currently no chlorine resistant bioassays.[29] Ruggedness also implies that sensors should be able to function well over at least several months. Methodologies minimizing or even eliminating calibration would definitely assist the notion of self-sustainable sensors.

There are several general approaches to solving the calibration problem. Ideally, one could identify and employ sensing devices whose response is completely stable and nearly immune to fluctuations in the operating conditions. However, relatively few chemical sensors are available that meet this standard at a practical level. Alternatively, one could try to achieve remote calibration by packaging appropriate standard solutions onto the sensor platform along with a suitable flow system (pump, valves, etc.). This latter approach would make actual on-site calibration possible, with the major drawbacks being increased device cost and complexity. These are serious drawbacks to the ability of smart sensor networks to function remotely in the field since device complexity in general leads to an increase in the frequency of failure, which in-turn requires more

frequent maintenance. Collectively, these additional costs reduce the practicality of a large number of sensors in a network.

Lastly, and perhaps the most preferable approach, is to explore and utilize in situ electrodes with regeneration/calibration capabilities and also to identify and employ analytical measurement methods that are both compatible with field deployment and also provide absolute quantitative results and therefore can be considered "calibration free". Most electroanalytical measurements are directly linked to the electrode area and, therefore, are not the best choice for possible unattended monitoring operations. Fortunately, two electrochemical methods that are insensitive to changes in the electrode area are available: potentiometry and coulometry.

1.3.1. Monitoring of drinking water

One area of environmental monitoring that has attracted great attention in the past decade is the surveillance of water resources. Rivers, lakes, estuaries, and open oceans receive most of the research community's attention. Many researchers have realized that under-sampling of time varying processes results in misrepresentation of real occurring chemical processes like the fluctuation in nitrate concentrations.[30] To gain a better understanding for natural occurring processes, high frequency sampling is essential. Additionally, the accidental or intentional contamination threat of water resources also highlights the need for continuous monitoring. This issue can be addressed properly only through a network of chemical sensors delivering directly real-time data.

Monitoring of drinking water quality is of great importance for several reasons. First, the threat of chemical, biological and radiological contamination of drinking water has

attracted great attention since September 11, 2001. Second, the everyday assurance of producing safe drinking water through disinfection is the foremost objective of water companies.[31] The Homeland Security Presidential Directive 9 requires the US Environmental Protection Agency (USEPA) to ensure public water quality through surveillance and monitoring initiatives.[32] Water companies do measure water quality parameters at their facilities. For the two most important parameters (at the example of the Hardin County Water District No. 2), free chlorine and turbidity are measured with commercially available online systems at their facility. Other parameters like pH and total dissolved solids (also known as conductivity) are measured three times a day by their in-house laboratory. Total organic carbon and dissolved oxygen are on a quarterly testing schedule, whereas nitrate is only checked once per year.

However, the complete surveillance of their product at multiple locations throughout their entire distribution system is highly desired but for now not achievable. At the present stage, water quality in the distribution system is mainly monitored through grab sampling with subsequent analysis in laboratories. These analyses rely on sophisticated instrumentation such as GC/MS, inductively coupled plasma chromatography, and ion chromatography which makes it in turn quite costly, lengthy, and incompatible with on-line monitoring goals. Consequently, water sampling and testing are occasionally performed at different locations unless requested by consumers. Additionally, contamination threat management requires available data for unusual water quality in real time which can be accomplished with on-line monitoring. Typical water quality parameters monitored by water companies are listed in Table 1.1.[33-34]

	Water Quality Parameter		Methods
1	Free chlorine	4 mg/L MCL	(DPD) colormetric method
2	Oxidation reduction potential (ORP)		Potentiometry
3	Total organic carbon		UV-persulfate oxidation
4	Turbidity	0.5 NTU	Nephelometric signal
5	pH	6.5-8.5	Glass combination electrode Proton selective electrode Proton selective metal oxide
6	Dissolved oxygen (DO)	N/A	Membrane electrode method Three electrode voltametric method
7	Specific conductance	100-1500μS/cm	Pt electrode method Four nickel electrodes
8	Chloride	250 mg/L NSDWR	Ion selective electrode
9	Ammonia		Ion selective electrode Colorimetric method
10	Nitrate	10 mg/L MCL	Ion selective electrode
11	Temperature	N/A	Thermistor

MCL is the maximum contamination level/ NTU is the nephelometric turbidity unit/ NSDWR is the national secondary drinking water regulation

Table 1.1 Typical water quality parameters monitored by water companies

On-line monitoring systems are already commercially available to monitor some of these parameters. Most are single-parameter sensors (electrodes), although a few are multi-parameter sensors which are bundled into one unit making the assembly rather bulky and inconvenient (YSI 6600 Sonde from Fondriest Inc. &Hydrolab Data Sonde 4a form Hach). To date, only one manufacturer offers a microfabricated multi-sensing chip (Dascore Six-Sense Sonde from Censar Technologies) located in a probe head which can be installed into main pipes of the water distribution system. Hall et al[33] tested the above mentioned commercially available monitoring systems of performance and response to possible contaminants in a drinking water simulation pipe line system. Results indicated that weekly calibrations with commercial standards were necessary for accurate measurements. Even more frequent calibrations were needed for the microfabricated multi-sensing chip.[33] These systems will suffice where trained personnel is not a time or cost issue, but they definitely are inadequate for true remote monitoring scenarios.

The Water Security Initiative (WSI) is a program of the USEPA which is addressing the risk of deliberate contamination of drinking water distribution systems. Five distribution systems (Cincinnati, San Francisco, New York, Philadelphia, and Dallas) have been engaged by the WSI to utilize real-time monitors at specific locations in order to detect possible contaminates and also function as early warning systems.[35-36] The main parameters to monitor the water quality are pH, chlorine, temperature, conductivity, total organic carbon (TOC), and turbidity. Commercially available instrumentations e.g. the Hach Guardian Blue Early Warning System, Sievers 900 Online TOC Analyzer, and INFICON Online GC-MS are installed at the surveillance stations.[37] It becomes obvious that such elaborate instrumentation requires not only trained personnel but it also comes with high power consumption and the need of frequent maintenance. In the case of the

multi-parameter technology, weekly (or more frequent) maintenance is required for calibrations.[33] Large scale monitoring incentives are hampered by just considering the cost involved to operate only a handful of surveillance stations.

A more cost effective alternative compared to the current surveillance stations employed by the WSI is to consider the construction of microfabricated electrochemical smart sensors that can be deployed autonomously at multiple points along the distribution system. These sensors need to be able to detect some of the above mentioned water quality parameters e.g pH, free chlorine, conductivity and temperature. Of course, a complete qualitative water analysis is not possible, but this is not the device's function. The sensor's task simply is to monitor the water continuously and, in case of unusual water quality, transmit real-time data directly to a central processing point from which immediate warning and shut off actions can be performed.

1.3.2. Electrode regeneration/calibration strategy for water pH sensing

pH readings are not only important for water companies to ensure the quality of their product it is in fact the most used analytical method encountered daily in ordinary life. It is an important parameter in many different areas such as medicine, agriculture, forestry, food industry, environmental science, chemistry, biology etc. Even the average person will occasionally need to measure the pH of the pool water or garden soil.

At the present time, pH measurements are typically performed with glass pH electrodes, metal/metal oxide electrodes, polymer matrix electrodes and CHEMFET sensors.[38] Excellent electrode performances (Nernstian-behavior), long term stability, high selectivity, low detection limits and less sensitivity to interference are great

advantages of the common glass electrode. Unfortunately, pressure and temperature dependence, mechanical fragility and limitations regarding miniaturizations and microfabrication lead to the development of solid state electrodes for pH measurement applications.[39]

Several solid state metal oxides have been of particular interest in pH applications for decades. Metal oxides have been known for decades to exhibit acceptable pH sensitivities. Many investigations and characterizations have focused on IrO_2 and RuO_2 since they display a near Nernstian response over a wide pH range.[40-42] As for iridium oxide, the main advantages include good stability over a pH range form 2-12 even at high temperatures (250°C) and pressures, great resilience in harsh environments (HF solutions), and fast response times in aqueous and nonaqueous solutions.[43-46]

Iridium oxide films can be divided into the hydrous and anhydrous form, whereas the former one can be prepared electrochemically and the later one via microfabrication or thermal deposition. Dissimilarities in electrode stabilities, film thicknesses, sensitivity to interferences and hydration states are apparent. Those differences can be attributed to the various fabrication techniques and conditions utilized during film deposition. Galvanostatic and potentiometric deposition are the two electrochemical methods to form hydrous iridium oxide. It is the least expensive method in which a solution containing an iridium complex for deposition of IrO_x onto various substrates e.g. glassy carbon, Ti, Pt or Pt-Kapton films. A somewhat more expensive method is to grow an oxide film onto an Ir metal surface via cyclic voltammetry (CV). Anhydrous films prepared by microfabrication offer great stability and reduced redox interference, but the low deposition rate (5Å/min) and the enormous price of the Ir target prevent its common

use.[22,23] The most frequent techniques for thermal depositions include pyrolysis of $IrCl_3$ on Ti substrates (400-500°C), oxidation of Ir wire in molten KNO_3 (425°C) and oxidation of Ir metal wetted prior with NaOH solution (800°C).[39, 47]

For us, electrochemical deposition of IrO_x onto conducting substrates is most useful, since it allows the post-modification of complex microfabricated electrode structures. Due to this advantage we are able to construct multiple copies of the same electrode onto one sensing platform and evaluate each individual electrode performance under the same set of conditions (exposing electrodes to different pH containing solutions and oxidizing/ reducing agents). Furthermore, real pH water monitoring scenarios are simulated and the chip's suitability and durability under those conditions are evaluated.

1.3.3. Coulometry

There are not many analytical measurement methods that are both compatible with field deployment and *potentially* calibration free. One of them that should be considered to be adaptable to large sensor networks is electrolysis. In particular, coulometry is one of the few analytical methods that are capable of absolute quantitative results, given that certain variables are controlled. If a precisely defined volume of analyte is oxidized or reduced completely and the associated current is integrated over time, Faraday's law can be used to convert the charge in coulombs to the absolute quantity of material electrolyzed. In principle, as long as the cell volume is accurately known and the electrolysis is carried out to completion, the corresponding charge is an absolute determinant of the analyte quantity and concentration; no additional experiment is required for quantitation. In addition, any changes in electrode area that occur over

extended periods of operation should be also less problematic. As long as the cell volume remains constant, partial passivation of the electrode surface affects the time dependence but not the final magnitude of the coulometric signal.

There are numerous examples that suggest that this approach has much to offer. For example, a 45μL thin-layer coulometric system containing a Cu anode was utilized by Karube's group to measure the chemical oxygen demand in lake water samples requiring 3-10 minute of analysis time.[48] Another study conducted by Fukuda et al. utilized a micro-bulk electrolysis cell containing a carbon felt electrode to study mediated enzyme reactions and the coulometric analysis of the substrate in 10 - 15 μL sample volumes.[49] Neither of these approaches was intended for, or applied to, remote sensing as both required extensive operator interaction.

For these reasons we developed a microfabricated electrochemical sensing system in order to investigate the concept of exhaustive coulometry. A custom flow cell containing fluidic connections and counter electrode chamber was constructed to integrate a sensor and to create an electrolysis chamber with a fixed volume. To initially evaluate and characterize the thin-layer cell ferro-ferricyanide was chosen as the model analyte. With the initial characterizations of the coulometric sensing system we can demonstrate many potential advantages of developing microfabricated coulometric devices for sensor networks.

A more practical application for utilizing exhaustive coulometry is the determination of free chlorine (in the form of OCl^-) in drinking water. For water companies, free chlorine is of interest since it is an important parameter during the chlorination of drinking water.[31] Chlorine is introduced to water via chlorine gas, calcium hypochlorite

($Ca(OCl)_2$), or sodium hypochlorite (NaOCl). It then hydrolyzes to form hypochlorous acid (HOCl), which in turn undergoes ionization to form hypochlorite ions (OCl^-).[31] More importantly, hypochlorite can be electrochemically reduced in a two-electron process without the oxygen reduction interference at a gold electrode surface.[50-51] This feature allows us potentially to determine absolute quantities of OCl^- via exhaustive coulometry using our microfabricated sensing system.

1.3.4. Summarized sensor requirements

The specific goal of our work is to investigate simple ways in which the microfabrication approach can be used to make electrochemical sensors behave "more intelligently" and thereby provide important information and possibly improve upon device performances for long-term remote monitoring applications. Important features that are investigated to enhance a sensor's capabilities and therefore make the sensor smarter are:

1) the inclusion of redundant sensing electrodes to function either as a back up when one sensor fails or as a way of verifying questionable results,
2) the development of in situ electrode regeneration and calibration procedures,
3) the construction and utilization of a coulometric system for absolute quantitative analysis, and
4) the integration of reference and auxiliary electrodes onto the sensor platform

1.4. Chapter overview

In this dissertation, Chapter II will describe a low adhesive bonding procedure for lab-on-a-chip glass devices for capillary electrophoresis application. In particular, fabrication details, advantages, and their overall long-term performance will be discussed and directly compared to their thermally bonded counterparts. This project also served as a lesson to obtain valuable microfabrication skills for the subsequent "smart sensor" project. The main objective is to develop microfabricated sensing systems which can be employed to measure water quality parameters for an extended period of time, require less maintenance, and can be operated remotely. The first progress in the development of smarter behaving sensors is presented in Chapter III, where a self-calibrating microfabricated iridium oxide pH electrode array is described. The array can be ultimately applied for remote sensing applications. Chapter IV entails an evaluation for a first generation microfabricated coulometric sensing system which can be potentially deployed for calibration-free sensor network operations. Different chip designs are evaluated as exhaustive coulometric sensors in terms of reproducibility and longevity using $Fe(CN)_6^{3-/4-}$ as a model analyte. Hypochlorite is the second water quality parameter of interest for on-line sensing systems, and it is therefore employed for exhaustive coulometry applications as discussed in Chapter V.

CHAPTER II

ROOM TEMPERATURE UV ADHESIVE BONDING OF CE DEVICES

2.1. Introduction:

A key step in the fabrication of lab-on-a-chip (LOC) or micro total analysis (μTAS) devices involves the bonding of two substrates or wafers. The specific approach employed for this bonding process depends, of course, on the nature and composition of the substrate materials. However, for standard glass or silica wafers, the conventional method used is direct thermal bonding. In this approach, the two substrates, each already containing a desired set of microfabricated channels or other structures, are brought together in cleanroom conditions at a temperature sufficient to soften and allow fusion of the substrate materials - which, for glass, typically involves temperatures of 600 °C and higher. The principal advantage of the thermal bonding approach is the relatively high bond strength that results. Potential disadvantages are the high degree of surface flatness required for the bonded substrates, the length of time required (because the temperature applied must be ramped up and down by only 1–2 °C min^{-1}), the possibility of distortions in channel dimensions, and, of course, incompatibility with any substrate features that are temperature sensitive (*e.g.*, most biomolecules or organisms). Furthermore, at least in our experience, the yield of successful LOC devices from thermal bonding is far below 100% due to fracturing of the wafers at some point in the process or formation of incomplete or leaking bonds. Of the several alternatives to thermal bonding, one of the most attractive is

adhesive bonding.[52-53] In this approach, an intermediate adhesive layer is placed between the two substrate wafers to create the desired bond. Typically, a polymer adhesive is applied to one or both of the wafer surfaces, modest pressure is applied, and the adhesive is cured by exposure to UV light (or slight warming). In addition to the avoidance of high temperatures, other expected advantages are that practically any substrate materials can be joined by adhesive bonding and that the process is, in principle, more tolerable to surface imperfections or roughness on the wafer. Further, the operations involved are more user-friendly - simpler, faster, and potentially reversible (by dissolving the cured adhesive contact layer) - than those in many alternative low-temperature bonding schemes which often require rigorous cleaning procedures,[54] hazardous reagents such as HF and concentrated H_2SO_4,[16-17, 55] and the use of 8–24 hour bonding times.[16-18, 55-57]

A particularly attractive low-temperature adhesive bonding approach is the so-called 'stamp-and-stick' method, introduced by Schlautmann[58] and Majumdar.[59] This technique involves 'stamping' one substrate wafer, already containing its set of microfabricated features, onto a blank wafer spin-coated with a UV-curable adhesive. This operation serves to transfer a thin layer of adhesive selectively onto protruding surfaces of the device substrate which, after removal from the sacrificial wafer, is aligned and bonded (*i.e.*, 'sticking') to the second microfabricated substrate.

The initial stamp-and-stick reports, although somewhat limited in scope, clearly showed the feasibility of the approach for fabrication of microfluidic devices.[58-59] In particular, these studies demonstrated its applicability to binding different materials (glass, silicon, silicon nitride, and poly(dimethylsiloxane)) with an acceptable bond strength and no apparent leakage problems.[59] Subsequently, this approach has been

employed as an alternative to thermal bonding in different kinds of microchip devices - *e.g.*, to facilitate bonding of substrates containing a thick surface layer of SiO_2,[60] to accommodate complex microfabricated features on one of the bonded surfaces,[61] and to allow the use of temperature-sensitive sensor elements.[62]

So far, however, tests of the stamp-and-stick bonding procedure have been limited either to static microwell/microarray devices or to systems involving pressure-driven bulk flow. To our knowledge, no studies have yet appeared regarding the suitability of this methodology for capillary electrophoresis (CE) based microfluidic applications such as those involved in the separation and analysis of DNA and proteins. Therefore, in this work, we present such a study that clearly demonstrates the advantages of the stamp-and-stick adhesive bonding approach for microchip CE applications. In particular, we have fabricated simple CE microchips (employing electrochemical (EC) detection) *via* the stamp-and-stick method and have examined both their quality of construction and separation performance. In general, we found that the new low-temperature adhesive bonding approach produced high-quality CE separations, equivalent to those seen for conventional thermally bonded devices. However, the fabrication process was significantly faster, resulted in a higher over-all yield of successful devices, and proved much more user-friendly in several ways.

2.2. Experimental:

2.2.1. Reagents

Chemicals were purchased at the highest purity commercially available and were used without further purification. A 20 mM pH 6.3 phosphate buffer solution (PBS) was employed as the electrophoresis medium for all CE experiments. For electrochemical detection purposes, the neurotransmitters dopamine and catechol (2.4 mM and 3.0 mM, respectively) were utilized as test analytes in order to take advantage of their convenient electrochemical activity.

2.2.2. Fabrication

The CE/EC microchip (shown in Fig. 2.1) consisted of a top substrate that contained the CE channels and access holes and a bottom substrate that contained the CE and EC electrodes. Both halves of the device were fabricated from 4" × 4" ultra-flat soda lime glass wafers pre-coated with a thin chrome layer and positive AZ1518 photoresist (Nanofilm, Inc., Westlake Village, CA). Chrome photomasks were printed using a laser pattern generator (Heidelberg DWL-66) and processed as previously described.[10-12] Since the final dimensions of the individual chips were only 28 mm × 50 mm, three separate substrates (top or bottom) were patterned on one glass wafer and fabricated during a single processing run and then separated with a dicing machine. Specific fabrication procedures for both top and bottom substrates were similar to those reported previously.[10-12, 14] Therefore, only an overview of this methodology has been included below, with full details indicated only where important changes were made. A complete summary of the fabrication process is in table format in the appendix (Tables A1 – A3).

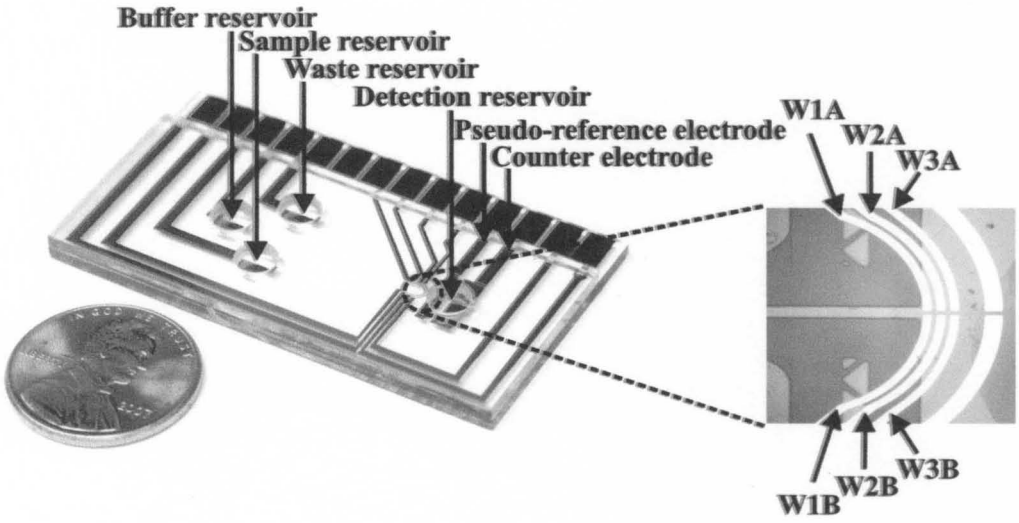

Figure 2.1 Photograph of the CE/EC device with a magnified view of the Pt working electrodes (W).

2.2.2.1. Top substrate

Prior to formation of the CE channels in the top substrate, access holes that would also serve as sample, waste, buffer, and detection reservoirs were created by a ultra-high-precision micromilling machine (Dover Instrument Corporation, Westboro,MA, USA) using a 4 mm diamond core drill-bit. Then the CE channels were isotropically etched into the wafer with buffered oxide etch solution (6 : 1 NH_4F : HF). Each of the four channel arms had a 1 cm length; the average width and depth were 55 μm and 16 μm, respectively.

2.2.2.2. Bottom substrate

The bottom substrate contained the platinum CE and EC electrodes. The EC working electrodes (shown in Fig. 2.1, exploded view) consisted of two sets of three finger-shaped electrodes aligned in a semi-circular configuration with the end of the CE channel. Each electrode had a width of 40 μm, and there was a 20 μm spacing between neighboring electrodes (*i.e.*, from W1 to W2 and W2 to W3) and a 20 μm middle gap between the two sets of fingers (*i.e.*, between W1A and W1B). Care was taken to ensure that the final distance between the first set of working electrodes and the end of the separation channel was between 10–20 μm. The pseudo-reference and counter electrodes for EC as well as the CE electrodes consisted of larger Pt strips that were positioned much further away from the CE channel. In all cases, a Ti adhesion layer and then the final Pt surface were deposited *via* sputtering (Technics 4604 RF/DC sputterer) with a cumulative Pt/Ti thickness of approximately 150 nm. All of the electrodes were recessed into the glass

substrate by etching an identically shaped trough into the substrate prior to Pt and Ti film deposition.

2.2.2.3. Bonding

Prior to performing the bonding procedure, both substrates (top and bottom plates) were cleaned with DI water and dried with nitrogen. The plates were then subjected to an evaporation bake at 115 °C for three minutes to remove any residual water. The top substrate was temporarily affixed to a glass plate within the mask aligner (AB-MIR mask aligner) by placing a water droplet onto it and then carefully bringing the two plates into contact. Parallel alignment of the top and bottom elements of the mask aligner was checked by placing a silicon wafer onto the bottom, bringing it into direct contact with the top substrate, and then manually leveling the two surfaces.

The optical adhesive Norland NOA 61 was spin coated (spread speed = 500 rpm for 5.5 s; spin speed = 7000 rpm for 20 s) onto a separate silicon wafer for transferring the adhesive to the top glass substrate. The 'transfer' wafer was placed on the bottom chuck of the mask aligner (Fig. 2.2A) and lifted into contact with the top glass substrate (Fig. 2.2B) for a few minutes. Subsequently, the transfer wafer was removed and replaced by the bottom glass substrate containing the patterned electrodes (Fig. 2.2C). The bottom chuck of the aligner was then raised to bring the two substrates into the final contact position. Once uniform contact was obtained, the chip was exposed to UV light for three minutes to initiate cross-linking of the polymer (Fig. 2.2D). Parallel orientation of the top and bottom plates, deposition and transfer of an even thickness of the adhesive (approximately 0.5 μm) onto the top wafer, and proper alignment of the features on the

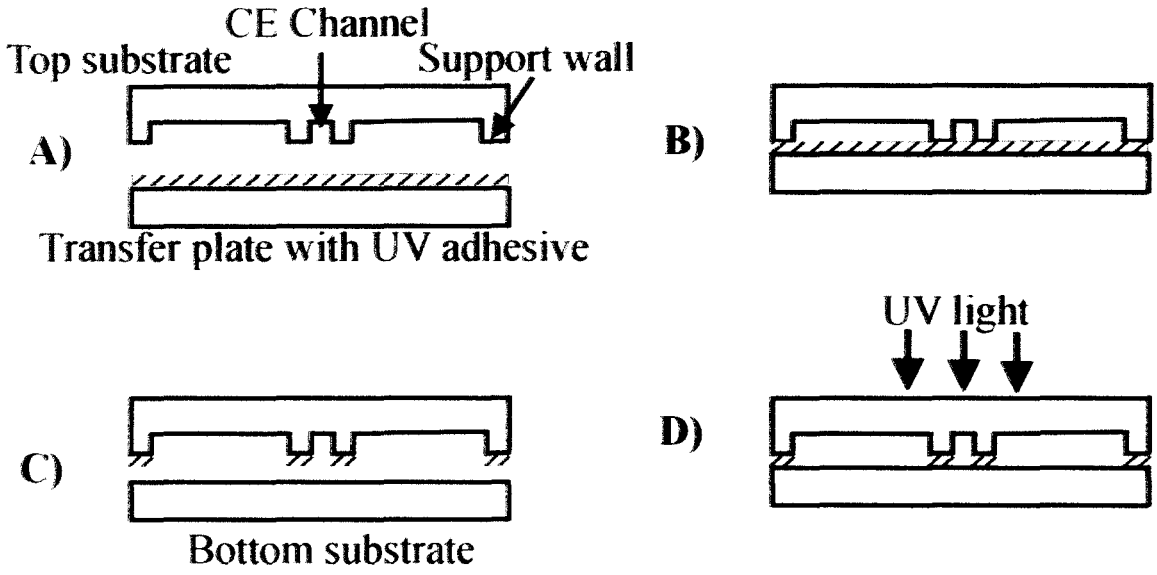

Figure 2.2 Schematic of the bonding process showing: (A) the starting position of the top glass substrate and the silicon transfer plate, (B) the stamping operation, (C) the alignment position of the bottom and top glass substrates, and (D) curing of the adhesive *via* UV light exposure.

two substrates were monitored continuously during the bonding process *via* the mask aligner's microscope/camera system. If non-uniform or faulty placement of the UV adhesive was observed prior to UV exposure, both substrates were simply separated by hand, cleaned with acetone, and recycled. If imperfections were observed after UV curing, a long-term soak (one day) in concentrated NaOH solution dissolved the cross-linked adhesive, allowing separation and re-use of the two substrates.

2.2.3. CE procedure

To evaluate the room temperature bonding technique, the chips were utilized in CE with EC detection experiments. The chips were placed onto an acrylic platform where electrical connections (for CE and EC) were established *via* spring-loaded contacts to connect to the electrode pads on the chip. A base wash of 0.1 M NaOH was frequently employed for cleaning purposes by flushing the channels for approximately 15 minutes with the solution. Channels and reservoirs were pre-conditioned by flushing with PBS before beginning a set of experiments. Next, the analyte solution (containing dopamine and catechol in PBS) was introduced into the sample reservoir. The sample was loaded into position by applying a voltage bias of - 205 V between the sample and waste reservoirs. The analyte plug (approximately 50 pL) was subsequently introduced into the separation channel by application of a 239 V (to give a CE field of $\approx$ 100 V cm^{-1}) across the buffer and detection reservoirs. The custom CE and EC detection instrumentation employed in this study has been previously described,[11] with the exception of an additional or second transimpedance amplifier to enable dual-electrode EC detection.

2.3. Results and Discussion

During the course of this study, numerous individual CE devices were fabricated and bonded. Early on, the device failure rate was higher than desired, primarily due to imperfect bonding and leakage problems during CE operation. Consequently, initial efforts focused on optimizing the chip design for use with the stamp-and-stick bonding approach. The lessons learned during this period are briefly summarized below. Subsequently, we report the comparative CE performance of several devices fabricated at the same time using the optimized chip design.

2.3.1. Optimized chip design

Early on, it became apparent that a conventional layout for the top LOC substrate, consisting of the CE channels etched into an otherwise featureless glass wafer surface, was not ideal for the adhesive bonding approach as the vast contact area afforded by such a large flat surface led to the transfer of excess adhesive during the stamping stage of the bonding procedure. As a result, it proved difficult to prevent seepage of the adhesive into the CE channels when the top and bottom substrates were pressed together. In order to avoid this problem, a thin wall system (240 μm thick) was constructed around - the CE channels and reservoirs of the top wafer. In addition, in order to stabilize the whole assembly, a similar wall structure surrounding the entire outside edge of the substrate was incorporated as well. Finally, a double wall system was constructed around the sample, waste, buffer, and detection reservoirs to provide extra protection against buffer leakage. Since most leakage problems were encountered at the detection reservoir, an extra design element consisting of an internal zigzag wall between the double wall of the detection

reservoir was added to minimize leakage effects due to any adhesion flaws in this area of the micro-chip. Fig. 2.3 contains an overview of the entire system, with the new wall structures highlighted in bold.

In general, the uniform application of UV adhesive along the straight sections of the channel walls was easily achieved; and it was relatively easy to complete bonding of the top and bottom substrates without noticeable contamination and occlusion of the CE channels by the adhesive material. This was especially true for straight channel sections located near the center of the chip. However, when the chip structure required turns in the channels, smooth curvatures were incorporated rather than right angles. Designs utilizing 90^{o} angles in their construction were often found to produce a webbing effect that resulted in seepage of the adhesive into the channel, which, if substantial, could lead to blockage.

The extra security provided by these design changes resulted in a dramatic improvement in the overall success rate of the fabrication process compared to conventional thermal bonding methodology - at least in our experience. Also, it is important to note that, even though the above changes led to a more complex top-substrate design, this did not make the actual fabrication of the final CE device any more complicated or time-consuming. This is due to the fact that all of the side wall construction was carried out in the same etching step in which the customary CE channels were created. Therefore, once the appropriate photomask incorporating the desired side wall elements was constructed, the required microfabrication operations for the top substrate remained exactly the same.

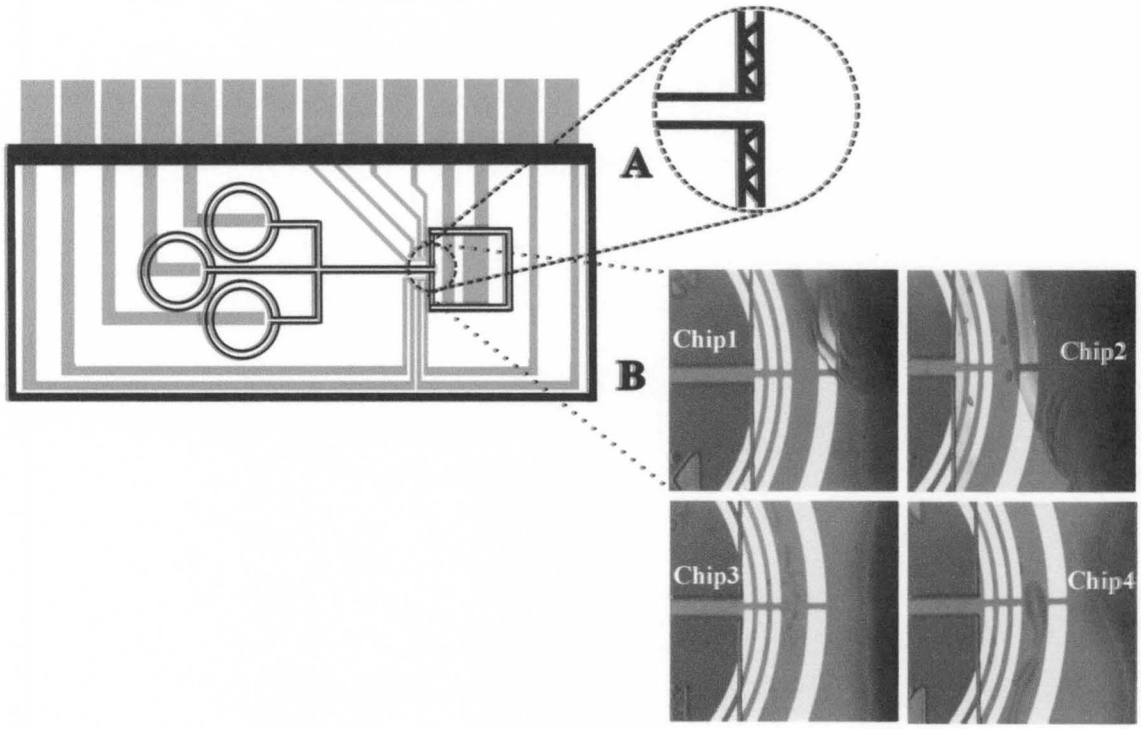

Figure 2.3 Photographs of the CE channels and walls (dark shaded region indicates UV adhesive).

2.3.2. Chip performance

2.3.2.1. General.

The use of the stamp-and-stick bonding method in the manufacture of lab-on-a-chip devices presents several broad advantages compared to the traditional thermal bonding method. Whereas thermal bonding requires several hours of controlled temperature ramping in a tube furnace, the stamp-and-stick method requires only three minutes of UV light exposure. As a consequence, the entire bonding process, from initial cleaning of the substrates to final product inspection, can be accomplished in less than 30 minutes. In this study, the majority of chip failures occurred during the manufacturing process and typically involved at least one of three specific defects: (1) incomplete or improper bonding of the two substrates, which induced leakage problems; (2) protrusion of the adhesive into the channel system, leading to complete channel occlusion; and (3) misalignment of the top and bottom substrates, which altered the position of the EC electrodes in relation to the CE channel. However, the severity of all three defects was greatly diminished by the 'stamp-and-stick' approach which enables the LOC manufacturer to actively intervene during several stages of the bonding process. The net result was that the stamp-and-stick method made possible a near 100% success rate in terms of viable chips produced.

The direct alignment capability made possible by the mask aligner used in the bonding process (as already described earlier in the Experimental section) allows highly reproducible alignment of the top and bottom halves of the device, which becomes important when specific features in both substrates need to be aligned simultaneously. For example, in this application, where CE channels are fabricated in the top glass

substrate and EC electrodes in the bottom, the precise placement of the electrodes at the end of the separation channel (Fig. 2.3B) is critical to limit undesirable broadening of the analyte plug prior to detection. In Fig. 2.3B, the distances from the channel outlet to the outer edge of the first set of electrodes for the four chips were found to be 16 μm, 13μm, 20 μm, and 33 μm, respectively. While this degree of control was adequate for the current study, an even more precise placement could have been achieved by simply incorporating alignment marks on the two substrates during fabrication.

In general, the stamp-and-stick approach represents a relatively forgiving bonding methodology as formation of clean and well-defined bond areas was fairly easily achieved in practice, especially for straight wall segments located near the center of the chips. (See Fig. 2.4A, for example.) However, even in instances where there were visible imperfections in the film application, the resulting flaws were seldom seen to affect chip performance. Examples of such non-uniform adhesive application are shown in Fig. 2.4B and C. However, in neither of those cases did the imperfections result in fluid leakage, inhibit fluid flow, or compromise the CE performance of the chips to any observable degree.

2.3.2.2. Chip evaluation.

Once the chip design had been optimized as explained above, the resulting chips were evaluated for performance in actual CE experiments. Of specific concern were both an evaluation of how the CE devices produced by the new procedure performed compared to chips fabricated *via* thermal bonding and an examination of the consistency with which the new devices could be fabricated. In order to accomplish this, several chips using the

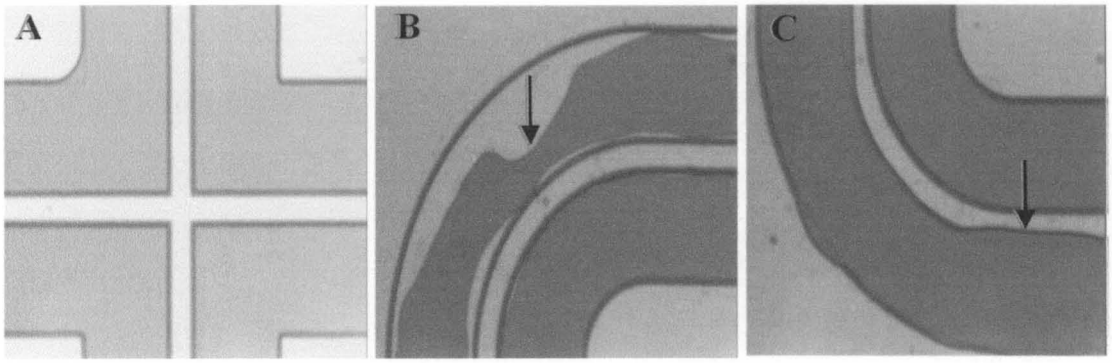

Figure 2.4 Photographs of the CE channels and walls (dark shaded region indicates UV adhesive). Picture (A) is depicting the correct UV adhesive application for the wall segment near the center of the chip, whereas pictures (B) and (C) illustrates imperfections in the film application.

room temperature bonding methodology were constructed in a single fabrication run; and conventional CE/EC experiments involving the separation and detection of the model electroactive compounds dopamine and catechol were carried out. Results are described below for three such 'identical' devices. On all chips, six independent working electrodes, arranged in an array of three left/right pairs (*e.g.*, Fig. 2.1: W1A & W1B), which were located in 20 μm increments away from the CE channel exit. Ideally, of course, the left/right electrodes of each pair should provide identical detection properties.

Fig. 2.5 depicts representative electropherograms collected at all six electrodes on Chip 1. This chip (as well as all the other chips tested) exhibited reproducible electropherograms with flat and stable baselines and well-shaped analyte peaks. The migration times for both dopamine and catechol increased slightly as the detection site was moved from the W1 to W3 electrode pairs due to the increase in the electrode distance from the separation channel outlet. This increase in distance also led to a slight broadening of the peaks and decrease in peak amplitude due to diffusional effects as the sample plug migrated through the detection reservoir. Both the peak area and the migration time were nearly the same for each member of a given electrode pair (*e.g.*, W1A *vs.* W1B), which is indicative of the near perfect alignment of the electrode array and the CE channel seen in Fig. 2.3C. In general, the CE behavior seen for Chip 1 (and all other stamp-and-stick devices) was equivalent in every way to that seen for analogous thermally bonded devices.

Longer-term chip performance as monitored during usage over several weeks showed consistent and reproducible CE results. This is demonstrated in Fig. 2.6, where electropherograms are shown for electrode W2A on Chip 2 at different days over a

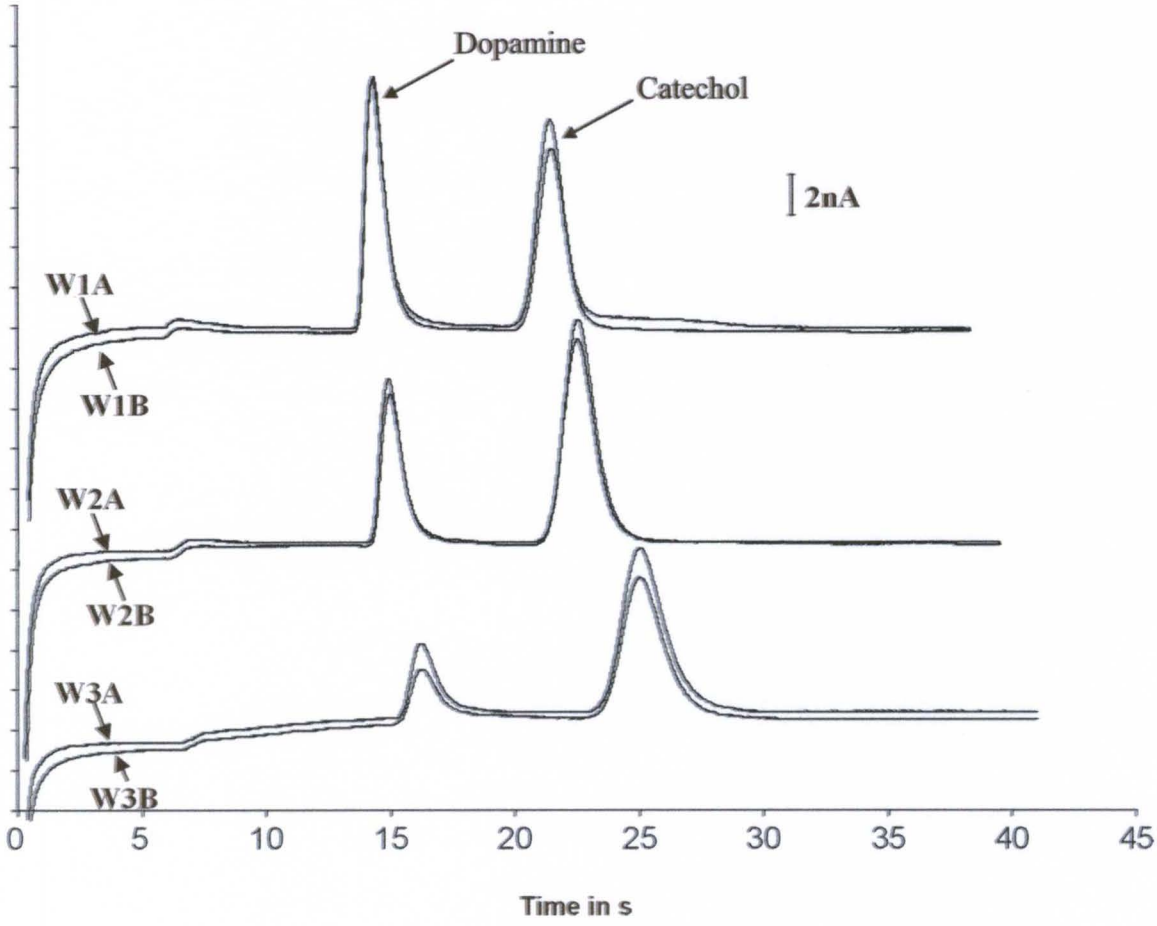

Figure 2.5 Electropherograms of all six working electrodes from Chip 1 at + 1.0 V. Dopamine and catechol (2.4 mM and 3.0 mM, respectively) in 20 mM pH 6.3 phosphate buffer solution where utilized as analytes. Note: the baseline of electropherograms was moved from the original position for presentation purposes.

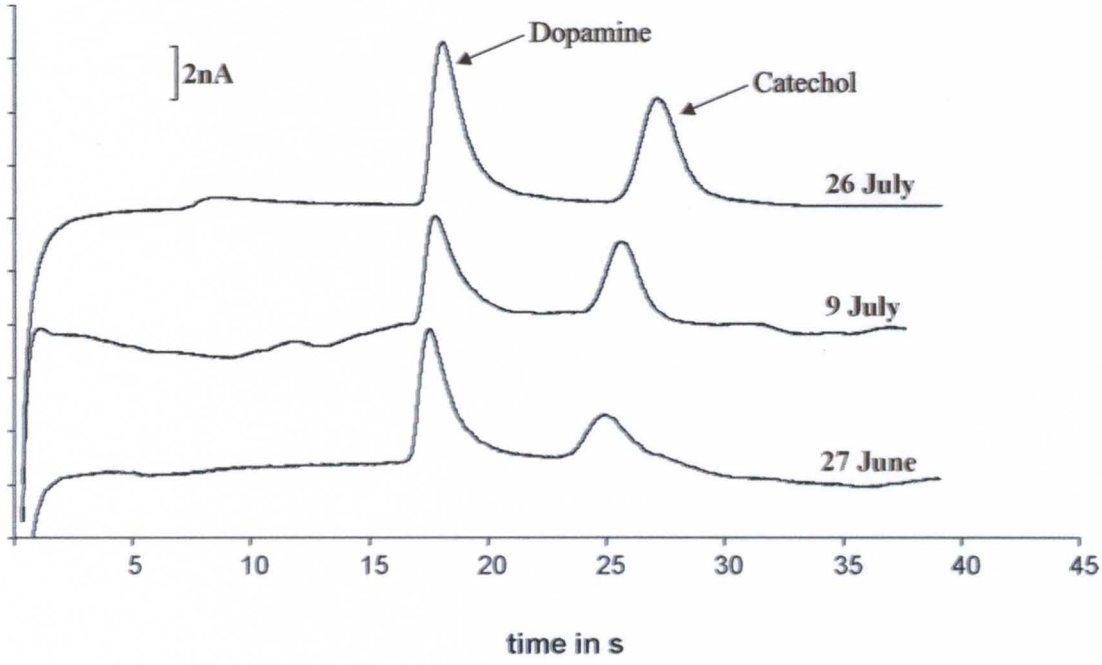

Figure 2.6 Electropherograms from working electrode W2A of Chip 2 taken on different days. Conditions are the same as in Fig. 2.5.

month-long period. During this time, Chip 2 experienced over 140 individual CE runs without any bonding failure or observable change in performance. The day-by-day variations seen in the electropherograms were similar in nature to what we have typically seen with thermally bonded devices. Most important, there was no apparent evidence of deterioration in chip integrity or performance.

To validate consistency between different devices fabricated *via* the stamp-and-stick technique, three different chips with the same CE and EC features were subjected to identical testing procedures. That is, the analyte and buffer concentrations as well as the CE and EC applied voltages were all held constant between individual CE runs and day-to-day CE experiments. Typical electropherograms obtained for the three chips are shown in Fig. 2.7. Clearly all three chips provided qualitatively similar CE performance, with chip-to-chip variations that were on the same scale as the day-to-day variations seen for a single chip.

A quantitative comparison of chip-to-chip performance is shown in Table 2.1. The current in the side arms represents the amount of current measured between the waste (or sample) reservoir and the channel intersection. This value was identical for all three chips used in the comparison studies and is an indication of balanced fluid flow in a single chip and similar fluid flow properties for different chips. The same is true for the CE current values measured in the separation channel. Migration times for the three chips with respect to dopamine and catechol showed only slight variation, as is common in these types of devices. Values obtained for peak area showed the greatest variability among the

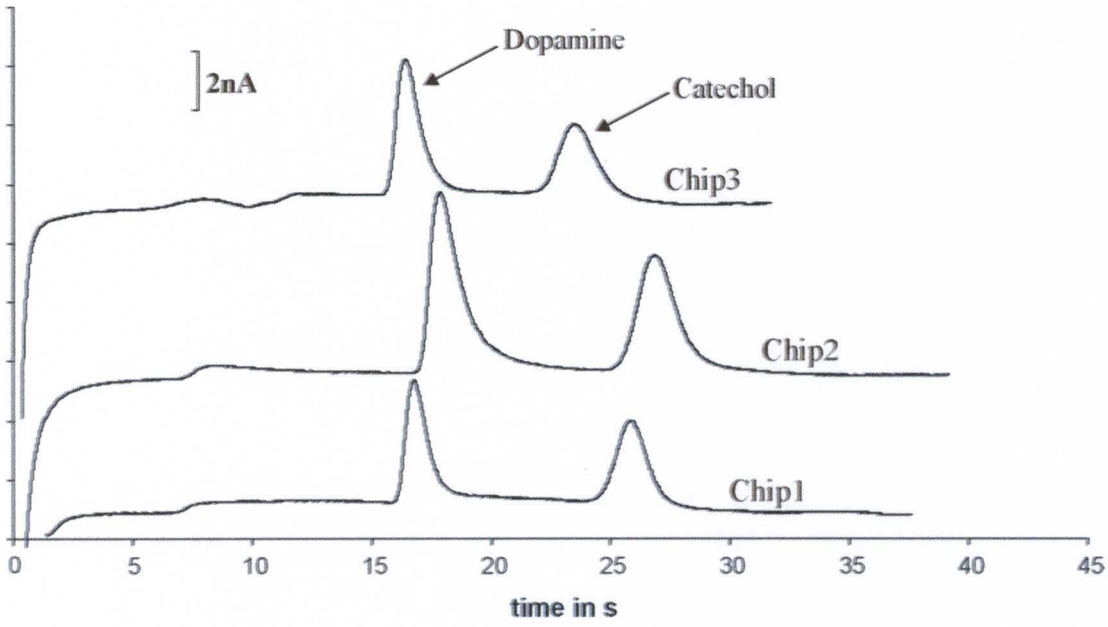

Figure 2.7 Electropherograms of analyte detection at electrode W2A of three different chips. Conditions are the same as in Fig. 2.5.

Table 2.1

	Applied CE field/V cm^{-1}	Current in side arms/μA	Current in separation channel/μA	Migration time/s	Peak area (arbitrary units)	Plug velocity/μm s^{-1}	Electroosmotic mobility/cm^2 V^{-1} s^{-1}	Efficiency/ plates m^{-1}	Absolute number of plates
Dopamine									
Chip 1	100 ± 2	0.44	2.25	17.3	205	579		122 900	1229
Chip 2	100 ± 2	0.44	2.25	18.6	404	536		117 200	1172
Chip 3	100 ± 2	0.44	2.29	16.9	248	591		110 100	1101
Catechol									
Chip 1	100 ± 2	0.44	2.25	26.3	184	381	3.81×10^{-4}	174 100	1741
Chip 2	100 ± 2	0.44	2.25	27.6	335	362	3.62×10^{-4}	149 500	1495
Chip 3	100 ± 2	0.44	2.29	24.0	180	417	4.17×10^{-4}	130 900	1309

[a] Note that for thermally bonded devices with identical CE channel length and applied voltage the efficiency seen for dopamine and catechol were 98 900 plates m^{-1} (989 total plates) and 68 000 plates m^{-1} (680 total plates), respectively.[16]

chips, with Chip 2 displaying nearly twice the response of the other two chips. The electroosmotic mobility (EOF) calculated for the chips was similar to that reported for other devices incorporating silica glass substrates, including thermally bonded chips.[11, 63] In all cases, the separation efficiency-over 100 000 plates per meter (or 1000 plates for the 1 cm long channel) - was similar to what our group has previously obtained for analogous thermally bonded devices.[11] (It should be noted that, due largely to the lower applied voltages normally employed with microchip CE devices, the separation efficiencies observed for these systems are typically lower than those expected for CE separations carried out in conventional capillaries. These appear, however, to be comparable to what has been reported for chip-based CE devices for similar channel length and applied voltage *e.g.*, ref.[64-66].) This indicated that there was no adverse effect from the adhesive in terms of CE performance.

One of the factors governing our selection of Norland NOA61 as the specific adhesive material for the stamp-and-stick procedure was its expected tolerance of most of the chemical conditions commonly encountered in CE operations, including both high and low pH as well as a broad variety of organic solvents.[67] Of particular concern was the resistance of cured adhesive layer toward: (1) solvents such as methanol and acetonitrile routinely employed as CE buffer additives; and (2) highly basic solutions routinely employed in CE to pretreat or restore the channels. In both of these cases, specific tests confirmed the adhesive's stability. Specifically, microscopic examination of bonded chips after overnight soaking in both methanol and acetonitrile showed no indication of any leakage or deterioration of the adhesive seal (seen in Fig. 2.8). In addition,

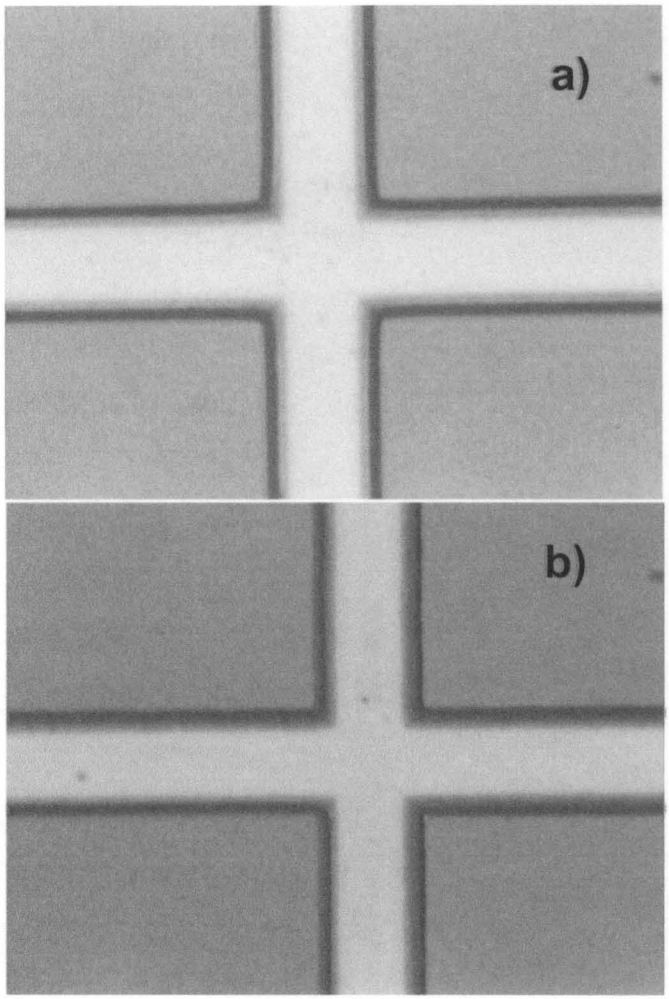

Figure 2.8 Photographs depicting the CE channel cross section (darker shaded region indicates UV adhesive) before a) the 16 hour soak in 20% methanol and 20% acetonitrile and after b) the soak.

subsequent CE runs in which the electrophoresis media consisted of PBS containing either 20% methanol or 20% acetonitrile (by volume) exhibited completely normal CE flow characteristics, with no leakage observed and no apparent change in the adhesive layer. Finally, the devices also proved compatible with high pH media such as 0.10 M NaOH as flow of this medium through the channels was routinely employed to periodically restore/improve CE performance.

Conclusions

The stamp-and-stick adhesive bonding approach has been shown to be a simplified and effective approach for bonding glass CE microchips under room temperature conditions. While the analytical performance of devices prepared by this process was essentially the same as that seen for conventional thermally bonded chips, the former technique offers clear practical advantages that include speed (30 min *vs.* several hours), success rate (nearly 100%), ease of alignment of the bonded substrates, and overall experimental simplicity. Furthermore, the necessity for special measures such as the use of ultraflat glass,[54] extensive pretreatment with sulfuric acid or piranha solution,[17, 54, 57] or plasma surface activation[18] was avoided. Of course, this approach is compatible with the presence of temperature-sensitive materials or structures on the bonded substrates (although this feature was not highlighted in this study). One requirement of the stamp-and-stick method is the availability of a suitable quality mask aligner such as is available in most state-of-the-art cleanroom/microfabrication facilities.

CHAPTER III

SELF-CALIBRATING MICROFABRICATED IRIDIUM OXIDE pH ELECTRODE ARRAY FOR REMOTE MONITORING

3.1. Introduction:

It seems clear that microfabricated instrument systems should have numerous unique applications in many areas of analysis. One such application for which microfabrication seems particularly well suited is the development of "smart" sensors suitable for numerous environmental, industrial, and security applications requiring long-term, on-site measurements. Such experiments entail analyses that need to be carried out with minimal operator intervention (preferably none at all) but nevertheless with a reasonably high degree of reliability over extended periods of time.

As mentioned in Chapter I, microfabrication is advantageous for electrochemical applications. It allows the freedom to customize electrodes and easily create complex electrical systems. Literally hundreds of electrode systems have already been reported for many important analytes. Additionally, microfabricated electrodes can be modified and optimized for specific applications by appropriate electrochemical postprocessing operations, leading to the construction of customized electrode designs for specific applications. Completely original electrode schemes do not need to be developed but rather these already well characterized electrodes may often only need to be adapted appropriately to the microfabricated format.

The specific goal of this work is to investigate simple ways in which the microfabrication approach can be used to make electrochemical sensors behave "more intelligently" and therefore provide improved performance for long-term remote monitoring applications. Specific features that can be incorporated onto the microfabricated sensor platform are (1) the inclusion of redundant sensing electrodes to function either as a back up when one sensor fails or as a way of verifying questionable results, (2) the integration of reference and auxiliary electrodes onto the sensor platform, and (3) the development of in situ electrode regeneration and calibration procedures.

The specific analytical problem that we consider here is the continuous pH monitoring of drinking water. Traditionally, the ideal sensor for pH monitoring has, of course, been the glass pH electrode. However, despite its attractive analytical capabilities with respect to selectivity and pH range, the glass electrode is rather poorly suited to conventional microfabrication techniques. A logical alternative is provided by metal oxide-based pH sensors that have been developed over the past 20-30 years and not only offer attractive pH measurement capabilities but also seem to be compatible in most respects with incorporation into microfabricated systems. A wide variety of metal oxides have been characterized and applied to pH measurement, including those involving Sb, Bi, Pd, Pt, Ir, Ru, Os, Ta, Rh, Ti, and Sn.[68-70] Although several of these oxide systems may be suitable, iridium oxide (IrO_x) was selected for use in this study because of its attractive stability and relative freedom from interferences. Most important, IrO_x can be prepared electrochemically and deposited onto a variety of conducting substrates by electro-oxidation/reduction of appropriate Ir complexes.[43-44, 71-79] This characteristic makes IrO_x-based sensors well suited for use in microfabricated devices in which noble

metal substrates have been patterned photolithographically and then modified as needed with the pH-sensitive IrO_x film.

Previously, there have been a few instances reported of microfabricated metal oxide sensor systems. For example, Marzouk et al. described the design and performance of implantable IrO_x-coated Pt electrodes for measurement of extracellular pH associated with myocardial ischemia.[44] Subsequently, Baudenbacher's group used similar procedures to place IrO_x electrodes on microfluidic chips for monitoring pH changes related to growth and activity of cell cultures.[71, 75] In all of these cases, the microfabricated electrodes exhibited excellent analytical performance, especially with respect to pH range, response time, and lack of drift. However, these studies took advantage primarily of the small electrode dimensions and precise electrode orientation made possible by microfabrication and were not concerned with the use of this methodology to create electrode arrays or systems that offered the increased reliability and independence required for remote monitoring applications. A promising approach in this direction was suggested by Vonau et al. who proposed the integration of a RuO_2-based pH electrode with Cl^-, NO_3^-, and NH_4^+ ion selective electrodes to create a "smart card" that might be used on-site for routine analysis of samples such as drinking water.[42] However, despite the intriguing nature of the study, only minimal information regarding the fabrication processes employed and almost no performance data were provided.

In this work, we report the construction of a microfabricated platform specifically designed for pH measurement and incorporating features to facilitate subsequent applications targeting independent on-site analysis. The resulting microchips (Figure 3.1) consisted of a flow-through silicon platform containing a patterned array of gold

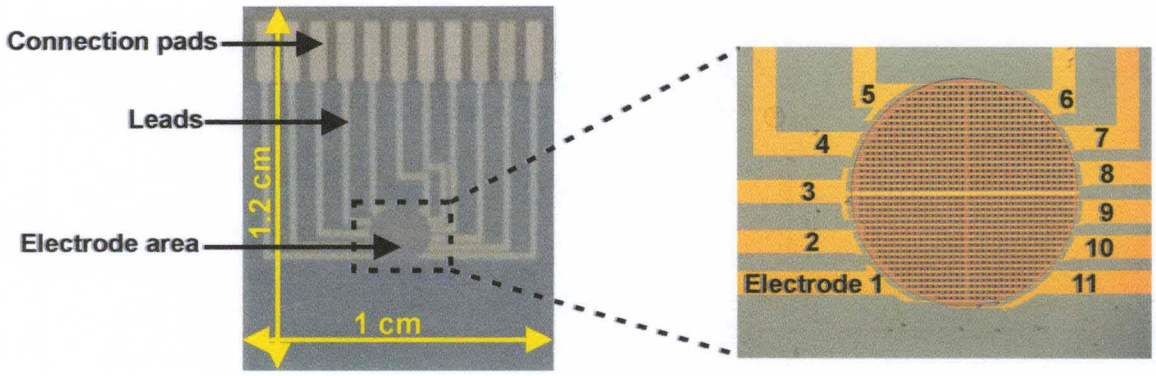

Figure 3.1 Photographs illustrating the entire microchip (left) and a close-up of the flow-through area containing the interdigitated working electrodes (right).

electrodes which were converted to pH electrodes via postprocessing electrodeposition of an IrO_x coating. The designs included as many as 11 equivalent pH sensors whose performance was evaluated for factors such as electrode-to-electrode reproducibility, short- and long-term drift, and the effectiveness of on-chip calibration procedures.

3.2. Experimental:

3.2.1. Materials

Universal pH buffers (4, 7, and 10), oxalic acid, and potassium carbonate (anhydrous) were purchased from VWR International (Batavia, IL). Iridium (IV) chloride hydrated and platinum wire (99.95%) were obtained from Strem Chemicals, Inc. (Newburyport, MA). All chemicals were used without further purification. Phosphate buffer solutions (0.2 M, pH ~ 6.6) and other solutions were prepared as needed using deionized (DI) water.

3.2.2. Chip Fabrication

Only a brief overview of the microfabrication process will be given here, since the production procedure has been reported separately.[13] In general, an oxidized 4 in. silicon wafer was employed as the substrate onto which various gold electrode arrays were patterned via photolithography. First, the gold electrodes (with a tantalum adhesion layer) were created by sputtering to a thickness of approximately 250 nm. Next, a polyimide layer, approximately 3 μm thick, was created to define the exposed electrode area and to insulate the electrical leads between the electrode area and the connection pads. Holes extending through the wafer for flow-through operation were created in two steps:

reactive ion etching of the electrode-side of the chip (after protection of the polyimide with a layer of aluminum) and deep reactive ion etching of the backside of the chip. A cross-sectional view of the resulting structure is shown in Figure 3.2. In all, four separate photolithography steps were required: to pattern the Au electrodes, the polyimide coating, and the front- and backside perforations.

Specific device designs ranged from a simple microchip containing a single electrode to one containing 11 interdigitated electrodes. This 11-electrode array, which was the design mainly utilized in this study, is depicted in Figure 3.1. A total of 38 finger electrodes with a width of 15 μm and varying in lengths were contained in the 2 mm diameter electrode area. All 11 electrodes had different surface areas, ranging from the smallest area (electrode no. 6) of 0.055 mm^2 to the largest (electrode no. 3) of 0.196 mm^2. This area was perforated (hole size 25 × 25 μm) enabling the chip to be incorporated into a flow through system to simulate drinking water detection scenarios.

3.2.3. Iridium Deposition Solution

The electrochemical iridium oxide deposition solution was prepared after a protocol first described by Yamanaka[78] and later utilized and modified by others.[43-44, 71, 75, 77, 79] A total of 75 mg of iridium(IV) chloride was dissolved in 50 mL of DI water and stirred for 15 minutes. Next, 0.5 mL of 30% H_2O_2 was added and stirred for 10 more minutes, and then 250 mg of oxalic acid was added with another 10 min stirring period. The resulting solution was slowly adjusted to pH 10.5 with anhydrous potassium carbonate and left to

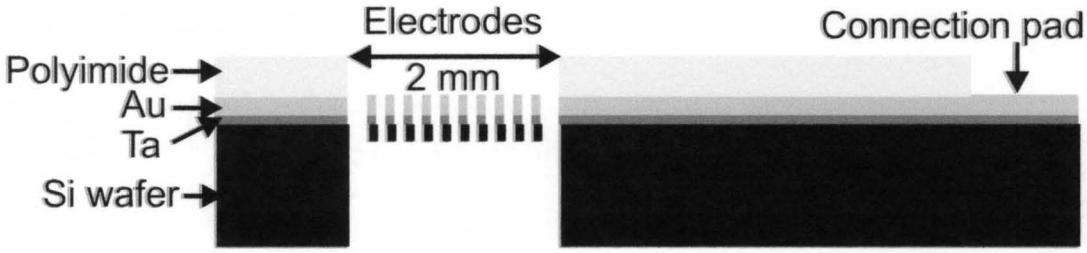

Figure 3.2 Schematic side view of the microchip illustrating the arrangement of the different material layers.

stabilize at room temperature for 2 days. Afterwards, the iridium solution was stored in the refrigerator and could be used for several weeks.

A pulsed potential deposition method was found to work best to deposit IrO*x* electrochemically onto the microfabricated gold electrodes.[76] The IrO*x* film was formed by potential pulsing between 0.0 V and 0.55 V (versus Ag/AgCl reference and a Pt wire counter electrode) at a 2 Hz frequency for 2400 cycles (40 min). When not in use, the IrO_x electrodes were stored in pH 7 buffer.

3.2.4. Instrumentation

Cyclic voltammograms (CVs) and constant potential treatments were carried out using a Bioanalytical Systems CV-50W voltammetric analyzer. Pulsed potential iridium depositions were accomplished employing a CHI 660A Electrochemical Workstation. All voltammetric experiments used a three-electrode cell with Ag/AgCl (3 M NaCl) reference and Pt wire counter electrodes.

All pH measurements were performed with a Thermo Orion model 320 potentiometer and verified by a commercially available glass electrode. A custom fabricated Delrin flow-through cell containing an access hole for a commercial Ag/AgCl reference electrode (1.9 cm downstream of the electrode area) was utilized to conduct flow through experiments with buffer solutions and drinking water. Solution flow was gravity driven, and the flow rate was determined by adjusting the height of the solution reservoir above the cell. Two water reservoirs were connected to the flow through system enabling a rapid switching from one solution to another.

3.3. Results and Discussion:

3.3.1. Iridium Oxide Deposition Process

Over the past 20-25years, many different groups have explored various strategies for preparing IrO_x deposits suitable for use as pH sensors, reference electrodes, and neural stimulation electrodes. In general, these fabrication methods can be grouped into four principal classifications: thermal treatment/decomposition of iridium or iridium compounds, sputtering from an iridium target onto the surface of a suitable substrate, electrochemical oxidation of an iridium substrate, and electrodeposition of IrO_x onto a substrate surface from a solution containing a suitable iridium complex. The resulting IrO_x films, though all suitable for pH sensing, have been shown to exhibit a wide variation in pH response (i.e., sensitivity, drift, etc.) depending on whether the IrO_x deposit is considered to be "anhydrous" or "hydrated". The former tends to result from the thermal and sputter-coating fabrication methods while the latter is usually associated with the electrochemical-based methods. A useful summary can be found in Madou's 2001 review.[39] For our intended applications, involving microfabricated pH sensing devices, the most attractive IrO_x formation approach seemed to be that utilizing Ir electrodeposition. First and foremost, this procedure was the most flexible, allowing the use of completely conventional microfabrication techniques to create the device platform and then the application of relatively straightforward electrochemical postprocessing to convert selected electrodes to IrO_x pH sensors. In addition, the electrodeposition also avoided high temperatures during the fabrication process and the need for a dedicated Ir sputtering target.

However, even with the electrodeposition approach to IrO_x film formation, there is still a wide variety of specific experimental procedures that have been reported. As summarized recently by Majda,[74] these variations center around (1) the nature of the Ir solution used and whether Ir oxalate complexes are employed or not and (2) the nature of the electrochemical procedure, constant current vs constant potential vs pulsed or scanned potential, used to carry out the deposition.

The former issue proved to be straightforward, and oxalate based solutions analogous to that described initially by Yamanaka[78] were always employed in this study. The behavior reported previously, namely, a 2 day induction period required for formation of the stable blue deposition solution, was observed consistently here, and the resulting IrO_x electrodes consistently exhibited the expected pH activity. However, the latter question concerning the electrochemistry operation was much more problematic; and during the course of this work, nearly all of the earlier procedures were investigated. In particular, we found that although the constant current or galvanostatic approach[43-44, 71, 75, 77-78] appeared to work acceptably for IrO_x deposition onto either carbon or platinum substrates, it did not yield uniform films on gold electrodes, either for large Au disk electrodes obtained commercially or for our smaller microfabricated Au electrodes. Rather, with Au, visual inspection showed that the deposited IrO*x* films usually varied greatly in color and thickness across the electrode surface and that the surface coverage of the underlying Au was often incomplete (seen in Figure 3.3). In addition, when used to monitor pH, IrO_x films deposited onto Au electrodes regularly exhibited unacceptable short-term and long-term drifts in the observed potential readings and were sometimes

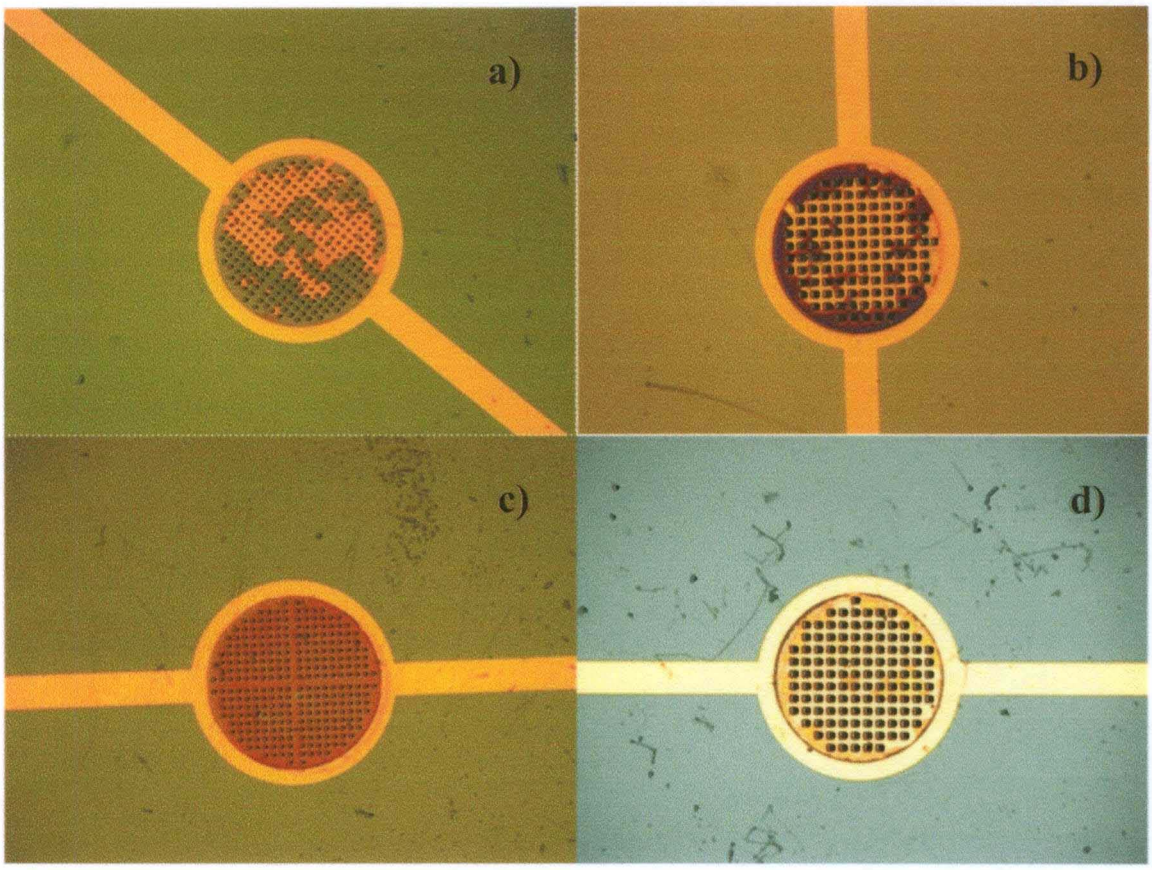

Figure 3.3 Photographs of galvanostatic modified gold electrodes depicting the irregularities in IrO_x film depositions and color variation ranging from a) blue, b) purple, c) light brown to d) clear.

prone to delamination from the Au substrate. Similar problems were also encountered with Au when the alternative constant potential approach[79] was employed.

Fortunately, greatly improved IrO_x films were obtained after switching to a pulsed potential electrodeposition strategy, similar to that developed by Meyer et al.[76] for preparing IrO_x coatings for implanted electrodes used for electrostimulation treatment of muscle and nerve tissue. In this protocol, the IrO_x deposit is grown by repeated application of brief oxidizing potentials, with the layer thickness determined by the length of time for which the potential pulsing was allowed to continue. The specific protocol that proved optimum for our microfabricated Au electrodes, pulsing between 0.0 V and +0.55 V (vs Ag/AgCl) for 40 min, was found to produce thick, visually uniform, and reproducible IrO_x deposits that were chemically and mechanically stable in buffer solutions for months and exhibited only very small drifts in both absolute potential and pH sensitivity. In addition to visual inspection, CV was also used to examine the nature of the electrodeposited IrO*x* and any qualitative or quantitative changes that may have occurred overtime. As shown in Figure 3.4, a typical CV, run in pH 6.6 phosphate buffer for a freshly prepared IrO_x-coated Au electrode, contained the expected Ir^{3+}/Ir^{4+} oxidation peak at ~250 mV and the corresponding reduction peak at ~50 mV, and scanning across the oxidation wave caused the appearance of the coating to change from colorless (Ir_2O_3) to bright blue (IrO_2). This CV behavior is identical to what has been described for the IrO_x in numerous earlier studies.[10-12, 14, 16, 20]

The optimization of the IrO_x deposition procedure described above was carried out primarily using commercial macro-sized Au disk electrodes. Therefore, once the optimization was completed, the next step was to establish how effectively this procedure

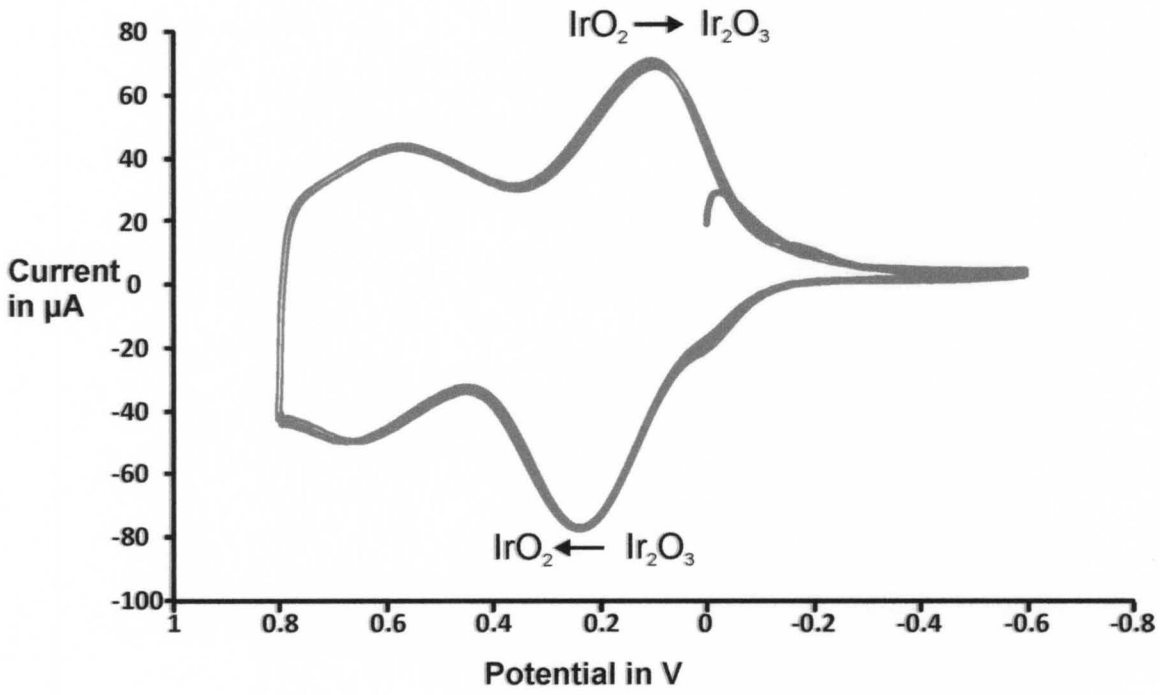

Figure 3.4 Cyclic voltammogram of an iridium oxide-coated Au electrode performed in pH 6.6 PBS at a scan rate of 50 mV/s.

could be extended to microfabricated the Au electrode arrays. Since our overall goal was to obtain a smart sensor that can operate in remote sensing settings with little or no external assistance, one strategy was to incorporate several redundant sensing electrodes on a single microchip platform. With this objective in mind, IrO_x was deposited onto a chip (see Figure 3.1) that contained 11 independent Au microelectrodes. For this procedure, all the electrodes were connected together; and the IrO_x was deposited onto all 11 in a single operation using the same experimental conditions developed above for conventional Au electrodes. Subsequently, the 11 electrodes were disconnected from one another, and the pH-sensing performance of each of the individual electrodes was evaluated and compared.

The results of this operation are summarized in Table 3.1. In general, the IrO_x deposition proceeded on the microchip exactly as expected, with visual and microscopic inspection indicating a complete and uniform coating of all 11 electrodes. In addition, CVs run separately on each electrode were all similar in appearance to that shown in Figure 3.4 for a Au/IrO_x macroelectrode and confirmed further that the deposition process had proceeded similarly. Because the individual microelectrodes were all different in size for this chip design, the magnitude of the CV currents was not identical for each but rather was determined by the electrode area. Of course, for the potentiometric pH measurements of interest here, these differences in electrode size had no influence on electrode performance. Most important, when examined in pH 4, 7, and 10 buffers, all 11 exhibited similar potential response, with slopes ranging from -63.8 to -69.5 mV/pH. This corresponds well to the pH behavior reported previously for hydrated IrO*x* films.[19] Finally, when examined over a long period of time, the Au/IrO_x electrodes

(A) Without treatment											
	Electrode										
	1	**2**	**4**	**5**	**6**	**7**	**8**	**9**	**10**	**11**	**ΔE**
pH10(mV)	97	81	62	60	65	51	14	32	24	75	83
pH7 (mV)	310	297	274	272	274	262	222	241	226	271	88
pH4 (mV)	505	498	470	473	470	458	422	440	419	458	86
Slope (mV/pH)	-68.0	-69.5	-68.0	-68.8	-67.5	-67.8	-68.0	-68.0	-65.8	-63.8	5.7mV/pH
(B) After 200mV treatment											
pH10(mV)	-3	-8	-7	-7	-9	-14	-12	-6	-13	-10	17
pH7 (mV)	205	205	206	206	201	197	201	206	199	199	9
pH4 (mV)	408	411	414	418	407	398	407	415	404	401	20
Slope (mV/pH)	-68.5	-69.8	-70.2	-70.8	-69.3	-68.7	-69.8	-70.2	-69.5	-68.5	2.3mV/pH

Table 3.1 Absolute potential responses and sensitivities for ten IrO_x electrodes before (A) and after (B) treatment. ΔE represents the range of the absolute potentials and sensitivities.

proved quite durable. The particular microchip that gave rise to the data in Table 3.1 was used on a daily basis for at least 4 months during which time hundreds of pH measurements were performed.

3.3.2. On-Chip pH Calibration.

For routine pH monitoring, the performance shown in Table 3.1A would probably prove acceptable. However, for the remote monitoring applications envisioned here, where conventional calibration with pH buffers would not be convenient, it is imperative that any single electrode behaves exactly the same over its entire lifetime and that drift in response over time, whether due to electrode aging, temperature, or other factors, should either be insignificant in extent or easily correctable. In addition, if any single electrode, upon malfunction, is to be replaced by another residing on the microchip, it is also essential that all redundant electrodes behave identically to one another. Unfortunately, Table 3.1A shows that this was not the case as the electrode-to-electrode variation in absolute potential readings seen for the pH 4, 7, and 10 buffers was 86, 88, and 83 mV, respectively, and electrode-to-electrode variation in the calibration slope over this pH range was 5.7 mV/pH. A practically useful solution to this problem was provided by the fact that the potentiometric pH response mechanism for the IrO_x electrode is fundamentally different from that of traditional ion selective electrodes. For most such systems (e.g., the glass pH electrode), the potential is generated at the solution/electrode interface and depends primarily on the solution-phase activities of the relevant ions. However, in the case of metal oxide electrodes, the pH response not only depends on the

H^+ activity but also on the oxidation state of the iridium film, with the suggested working reactions typically given as[75]

$$2IrO_2 + 2H^+ + 2e^- \leftrightarrow Ir_2O_3 + H_2O \quad (3.1)$$

for an anhydrous IrO*x* electrode and

$$2[IrO_2(OH)_2 \cdot 2H_2O]^{2-} + 3H^+ + 2e^- \leftrightarrow [Ir_2O_3(OH)_3 \cdot 3H_2O]^{3-} + 3H_2O \quad (3.2)$$

for the hydrated IrO_x system. Thus, for electrodes prepared via different methodologies, the Nernstian response slopes can range between 59 and 88.5 mV/pH; and electrodes such as ours that exhibit intermediate slopes (60-70 mV/pH) are generally assumed to have a mixed IrO_x composition and to be operating under a correspondingly mixed reaction mechanism.[20] Further, consideration of the related Nernst equations,e.g.,

$$E = E^0 - 2.3RT/2F \log[Ir_2O_3]/[IrO_2]^2[H^+]^2 \quad (3.3)$$

and

$$E = E^0 - 2.3RT/2F \log[Ir_2O_3]/[IrO_2]^2[H^+]^3 \quad (3.4)$$

suggests that any variation in the Ir^{3+}/Ir^{4+} ratio should also have a predictable effect on the pH response. In fact, this latter consideration has frequently been invoked to explain variations in potentials observed not only for IrO_x electrodes prepared by different methods but also for IrO_x electrodes as they age or are exposed to redox agents during operation. For example, newly prepared electrodes have been reported to vary in their potential response up to 100 mV,[21] and deliberate exposure to redox agents such as $Fe(CN)_6^{3-/4-}$ has been shown to eliminate pH sensitivity entirely.[17]

The most important implication of this analysis is that, just as variations in the Ir^{3+}/Ir^{4+} ratio during usage may cause an electrode's pH response to vary, restoration of an electrode's initial redox state might restore it to its original activity. In fact, as early as

1992, Hitchmann, working with thermally prepared anhydrous IrO*x*, showed that both the absolute starting potential reading and the overall stability of a series of electrodes could be dramatically improved after application of an appropriate potential for a 5-30 min period.[21] By this approach, the variation in response of four IrO_x electrodes whose starting potentials varied over nearly 100 mV was made to converge to just a 10 mV range. Despite the obvious utility of this technique, it seems to have been largely overlooked since its initial report and we have been able to find no subsequent application of analogous potential pretreatment schemes in the production or use of metal oxide pH electrodes. Nevertheless, for our microfabricated electrode arrays, Hitchman's electrochemical treatment approach presented a very attractive method both to improve interelectrode reproducibility and perhaps to allow a simple and effective way to "recalibrate" pH electrodes in the field without the need for standard buffers.

Accordingly, the same IrO_x electrodes whose response is shown in Table 3.1, A were subjected to a potential treatment that consisted of immersion in pH 7 buffer and application of 200mV (vs Ag/AgCl) for 3 min. (At the time of this treatment, the microchip had already undergone over 3 months of routine testing and the electrodes had already shown clear deviations from their original potentials and slopes.) This particular potential, which was reasonably close to the electrodes' original potential reading for pH 7, was chosen because, based on the IrO_x CV in Figure 3.4, it should ensure significant amounts of both Ir^{3+} and Ir^{4+} oxidation states. Table 3.1, B shows that, after this 3 min treatment, the absolute potential readings obtained in pH buffers converged dramatically. Compared to the earlier 80-90 mV differences, the interelectrode responses were reduced to 10-20mV (±4 mV). This corresponds to a difference in pH of 1.4 and

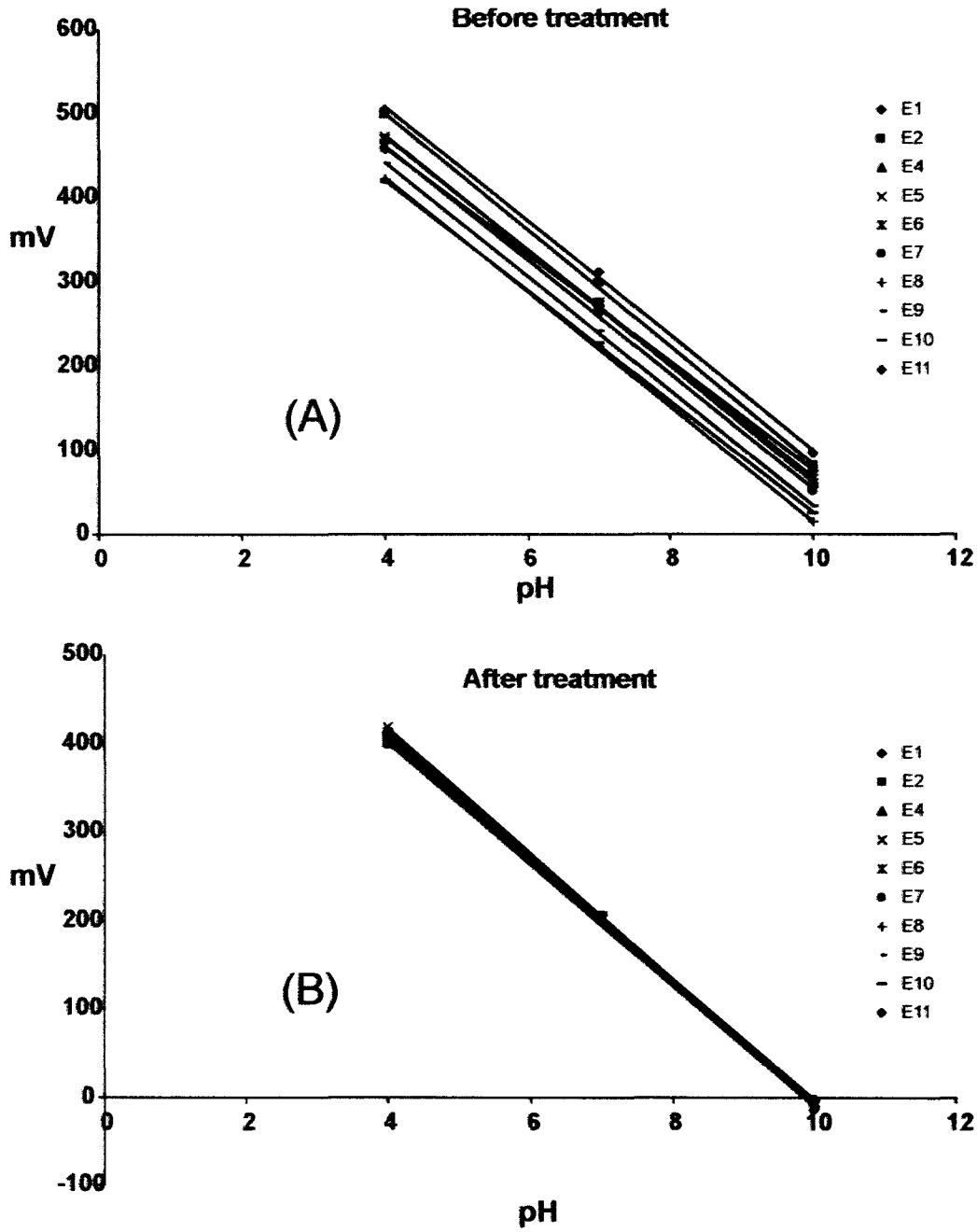

Figure 3.5 Calibration curves of the IrO_x electrodes in pH 4, 7, and 10 buffer solutions before (A) and after (B) potential treatment.

0.29, respectively. In addition, the variation in the calibration sensitivity was also significantly reduced, with the range of slopes decreased from 5.7 mV/pH before the potential treatment to 2.3mV/pH (±1 mV/pH unit) following it. The effect of the 200 mV treatment is perhaps best illustrated in Figure 3.5 where the overall pH response is shown graphically both before and after the procedure.

3.3.3. Rationale

The apparent explanation for the success of the 200 mV treatment procedure is that, during preparation or during extended usage, the Ir^{3+}/Ir^{4+} composition of the IrO_x electrode can vary and that, as suggested by Hitchman,[21] the application of an external potential provides a convenient mechanism for both restoring the composition of an individual electrode to its initial state and bringing that of different electrodes into a close degree of convergence. Several observations made during this study provide qualitative support for this explanation. For example, we noted early on distinct differences in pH behavior for the electrodes depending on the ending potential for the IrO_x deposition which could be either reducing (0.0 V vs Ag/AgCl) or oxidizing (+0.55 V) in view of the pulsed potential electrodeposition procedure employed. Next, it is well-known that Ir^{4+} oxide species tend to be blue in color. As our IrO_x electrodes aged during use, they gradually lost their initial blue color and took on a largely colorless appearance indicative of Ir^{3+}. Finally, we electrodeposited IrO_x onto an optically transparent indium/tin oxide slide and then observed its absorbance *in situ* as a function of applied potential. Potentials ranging from 600 to -200 mV were applied in 100 mV increments in pH 7 buffer, and absorption spectra were taken from 400 to 800 nm. At the initial 600 mV potential, the

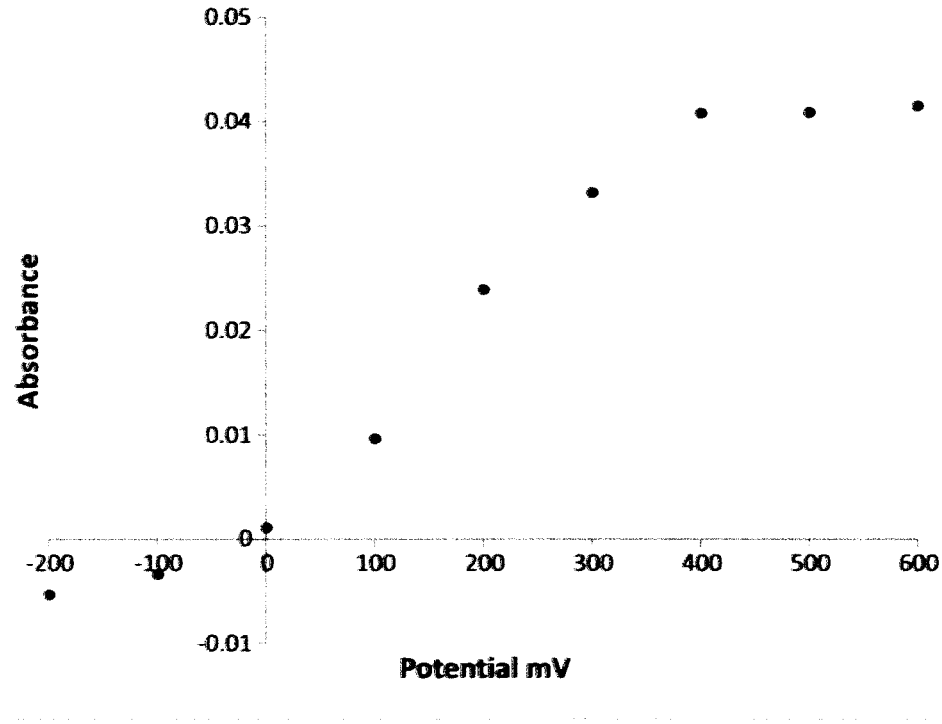

Figure 3.6 Absorption spectrum of IrO_x taken at 100 mV incremental steps at the maximum absorption wavelength of 635 nm.

IrO_x deposit was blue in color, with a maximum absorbance at 635 nm. Almost no changes in the spectrum were observed down to 400 mV, but at 300 mV the 635 nm absorbance started to decrease (as shown in Figure 3.6). This suggested that, at the 200 mV pretreatment potential, some of the Ir^{4+} was already converted to the colorless Ir^{3+} form and that a mixture of the two redox states is necessary to obtain an ideally functioning pH electrode.

One of the strengths of IrO_x in pH sensing is its relative freedom from interference from many simple ions and complexing agents.[44, 72, 80] However, like most metal oxide systems, IrO_x response is known to be particularly sensitive to the presence of redox species.[72, 80] Accordingly, as a final test of the above treatment procedure to provide an effective calibration approach, exposure of the IrO_x to redox agents was also investigated. In particular, the ferri-/ferrocyanide couple was selected as the interfering agent of choice because Bezbaruah and Zhang[72] recently showed that the pH sensitivity of IrO_x can be blocked completely by the presence of this redox couple. Our experiments, shown in Figure 3.7, confirmed the severity of this problem. While a freshly prepared IrO_x electrode exhibited the expected pH response for pH 4-10 buffers (Figure 3.7, trace A), addition of 0.01 M ferri-/ferrocyanide to the buffers virtually eliminated the effect of pH on the observed electrode potential (trace B). While removal of the ferri-/ferrocyanide and return of the electrode to pristine buffer solutions did allow its general pH sensitivity to be restored, the new potential readings were displaced by more than 150 mV from their initial values (trace C). In practice, such a displacement, which is consistent with a net reduction of the Ir deposit, would have a serious effect on the measurement; and without

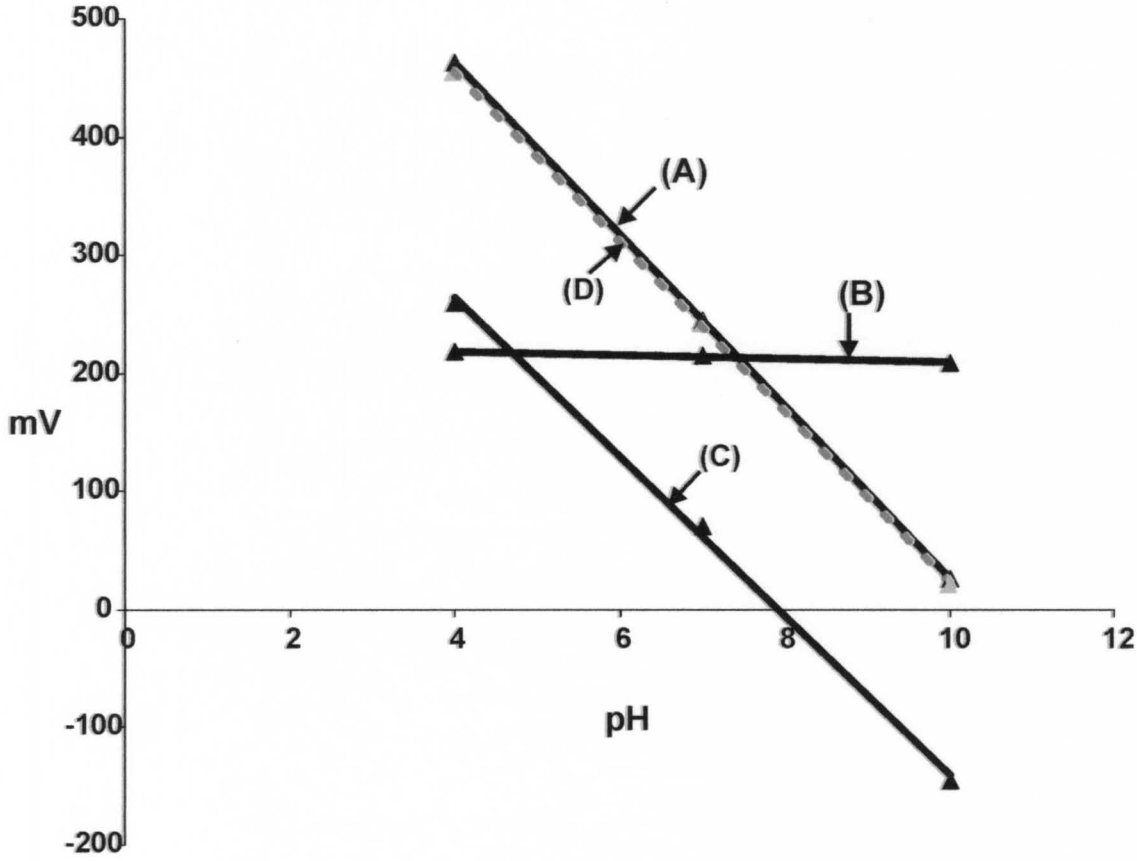

Figure 3.7 Calibration curves of a freshly prepared IrO_x electrode in pH 4, 7, and 10 buffer solutions. Trace A shows the original pH response. Trace B was acquired after addition of 0.01 M ferri-/ferrocyanide to the buffer solutions. Trace C is the response curve after removal of the ferri-/ferrocyanide, and trace D is the restored pH response after a 3 min treatment in pH 7 buffer (gray dotted line).

recalibration, the new pH readings would be changed by as much as 2 pH units. However, as can be seen from trace D, application of the above pretreatment procedure (i.e., 3 min in pH 7 buffer) returned the electrode's pH response nearly exactly to its starting state. This experiment showed obvious promise for the possibility of on-site sensor recalibration after exposure to oxidizing and or reducing agents that might be encountered in drinking water analysis.

3.3.4. Application in Flow System

Up to this point, all pH measurements and pretreatments had been carried out in bulk solution by simply immersing the IrO_x electrodes in an unstirred buffer/analyte solution. In order to simulate actual water quality testing scenarios, the microchip was integrated into a flow-through system which contained a downstream commercial Ag/AgCl reference electrode. The chip utilized for the flow-through experiments described below contained a six-segmented electrode array. One of the electrodes was coated with IrO_x for pH sensing, and the others were kept as bare Au electrodes, thereby enabling them to function as a counter electrode for any desired pretreatment experiments. Initial experiments employed standard pH buffers since, unlike actual tap water, these have a fixed and well-known composition with respect to ionic strength, dissolved organics, etc.

Typical flow-cell results are shown in Figure 3.8. In this experiment, the potential of an IrO_x was monitored over time as pH 10 and pH 4 buffers were alternately passed through the cell. As can be seen, although the observed potential readings were relatively stable initially, a substantial negative drift ensued that after 4 h amounted to

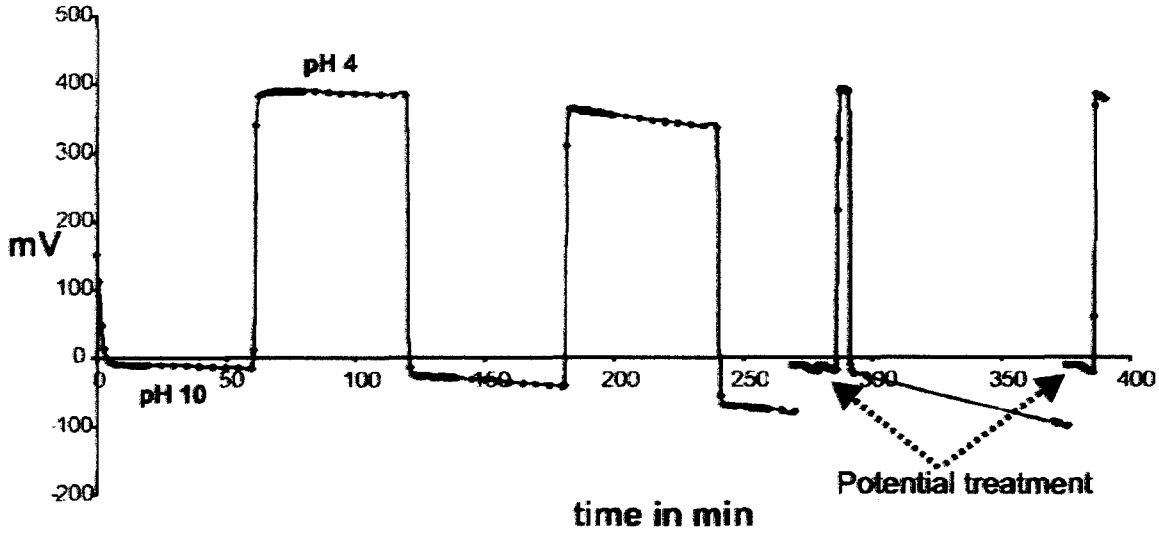

Figure 3.8 Potential response of the microchip containing IrO*x* electrode incorporated into a flow system. Buffer solutions (pH 4 and 10) were alternately passed through the chip; after 275 min, a potential treatment of -14 mV was applied to the working electrode to correct for negative drift (~60 mV).

approximately 60 mV. Other than this drift, the IrO_x electrode continued to respond rapidly to changes in the buffer pH. Subsequently, a potentiostatic treatment, consisting of holding the electrode at -14 mV for 6 min, was applied. (Note that a different treatment potential from that used earlier was employed here because, unlike the previously described +200 mV treatments that were carried out in pH 7 buffer, the treatment medium in this study was pH 10 buffer.) Clearly, this procedure was again successful in restoring that electrode's original response. Moreover, although the electrode output continued to drift after the treatment, the protocol could be repeated at will to restore the electrode response and make accurate pH readings possible. Only two treatment cycles are shown in the figure, but we found that the procedure remained effective for numerous pretreatments over periods of weeks.

Finally, the sensor performance under more realistic conditions was examined by obtaining longer-term pH measurements made directly on municipal (Louisville, KY) tap water. As above, these measurements were made by continuously flowing the water sample through the microchip for the entire duration of the experiment; and the sole pretreatment of the tap water consisted of filtration to remove particulates and prevent possible clogging of the perforated electrode area during such long time use. Throughout the course of the reported experiment, the pH of the specific water sample employed was 8.05 as determined at the outset and verified daily with a standard glass electrode.

Figure 3.9 summarizes the chip performance obtained over a16-day measurement period. For each set of pH measurements shown, the initial potential reading corresponded to the potential of the IrO_x electrode on that day without any treatment or modification. Clearly, there was a significant and mostly random drift in this potential

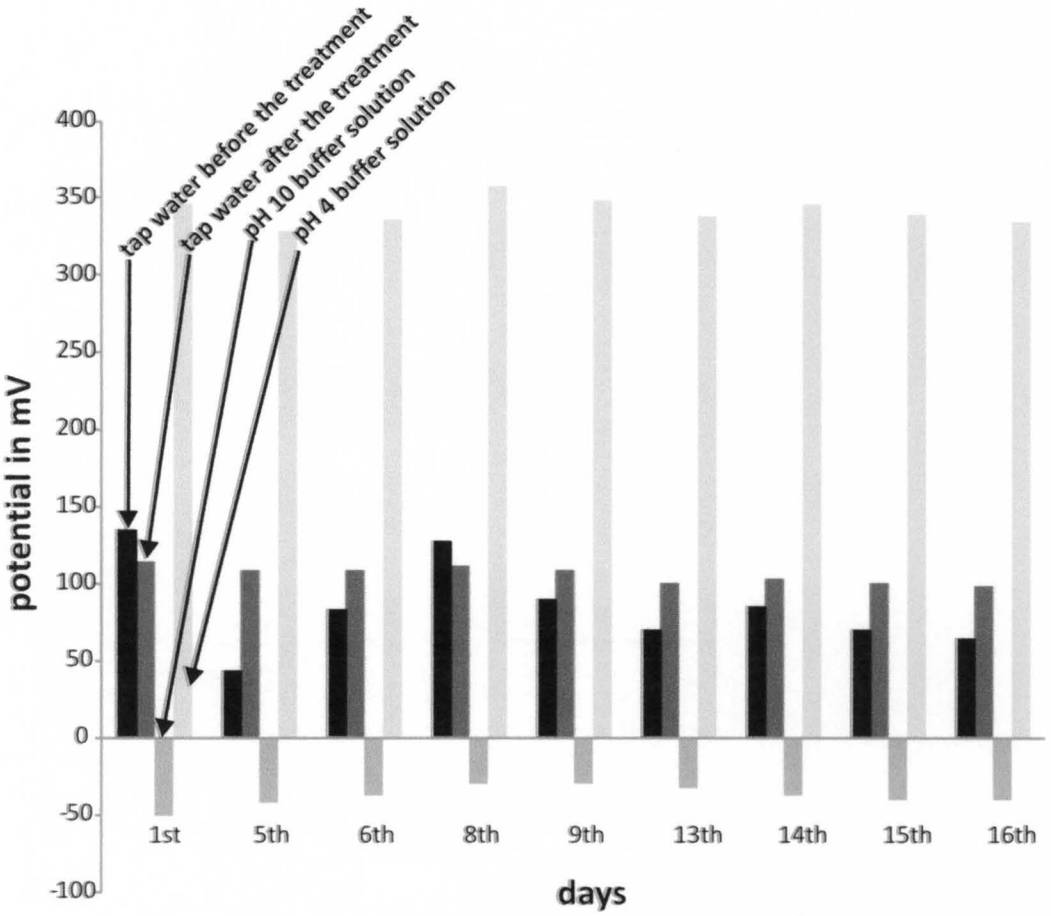

Figure 3.9 Potential responses of the microchip incorporated into a flow-through system for 16 days in tap water. Potential treatment of 115 mV (6 min) was applied, and the electrode pH responsive was verified by passing pH 4 and 10 buffer solutions through the chip.

reading from day to day. Subsequently, the electrode was treated by holding it at +115 mV for a 6 min period and then allowed to equilibrate for 5 min. The potential values, remeasured at this point, showed a maximum deviation of only 16 mV (±5.3 mV) over the entire course of the experiment. This corresponds to a maximum difference in pH readings of 0.24 (±0.08). In order to confirm that the electrode's overall pH response was still in place, the tap water was briefly replaced by pH 10 and pH 4 buffers, and potential readings were made in each of the media. Despite a relatively small random drift, the IrO_x electrode remained well calibrated over the 16 day test period.

Additionally, it was also important to verify that the pH electrode can be restored to its original pH response under realistic conditions when exposed to redox agents (ferri-/ferrocyanide). For this reason, the sensor was placed again into the flow through system and measurements were taken under continuous flow of tap water and the results are shown in Figure 3.10. During the introduction of tap water containing 0.01M ferri-/ferrocyanide, an obvious potential increase from 108 mV (±0.9) to 178 mV (±2.1) was observed. Not surprisingly, after removal of the interfering agent from the tap water, the absolute potential reading for the pristine tap water was displaced by 44 mV (±1.5), indicating an alteration of the IrO_x surface. By applying the same potential treatment as mentioned earlier (115 mV for 6 min), it was possible to restore the electrode to its original pH response of 108 mV under drinking water conditions.

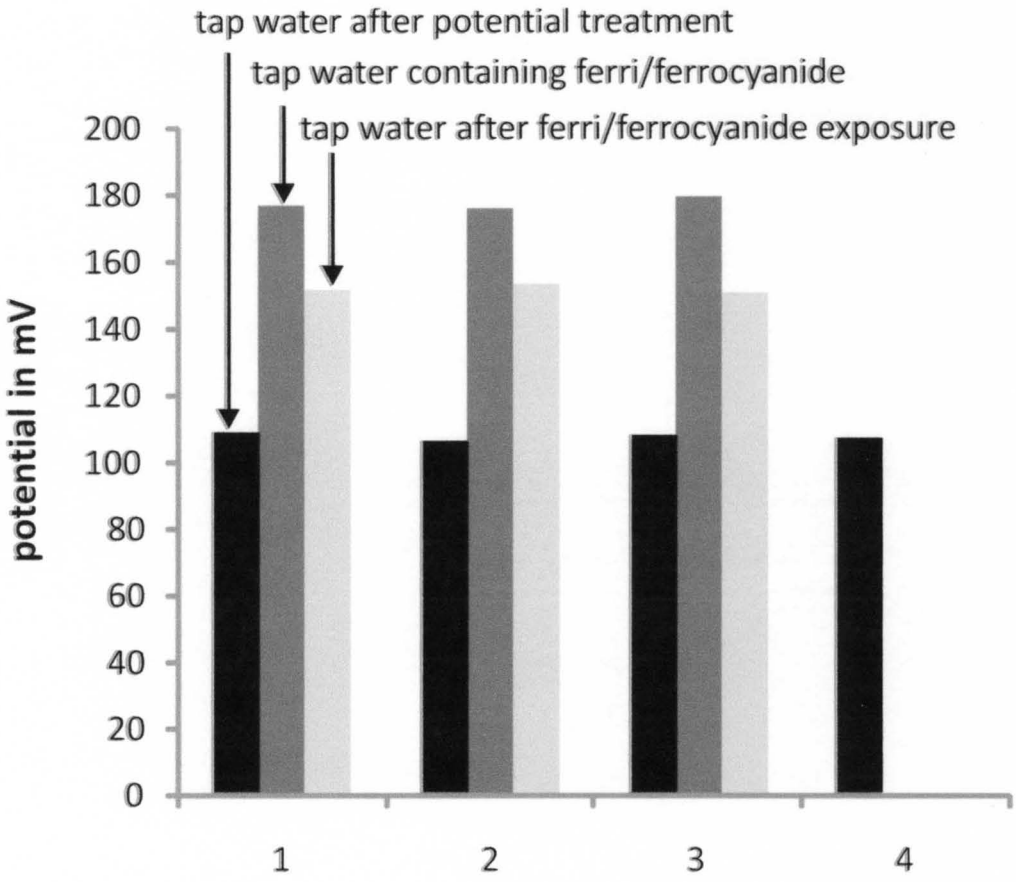

Figure 3.10 Potential responses for a microchip incorporated into the flow-through system for drinking water spiked with 0.01M ferri-/ferrocyanide. Potential treatment of 115 mV (6 min) was applied to restore the electrode to the original pH response.

3.4. Conclusion:

In this work, we have investigated a few simple strategies, made possible by microfabrication methodologies, for improving sensor performance for on-site and especially unattended operation. Specifically in the case of pH measurement, arrays of microfabricated Au electrodes coated with IrO_x films were shown to perform effectively for drinking water samples from municipal treatment facilities. Perhaps most important, a simple potentiostatic calibration procedure, requiring no external buffer solutions, was shown to be highly effective both for standardizing the absolute potential response of all the individual electrodes in the array and for restoring the potential response of a single electrode over an extended period of time. These represent a few examples illustrating simple ways in which microfabrication can be employed to allow instrumentation to operate at a more "intelligent" and independent level.

Although automated monitoring of pH alone may be important for some applications, integration of additional sensing functions would be necessary in order to achieve a practical device suitable for general surveillance of drinking water quality. For example, inclusion of sensors for other parameters such as conductivity, redox potential, and disinfectant level would certainly increase the available analytical information to a very useful level. Interestingly, not only do electrochemical approaches appear to be well suited o the design of sensors for all of these parameters, but also their actual construction and miniaturization seem highly amenable to conventional microfabrication techniques. Therefore, we expect that there will be rapid progress in the development of smart microfabricated sensors for routine monitoring of water quality. In addition, in view of the innumerable practical applications of electroanalysis that are already well-known, it

seems likely that the approach can be extended to very many important measurement situations.

CHAPTER IV

MICROFABRICATED ELECTROCHEMICAL SENSORS FOR EXHAUSTIVE COULOMETRIC APPLICATIONS

4.1. Introduction:

There currently exists a wide variety of environmental, industrial, and security applications where long-term remote chemical analysis is either required or at least highly desirable.[81-82] As a result, the design of "smart" sensors, capable of performing stable and reliable measurements without operator intervention has become an area of increasing interest in instrument and sensor development. At the same time, important progress has occurred in the microfabrication of analytical instruments and the production of so called "lab on a chip" (LOC) or "micro total analysis" (μTAS) systems. The benefit of miniaturization is not only smaller individual instruments but also the potential for incorporating multiple instruments on a single platform. The potential mass production of such miniaturized integrated measurement systems also allows, in principle, deployment of a network of devices which can simultaneously monitor many locations at once, especially when smart sensors that require little operator intervention are utilized. Consequently, it has been one of our group's objectives to investigate specific ways to utilize smart sensor design principles in conjunction with microfabrication.

Of course, there is a wide range of specific instrument characteristics that serve to make a sensor "smart". One approach to smart sensor design has been the inclusion of a number of independent sensor elements which are able to measure different sample attributes.[26-28] The inclusion of redundant sensor elements for self-verification and the availability of back-up sensors for enhanced longevity is another approach and was discussed in Chapter III on hand of the pH IrO_x array for drinking water monitoring.[6] A more difficult issue for operator-free smart sensors has been the issue of calibration. With the exception of a few commercial devices where a single sensor selected from a batch is used to initially calibrate the sensitivity of the entire lot,[83] there have been very few examples of sensors which do not require at least an initial calibration. To our knowledge, there have been no reports of sensors which are capable of extended field operation without calibration, which is a challenging requirement even under the best circumstances. The response of most instruments is sufficiently unstable as to require at least periodic calibration, even under well controlled laboratory conditions. A sensor deployed in a truly remote setting is expected to experience a variety of physical conditions (temperature, humidity, etc.). Additionally, sample pretreatment and conditioning procedures are limited with a remote sensor.

There are several general approaches to solving the calibration problem. Ideally, one could identify and employ sensing devices whose response is completely stable and nearly immune to fluctuations in the operating conditions. However, relatively few chemical sensors are available that meet this standard at a practical level. Alternatively, one could try to achieve remote calibration by packaging appropriate standard solutions onto the sensor platform along with a suitable flow system (pump, valves, etc.). This

latter approach would make actual on-site calibration possible, with the major drawbacks being increased device cost and complexity. These are serious drawbacks to the ability of smart sensor networks to function remotely in the field since device complexity in general leads to an increase in the frequency of failure, which in turn requires more frequent maintenance. Collectively, these additional costs reduce the practicality of a large number of sensors in a network. A third – and, we believe, preferable – approach is to identify and employ analytical measurement methods that are both compatible with field deployment and also provides absolute quantitative results and therefore can be considered "calibration free".

Besides potentiometry, which was discussed in chapter III, a second analytical approach that is adaptable to large networks of remote sensors is electrolysis. Amperometry has been described for both flow-by and flow through sensors[84-85] and amperometric sensors utilizing either flow-by or stopped flow analysis have been adapted to diverse applications including biosensing,[86-87] gas sensing,[88] and chlorine.[50] However, all of the amperometric methods require calibration since the collected current depends on mass transport of the analyte (i.e. temperature, solvent viscosity, etc.).[89] Amperometric measurements are also dependent on electrode area which may change with extended use due to fouling in a remote sensing application.

Of the electrochemical approaches for smart sensors, one that seems to have much to offer is coulometry[90] which is one of the few analytical methods that is capable of absolute quantitation. In principle, as long as the cell volume is accurately known and the electrolysis is carried out to completion, the corresponding charge is an absolute determinant of the analyte quantity and concentration. In addition, any changes in

electrode area that occur over extended periods of operation should be also less problematic; as long as the cell volume remains constant, partial passivation of the electrode surface affects the time dependence but not the magnitude of the coulometric signal.

In this chapter, we report on the development and evaluation of a first-generation microfabricated coulometric sensor system that shows promise for calibration-free remote monitoring applications. Although there have been many examples of quantitative coulometry, few seem to be ideally suited remote monitoring applications. High surface area flow-through electrodes not only would require precise control of sample flow rate for reliable quantitation and seem poorly suited to reproducible mass production. Rather, we have chosen to investigate the use of a small volume, thin-layer electrolysis cell employing readily fabricated planar electrodes. There are numerous examples that suggest that this approach has much to offer. For instance, Karube's group showed that a 45 μL thin-layer coulometric system constructed with a planar Cu anode permitted the measurement of chemical oxygen demand in lake water samples in a 3-10 minute time frame. [48] Fukuda et al. described a micro-bulk electrolysis cell suitable for the study of mediated enzyme reactions and the relatively rapid coulometric analysis of the substrate species in 10 μL sample volumes.[49] Neither of these approaches was intended for, or applied to, remote sensing as both required extensive operator interaction. More recently, Bakker has shown that passage of controlled currents through ion selective membranes can be used to release precisely defined quantities of calcium and barium ions into the surrounding solution with high selectivity.[91-92] This approach offers the potential of carrying out a wide variety of calibration-free coulometric measurements that should

eventually have interesting and useful applications in long-term remote sensing. In this chapter, we report on the design, construction, and performance of a miniaturized sensor system intended to carry out exhaustive coulometric measurements and have eventual application in remote monitoring. The electrolysis chamber is a thin-layer cell, approximately 2.2 μL in volume, that contains working and reference electrodes microfabricated onto a silicon wafer and whose dimensions are defined by a silicone rubber gasket placed on top of the wafer. The working and counter electrode compartments are isolated by means of a semi-porous membrane that permits current flow but limits physical exchange between the two halves of the cell. Here we evaluate the performance of the coulometric sensor platform using ferri-/ferrocyanide as a model electrochemical analyte and describe the design considerations most critical for successful calibration-free operation.

4.2. Experimental:

4.2.1. Reagents

For all coulometry experiments, potassium ferricyanide, potassium nitrate, and sodium chloride were purchased from Sigma-Aldrich (Milwaukee, WI) and potassium ferrocyanide from VWR International (Batavia, IL) at highest purity and were used without further purification. Analyte and electrolyte solutions were always freshly prepared using deionized (DI) water. A commercial silver plating solution (Technic Silver Cyless II RTU) obtained from Technic Inc., Cranston, RI was used to electroplate all reference electrodes.

4.2.2. Fabrication

4.2.2.1 Sensor

All sensor chips were fabricated in the cleanroom facility in the University of Louisville Center for Micro/NanoTechnology. The following discussion is intended to provide an overview of the fabrication process employed here. Detailed procedures steps are listed in the appendix in Table B.1.

A 4-inch silicon wafer was employed as the substrate onto which different sensor designs were patterned via photolithography. The individual chip platforms were 1.3 cm wide x 2.1 cm long, with patterned gold electrodes occupying a 4 mm x 8 mm elliptical area near the center. Thus, 18 different chips could fit onto a single wafer and be fabricated together during each processing run.

Each chip contained from two to six independent gold electrodes, one of which was subsequently transformed into a Ag/AgCl pseudo-reference electrode. Figure 4.1 shows the two different electrode schemes that were used in this work. The first (Design A) contained only two electrodes, a large Au oval with an area of 25.6 mm^2 surrounding a smaller Au strip with an area of 0.71mm^2. The second (Design B) contained six 50 μm wide gold finger electrodes arranged in a concentric spiral pattern with an inter-electrode spacing of 50 μm. The electro-active area of the working electrodes in Design B (W1-W5) was only 40.5% of the active working electrode area in Design A (W1). Details of the working electrode areas for electrodes on both chip designs are listed in Table 4.1.

The first step of the fabrication process consisted of growing a 600-nm thick oxide insulation layer onto the silicon wafer. Next, the desired pattern for the electrodes was transferred onto the wafer via photolithography and was etched into the wafer to a depth

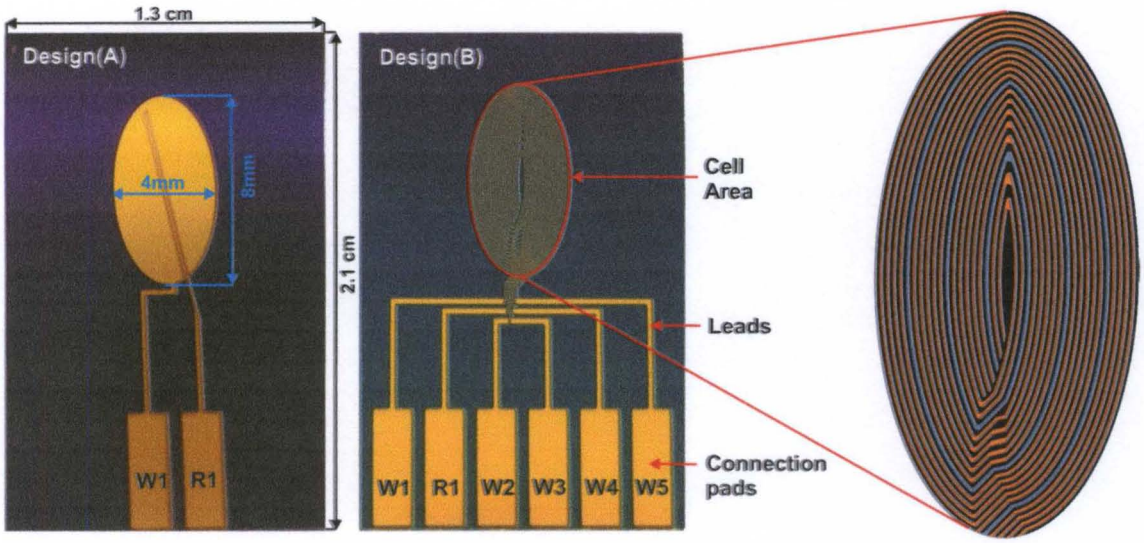

Figure 4.1 Photographs illustrating two sensor chip layouts. Design (A) contains working electrode (W1) and reference electrode (R1), whereas design (B) has five working electrodes (W1-W5) and one reference electrode (R1). Exploded view indicates detail of concentric spiral electrode design.

Design	W 1 Area (mm^2)	W 2 Area (mm^2)	W 3 Area (mm^2)	W 4 Area (mm^2)	W 5 Area (mm^2)	R 1 Area (mm^2)
(A)	25.6	-	-	-	-	.714
(B)	1.73	1.84	1.95	2.05	2.15	2.49

Table 4.1 Electrode areas of two sensor chips (design A and B)

of ca. 250 nm using a buffered oxide etch. Subsequently, the electrodes were formed by sputtering a similar thickness of gold (preceded by a thin tantalum adhesion layer) so as to fill up the etched recesses. A lift-off procedure was used to remove the unwanted Au and leave the final electrode structures intact. A Disco DAD 321 dicing machine was then used to cleave the wafer into individual sensor chips.

Thereafter, one of the patterned Au electrodes on each chip was converted via electroplating to a Ag/AgCl pseudo-reference electrode. The procedure used to do this was similar to that reported by Shanthi. [93] First, the chip (R1, cathode) was placed into a commercial silver plating solution along with a Ag sputtered Si wafer (anode) where a 560-mV pulse train (40ms on, 60ms off) was applied for 70 minutes to give an initial current density of approximately 0.7 mA/cm^2. This current density slightly increased over time and was adjusted when necessary; exceeding 1.2 mA/cm^2 led to destruction of the gold electrode. Chlorination was then performed by placing the chip in a 1M NaCl solution and applying a 50-mV pulse train (40ms on, 60ms off) to the electroplated silver electrode (R1, anode) using a Pt wire (cathode) for 15 seconds.

4.2.2.2. Flow Cell

The flow cell into which the microfabricated chips were inserted for analysis is shown in Figure 4.2. It consisted of two principal pieces that were fabricated from Lexan by precision CNC milling. The microfabricated chips were placed onto the bottom Lexan piece into a shallow trench that had the same dimensions as the chip and acted as an alignment guide. The working electrode compartment of the electrochemical cell was formed by cutting an elliptical hole of the desired size into a 120 μm thick silicone rubber

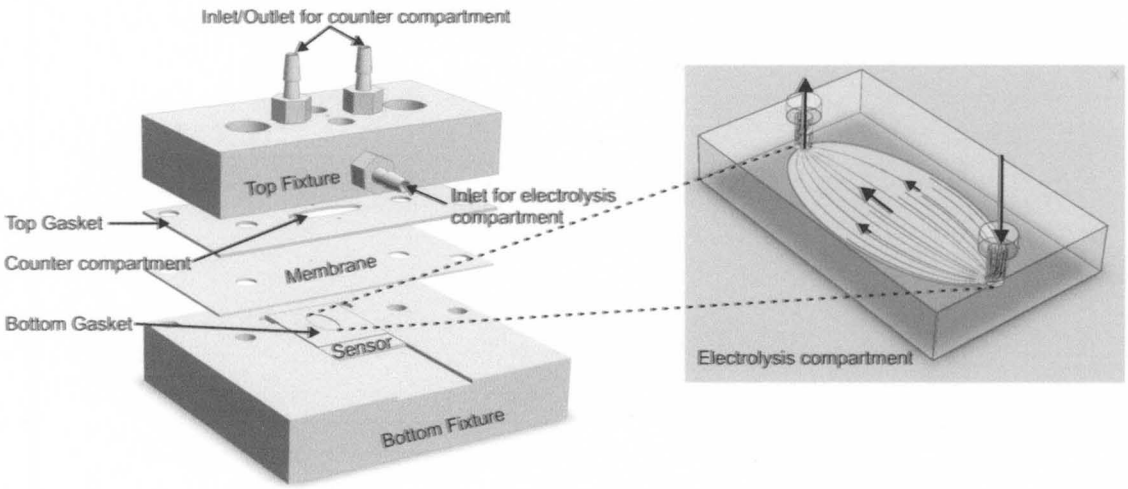

Figure 4.2 Schematic view of the flow cell assembly. Inset shows isometric view of simulated laminar flow inside electrolysis compartment (8 mm x 4 mm x .08 mm).

gasket and placing this gasket piece on top of the chip in the alignment trench. To isolate the working and counter electrode chambers, a semi-porous (200 dalton) membrane (SelRO MPF-34, Koch Membrane System, Inc., Wilmington, MA) was placed over this bottom gasket layer. The volume and shape of the upper counter electrode chamber was defined by yet another silicone rubber gasket layer. To complete the three-electrode cell, a large surface-area gold wire counter electrode was inserted into the upper compartment through the top Lexan piece. The top and bottom sections were attached together by screws which facilitated reproducible alignment and could be tightened sufficiently to prevent leakage of solution from the cell compartment. Since knowledge of the precise volume of the working electrode chamber was required to carry out the intended coulometry experiments, membranes and gaskets were precision laser cut. In most of the coulometry experiments described below, the gaskets were cut so that the resulting sample volume of the working electrode chamber was calculated to be 2.2 μL (maximum range 2.15-2.25 μL). Average geometrical dimensions obtained by profilometric measurements on the cell assembly were used to calculate the cell volume.

4.2.3. Instrumentation

Pulsed potential silver depositions were carried out with a 5MHz function generator (BK Precision 4011A), a multimeter (Agilent 34410A), and a digital oscilloscope (Rigol DS1052E). Electrochemical experiments were carried out using either a BASi epsilon potentiostat (Bioanalytical Systems, West Lafayette, IN) or a custom potentiostat designed in-house. The latter system, which utilized a LabVIEW (National Instruments, Austin, TX) interface designed to operate in one of many interrogation modes

(coulometry, amperometry, potentiometry, cyclic voltammetry, etc.) for maximum flexibility in the field, was of interest because of our final goal of creating a field-deployable, automated detection system. All voltammetric and coulometric experiments used a three-electrode configuration with Au working, Ag/AgCl pseudo-reference, and Au wire counter electrodes. Analyte solutions for the electrolysis compartment and electrolyte solutions (0.1M KNO_3) for the counter compartment solutions were introduced to the custom flow cell with a syringe.

4.3. Results and Discussion:

4.3.1. Design Considerations

The specific cell design employed for this study was decided upon after considering various properties that were viewed as especially important in a prototype sensor that might be used for calibration-free analysis operations in the field. A critical characteristic for any viable coulometry measurement is, of course, that the cell volume is fixed. Further, it is necessary that this volume be readily determinable either by calculation from known cell dimensions or by initial calibration. A second critical issue is that the electrolysis process of interest needs to be carried out to completion within a reasonable/acceptable time frame. These two considerations led us to choose a thin-layer (< 100 μm) cell design in which a large surface area working electrode would occupy the bottom surface of the coulometry compartment. Thus, the time required for complete electrolysis would depend solely on the analyte diffusion time across the narrow layer of solution above it. The time required for exhaustive electrolysis could be estimated from

the average diffusion distance given by $(2Dt)^{1/2}$ where D represents the diffusion coefficient (cm^2/sec) and t the time (sec). [84]

Beyond this, the system should be comprised of a flow cell which enables convenient replacement of the sample solution without manual dismantling of the cell. Additionally, the working electrodes ought to be isolated in a separate chamber in order to avoid possible interference from redox reactions occurring at the counter electrode. Finally, the microfabricated sensor chip itself should be able to be switched or replaced easily to allow different chips and electrode designs to be tested and compared.

After evaluating several different configurations in the early stages of this study, we settled on a single-gasket design with a 4 mm x 8 mm elliptical hole (i.e., cell) that covered the same area as the electrode pattern on the microfabricated chip. This elliptical shape was chosen in order to promote laminar flow of solution and complete clearing of the cell by eliminating corner areas where air bubbles and stagnant pools of sample might collect. The height of the alignment trench was chosen so that after assembly the cell thickness was 80 μm. With the compression needed to avoid leakage, the chip gasket creates a calculated nominal cell volume of 2.2 μL.

Microfabrication allows for the production of an essentially limitless number of electrode designs. In this work, the two specific electrode structures shown in Figure 4.1 were employed. In the first, the chip contained only a single large working electrode (W1) that covered nearly the entire bottom side of the electrolysis compartment along with a pseudo-reference electrode (R1) embedded as a narrow strip spanning the middle of W1. In the second, the chip contained five independent working electrodes (W1-W5) arranged in a spiral pattern. This latter design was selected because it allowed us both to

simulate a realistic sensing situation where the availability of several electrodes might be valuable and to select different electrode sizes and locations to obtain potentially useful information concerning the operation of the electrolysis cell. In all cases, for ease of fabrication, the material chosen for the surfaces of the microfabricated electrodes was Au. Although it will certainly be of interest in future studies to utilize additional working electrode materials, all the experiments described here used ferro-ferricyanide as a model analyte; and Au performed acceptably to carry out this redox process.

4.3.2. Chronoamperometry

Our basic experiment consisted of filling the working electrode compartment of the flow cell with an electroactive analyte species of known concentration and then stepping the applied potential to a value sufficient to cause the oxidation or reduction of this species; the electrode configuration used was normally that shown in Figure 4.1 Design (A), with a single working electrode covering essentially the entire bottom surface of the cell. Figure 4.3 shows the chronoamperograms obtained in this manner for a 250 μM ferrocyanide sample solution. The starting potential was -0.10 V, and the experiment was initiated by stepping to +0.40 V where the electro-oxidation to ferricyanide proceeded to completion. Subsequently, the applied potential was stepped back to -0.10 V in order to carry out the reverse redox process. (Note: these oxidation and reduction potentials were established earlier via cyclic voltammetry performed on an $Fe(CN)_6^{3-/4-}$ solution under the same solution/electrode conditions.) As can be seen from the Figure, each change in potential produced an immediate spike in current, anodic for the positive potential and cathodic for the negative, which decayed to near background within less than 30 s. Each

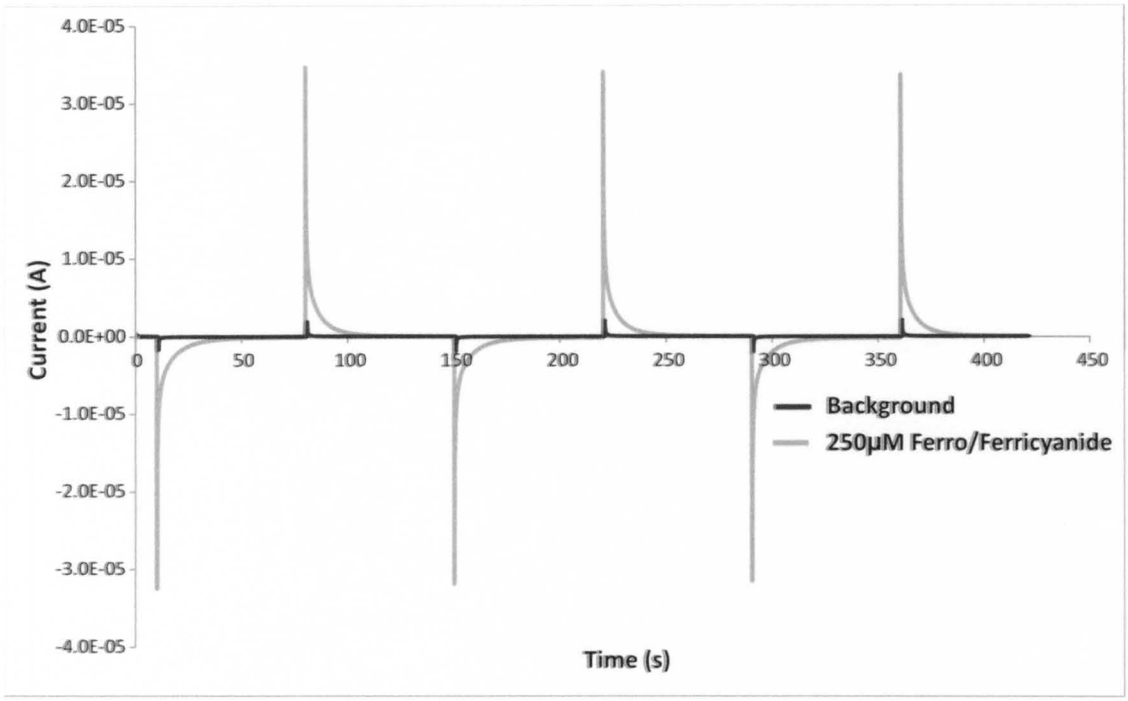

Figure 4.3 Chronoamperograms of 250 µM $K_4Fe(CN)_6$ and the 0.1 M KNO_3 background for the thin-layer cell are obtained by pulsing between +0.4V and -0.1V vs. Ag/AgCl pseudo-reference.

current spike was nearly equal in size, and the potential pulsing could be continued indefinitely with little or no change in the magnitude of the current spikes. When the identical experiment was carried out with a blank electrolyte solution, only a much smaller and more rapidly decaying current was observed, presumably due to charging current. Furthermore, when the same experiment was performed on solutions of different $Fe(CN)_6^{4-}$ concentrations, the amplitude of the current spikes was seen to track directly with this concentration, as shown in Figure 4.4. All these chronoamperometric observations were consistent with the reversible oxidation and reduction of ferro-ferricyanide in a thin-layer cell. Furthermore, the time frame of the current spikes following each potential step matched reasonably well the roughly 5-s average diffusion time estimated for the 80-μm thickness of our specific cell.

A closer look at the corresponding amperograms (as shown in the Figure 4.4 inset) revealed that, although nearly all of the electrolysis current had dissipated within 30 s after application of the electrolysis potential, there remained a very small but still significant current that was clearly above the background level and persisted throughout the entire measurement period. In fact, this long-term current decreased in magnitude only extremely slowly and persisted at an above-background level for several minutes. In addition, the magnitude of this long-lived current was directly related to the specific $Fe(CN)_6^{3-/4-}$ concentration employed.

One possibility for this observation was that there was an appreciable diffusion of $Fe(CN)_6^{3-/4-}$ analyte from the channels used to allow flow of the sample solution into and out of the electrolysis chamber. In our device, these consisted of pinhole-sized (500-μm diameter) openings which had been laser-cut through the membrane and gasket layers

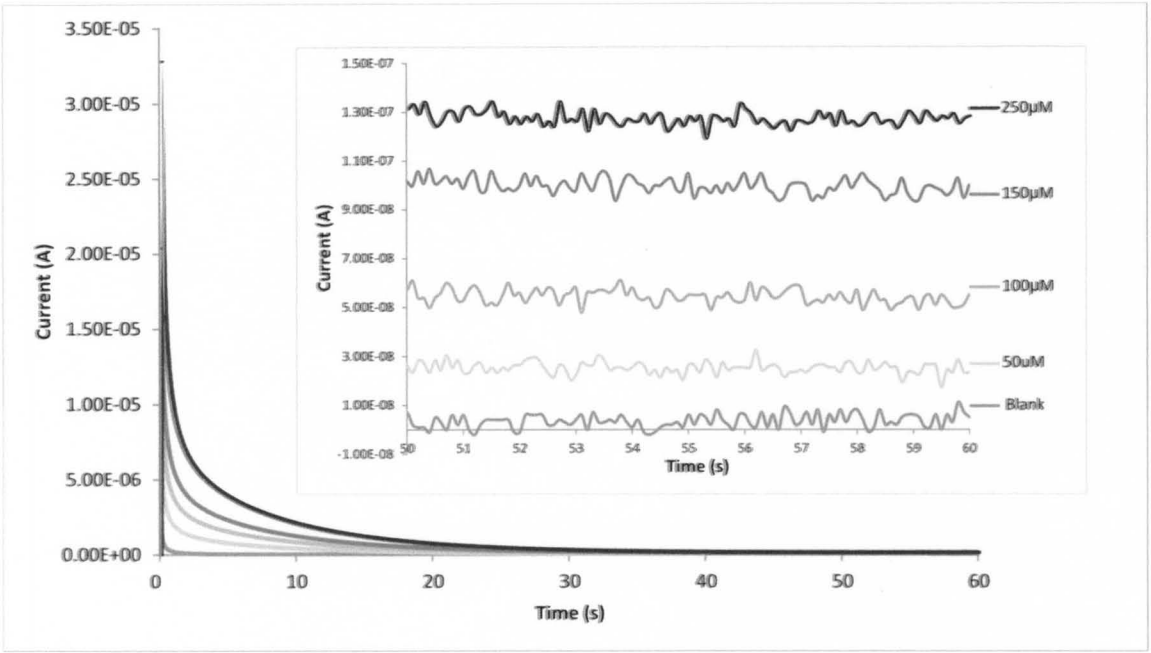

Figure 4.4 Current time curves obtained for the thin-layer cell at 0.4V vs. Ag/AgCl pseudo-reference for the background (0.1 M KNO_3), 50 µM, 100 µM, 150 µM and 250 µM $K_4Fe(CN)_6$ in 0.1 M KNO_3. A magnification of the ending current for the last 10 seconds is depicted in the inset.

used to isolate the top and bottom cell compartments. These channels remained open to the electrolysis cell and contained sample solution throughout the analysis. Complications arising from this condition have been reported in earlier thin-layer spectroelectrochemistry experiments [94] where it was shown that accurate coulometry depended on properly restricting inlet and outlet dimensions. In order to investigate this possibility, we compared the experimental i-t curve obtained for electrolysis of 100 μM $Fe(CN)_6^{4-}$ ($Conc_0$) with a calculated model of unrestricted linear diffusion (i.e., the Cottrell equation (COT(t))) and a model for a thin-layer cell (il(t)) of 80 μm thickness (len).[84]

$$COT(t) := \frac{n \cdot FC \cdot Area \cdot (D_0)^{\frac{1}{2}} \cdot Conc_0}{\pi^{\frac{1}{2}} \cdot t^{\frac{1}{2}}} \qquad (4.1)$$

$$il(t) := \frac{4 \cdot n \cdot FC \cdot Area \cdot D_0 \cdot Conc_0}{len} \cdot \sum_{m=1}^{200} e^{\left[\frac{-(2 \cdot m-1)^2 \cdot \pi^2 \cdot D_0 \cdot t}{len^2}\right]} \qquad (4.2)$$

For these calculations, a diffusion coefficient (D_0) of 6.67 x 10^{-6} cm^2/sec and faradays constant (FC) of 96485.3399 C/mol of were employed for the one electron (n) oxidation process. Direct comparison to the Cottrell and thin-layer models shows that the experimental results are intermediate in nature (Figure 4.5A). At short times, where the main contributor to the current is oxidation of the $Fe(CN)_6^{4-}$ present initially in the cell, the signal closely matches the initial rapid decay calculated for an ideal thin-layer cell. However, after 3-4 s, the presence of a more slowly decreasing component is evident. We

suspect that this longer-lived current, which is present throughout the 60-s measurement period but is always well below the predicted semi-infinite diffusion conditions assumed in the Cottrell analysis, is due at least in large part to diffusional leakage of $Fe(CN)_6^{4-}$ into the cell from its inlet and outlet channels. Classic Cottrell plots (i vs. $t^{-1/2}$) (Figure 4.5B) showed two linear regions, one at times less than five seconds, corresponding to diffusion in the volume of the thin-layer cell, and the other at longer times due, presumably, to diffusion from the inlet and outlet channels. The initial magnitude and slope of the experimental data both deviate from the Cottrell/thin-layer theoretical values due to limitations in data acquisition such as electronic transient response characteristics and noise filtering circuitry.

Regardless of the specific explanation for the extra current in the greater than 5 second regime, it seems clear that our electrolysis cell is not behaving exactly as an ideal thin-layer device, and we believe that a major contributor to this deviation is the relatively slow diffusion of analyte into the cell from the sample inlet and output channels. In the next flow cell design, it will be important to avoid, or at least minimize, this issue by decreasing the size of these channels. A distinct strength of the microfabrication approach to instrument construction is the number and variety of design changes that can be made with μm channel dimensions. Even complex designs can be executed with a high degree of fidelity.

4.3.3. Coulometry

The specific goal of this work was to evaluate exactly how well the microfabricated cell system behaved coulometrically. Therefore, the i-t data shown in Figure 4.4 for different

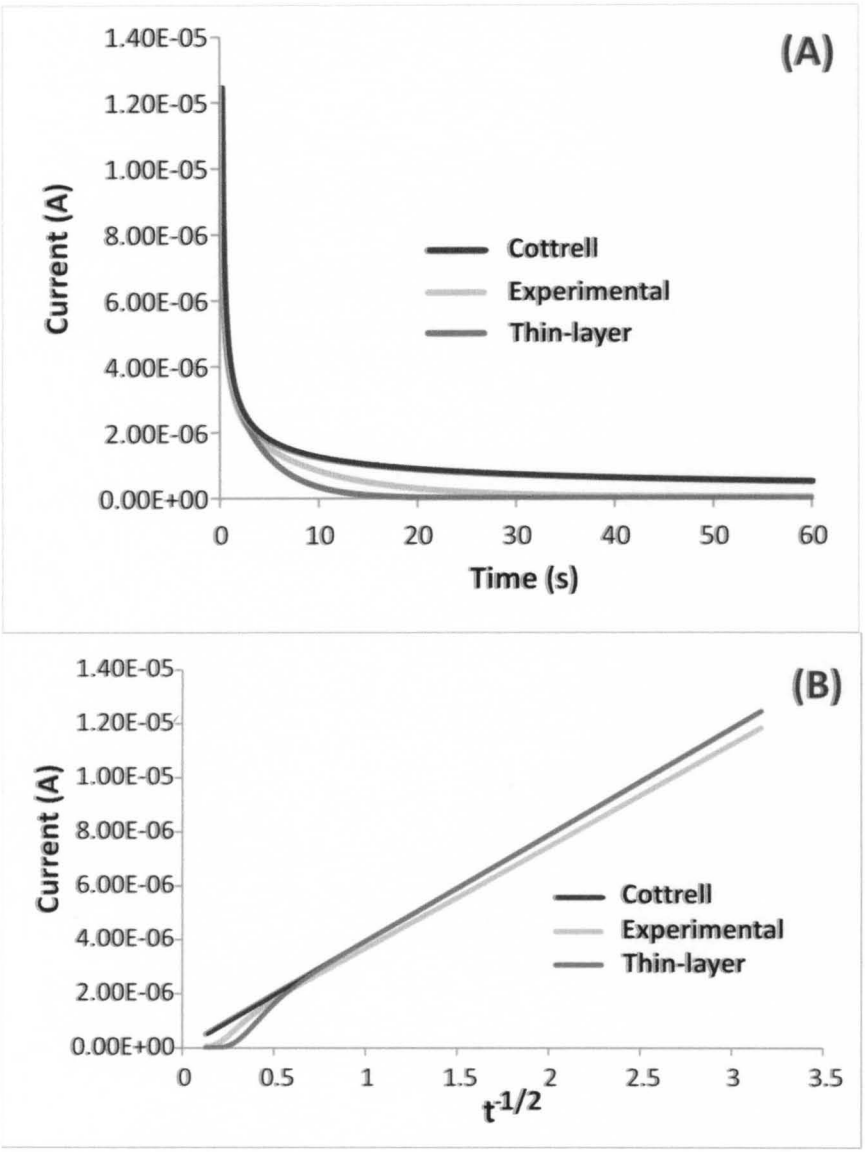

Figure 4.5 Current time plots (A) for calculated unrestricted linear diffusion (Cottrell), experimental data (for the oxidation of 100 μM $K_4Fe(CN)_6$), and a thin-layer cell. The corresponding Cottrell plots are depicted in (B).

$Fe(CN)_6^{4-}$ concentrations were integrated to produce the corresponding q-t results shown in Figure 4.6. Again, the results obtained were qualitatively as expected. The initial rapid increase in charge, corresponding to the electrolysis of the primary sample, was largely completed and the cumulative charge leveled off within 20-30 s. Further, the charge tracked the $Fe(CN)_6^{4-}$ concentration closely over a very wide range - 50 μM to at least 10,000 μM in this set of experiments.

However, detailed inspection of the Figure confirms that the charge did not actually reach a constant value even at long times but rather continued to increase slowly at a steady rate. This can be most easily seen for the q-t curves generated for the higher $Fe(CN)_6^{4-}$ concentrations; but, as shown by the numerical data in Table 4.2, this phenomenon occurred to the same extent for all concentrations. Of course, in view of the fact that the electrolysis current did not decay to the background level within the time frame of the experiment, the accumulated charge must continue to increase slowly as well. The Table also shows the total charge calculated from Faraday's law for each concentration for the 2.2 μL volume of the cell compartment. In every case, these target values were consistently reached within 10-15 s of the start of the electrolysis. This time frame was the same for every concentration used and also for both the $Fe(CN)_6^{3-/4-}$ oxidation and reduction processes.

One of the most attractive features of the coulometric measurement approach for applications involving remote or unattended monitoring experiments should be its reliability over time and its freedom from many specific operational variables. With thisin mind, we examined the performance of our device over a 6-7 week period. Results obtained with the same microfabricated chip for 250-μM $Fe(CN)_6^{4-}$ over this period are

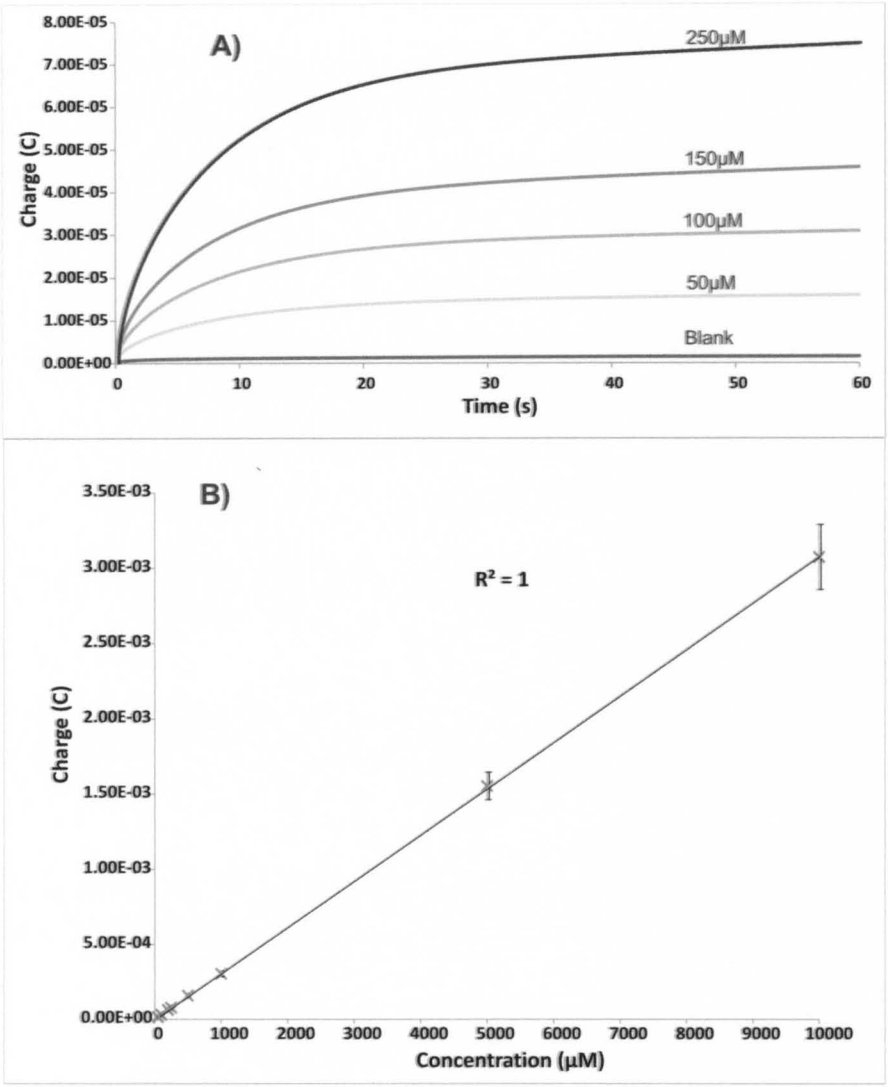

Figure 5.6 Charge time curves (A) for the background (0.1 M KNO_3), 50 µM, 100 µM, 150 µM and 250 µM $K_4Fe(CN)_6$ in 0.1 M KNO_3. Calibration curve (B) is generated from 60 seconds electrolysis data which were obtained over three different days for 50/100/200/250/500/1000/5000 and 10000 µM $K_4Fe(CN)_6$ in 0.1 M KNO_3 where n=9 for each concentration.

Reductions	**Expected Charge (μC)**	**Charge after 10s**	**Charge after 30s**	**Charge after 60s**
50μM (n=4)	10.61	9.71 (+/- 0.47)	12.56 (+/- 0.72)	13.50 (+/- 1.19)
100μM (n=4)	21.23	20.33 (+/- 0.54)	26.50 (+/- 0.58)	28.28 (+/- 0.66)
150μM (n=4)	31.84	30.78 (+/- 0.99)	40.40 (+/- 1.54)	42.88 (+/- 1.23)
250μM (n=4)	53.07	51.30 (+/- 2.41)	67.37 (+/- 4.38)	71.30 (+/- 4.58)
Oxidations	**Expected Charge (μC)**	**Charge after 10s**	**Charge after 30s**	**Charge after 60s**
50μM (n=5)	10.61	9.95 (+/- 0.89)	13.45 (+/- 1.16)	14.68 (+/- 1.50)
100μM (n=5)	21.23	20.57 (+/- 1.10)	27.92 (+/- 1.61)	30.3 (+/- 2.09)
150μM (n=3)	31.84	31.25 (+/- 0.71)	42.31 (+/- 1.92)	46.47 (+/- 2.49)
200μM (n=2)	42.45	41.51 (+/- 1.79)	56.46 (+/- 1.68)	60.53 (+/- 1.82)
250μM (n=5)	53.07	51.97 (+/- 0.58)	69.88 (+/- 1.29)	75.32 (+/- 1.87)

Table 4.2 Charge responses for the reduction/oxidation of ferri-/ferrocyanide at different concentrations and times. Data is reported along with the standard deviation (*n* represents the number of different days).

shown in Figure 4.7. The data shown for seven typical sets of runs spanning this length of time gave a relative standard deviation (RSD) of only 5.5%. During the course of the testing period, nearly 500 individual electrolysis experiments were conducted on this chip; and the entire cell was assembled and disassembled numerous times. In addition, no special cleaning or treatment procedures beyond occasional rinsing with water and ethanol were applied to the electrodes. There was no deterioration of the device, and presumably the evaluation could have been extended to a longer testing period if we had so desired. The variability between different microfabricated chips (RSD = 6.3%; n = 3) was essentially the same as seen above for different sets of experiments carried out on the same chip.

All of the amperometry and coulometry results described so far involved the use of the microfabricated chip with the simple electrode configuration shown in Figure 4.1 design (A). Beyond this, we chose to carry out some additional experiments with a chip with the more complicated electrode pattern shown in Figure 4.1 design (B). Initially, this arrangement, containing six independent spiral-shaped finger electrodes, was designed to demonstrate the capability of incorporating several redundant working electrodes in the same device. However, it also proved informative with respect to the device's coulometric operation as well. In particular, the electrode area could be minimized (and the analyte diffusion distances maximized) by using only a single finger electrode to carry out the electrolysis. Alternatively, an increasing number of electrodes could be connected together so as to systematically increase the working electrode area, thereby shorting the diffusion distance between individual electrodes and gradually approximating the single large electrode model.

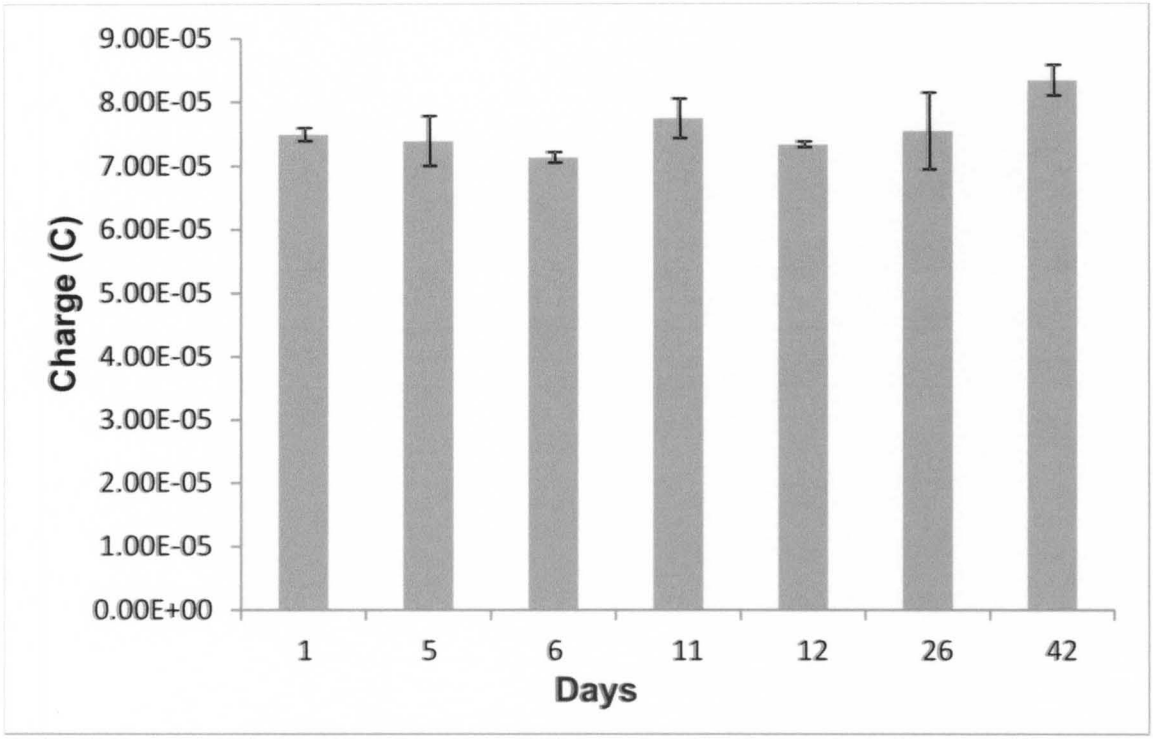

Figure 4.7 Coulometric responses obtained from one chip over a period of 42 days at a 250 μM $K_4Fe(CN)_6$ in 0.1 M KNO_3. The total charge obtained after 60 seconds is background corrected and reported along with the standard deviation where n=3.

Shown in Figure 4.8 (traces a-e) are the results of coulometry experiments when one to five finger electrodes were employed to carry out the $Fe(CN)_6^{4-}$ reduction. Shown for comparison in trace f is a q-t curve that was obtained when a single large working electrode (as in Figure 4.1A) was used. Clearly, when a single finger electrode (trace a) was employed the charge accumulated much more slowly and was less than half the total seen for the large electrode after a one-minute electrolysis. In fact, even when the electrolysis was allowed to proceed for 5 minutes, the charge with the single finger electrode remained well below that seen for the large electrode. As the number of finger electrodes linked together was increased, the rate of charge build-up increased as well. But only when all five fingers were employed simultaneously (see trace e) was the charge able to catch up with that seen for the large electrode within the 60-second time frame. Even in this instance, the $Fe(CN)_6^{4-}$ electrolysis occurred at a somewhat slower rate initially due to the smaller electrode coverage and the resulting larger diffusion distance still in effect. When evaluating the specific layouts for the five different electrode arrangements, it becomes clear that the maximum diffusion distance is no longer the cell height of 80 μm. Using the average diffusion distance calculation, the time required to complete electrolysis should increase by a factor of 1.25, 6.25, 14, 25, and 56 for the five, four, three, two and one electrode arrangements, respectively, when compared to the large electrode. By decreasing the number of electrodes, measurement of the Faradaic current may be enhanced through a reduction of the background current, with an associated lowered detection limit. However, the practicality of this approach should be contrasted with the increased time necessary to complete the electrolysis for increased diffusion distances.

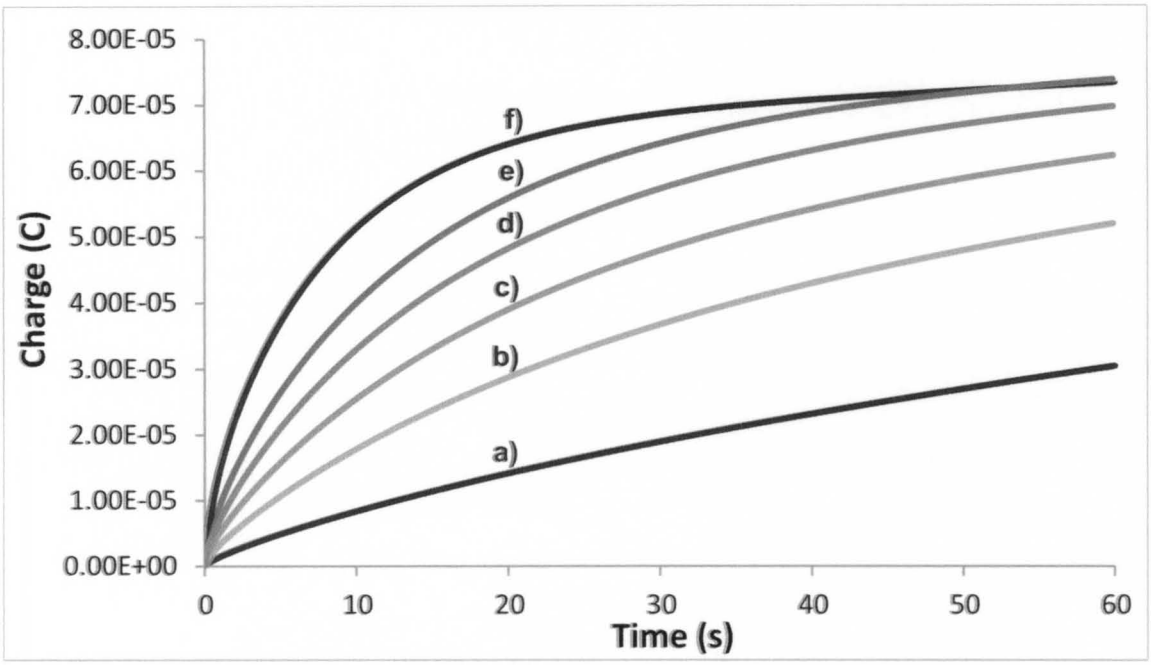

Figure 4.8 Background corrected charge time curves for a design (B) sensor where the charge for the oxidation of 250 μM $K_4Fe(CN)_6$ was obtained for one (a)), two (b)), three (c)), four (d)), and five (e)) connected electrodes. Trace (f) represents the charge for a design (A) chip at the same $K_4Fe(CN)_6$ concentration.

These results show that, although it is certainly possible to include in one chip multiple independent electrodes that might be useful in various applications, the particular electrode arrangement in Figure 4.1B seems not to be the ideal one for carrying out rapid coulometric measurements. However, it is apparent that creation and operation of a complex microfabricated electrode scheme is readily achievable. Beyond this, the results in Figure 4.8 serve to demonstrate another likely advantage of the coulometric approach for remote monitoring applications – namely, a substantial freedom from partial fouling or de-activation of the electrode surface. In conventional amperometric or voltammetric approaches, the critical quantity measured is the current, whose magnitude is directly tied to electrode area. Thus, dependable performance with real samples over an extended period of time often requires periodic restoration of the working electrode surface. In the laboratory, this can be accomplished by manual, chemical, and electrochemical procedures, all of which would be troublesome, if not impossible, without extensive operator interactions. Coulometry, on the other hand, still offers the possibility of accurate and reproducible results for a partially passivated electrode surface by simply allowing more time for the electrolysis process to reach completion. For example, for curve e in Figure 4.8 where the area of all the connected finger electrodes is only 40.5% of that of the large single electrode used for curve f, the measured charge has already caught up within less than one minute.

4.4. Conclusions:

This study has demonstrated many of the potential advantages of developing microfabricated coulometric devices for remote monitoring applications. By use of low-

volume thin-layer cells, exhaustive electrolysis can be carried out on the time scale of a minute or less and can be repeated for weeks with highly reproducible results. Most important, reliable quantitative results can be obtained over a very wide concentration range in a calibration-free manner that offers the possibility of long-term unattended operation. A second-generation device that allows the cell volume to be defined absolutely and, in particular, minimizes analyte entry by diffusion from the inlet and outlet channels is presently under development in our laboratory, and we hope to report on this device and its performance in realistic applications shortly.

CHAPTER V

EXHAUSTIVE COULOMETRY FOR THE DETECTION OF FREE CHLORINE IN DRINKING WATER

5.1. Introduction:

Chlorine is the most commonly used disinfecting agent for drinking water. It was first used to disinfect municipal wastewater in 1908 and has since been utilized as a disinfectant for public health protection.[31] At present, the majority of water companies, such as Hardin County Water District 2, disinfect the water by introducing chlorine gas. In water, chlorine gas hydrolyzes to form hypochlorous acid (HOCl) and hypochlorite anions (OCl^-).[95] Both forms (HOCl/OCl^-) are referred to as "free chlorine" and are considered strong oxidizing agents capable of destroying microorganisms.[31, 50]

$$Cl_2 + H_2O \rightleftharpoons HOCl + Cl^- + H^+ \qquad (5.1)$$

$$HOCl \rightleftharpoons H^+ + OCl^- \qquad pK_a = 7.5 \qquad (5.2)$$

During water processing, water companies must add enough disinfectant to the water to ensure complete destruction of bacteria and various microorganisms. Thereafter, the water is tested for residual chorine levels to guarantee consumers safe drinking water. The EPA's regulation for free chlorine levels in drinking water is 1 – 4 ppm.[33-34] A free chlorine level above 4 ppm are toxic and is considered to be a secondary water contaminate ion, while free chlorine levels below 1 ppm are too low to provide adequate germicidal strength and water containing such levels is considered unsafe for public

consumption. The challenge presented to water companies is to maintain the safe free chlorine levels throughout the entire water distribution system. For 800 miles of pipeline (referring to the Hardin County Water System, for example), drinking water can remain up to one week in the system before it reaches the consumer. Although the time that the water remains in the distribution system depends on seasonal demand fluctuations, water companies use frequent flushing to avoid providing water to the customer which has remained in the system for more than one week. This practice is performed in an attempt to maintain adequate residual chlorine levels. However, water companies usually monitor free chlorine levels only at water storage towers and by monthly grab sampling. In order to ensure public health and safety, it is apparent that on-line monitoring of free chlorine levels is highly important. Not only would on-line sensors better monitor the narrow range of free chlorine in drinking water, but they also would be able to function as early warning systems for unusual water quality resulting from intentional or unintentional water contamination.

Currently, the standard method for determination of free chlorine in drinking water is a spectrophotometric technique which uses N,N-diethyl-p-phenylenediamine.[50] Water companies are utilizing commercially available systems (e.g., Hach CL-17) to monitor the levels of free chlorine. Although these instruments are proven to be very reliable and offer detection limits as low as 35 ppb,[96] they require monthly maintenance and the addition of reagents. Electrochemical detection of free chlorine presents a possible reagent-free solution, and various groups have developed electrochemical chlorine sensors. Many of these sensors detect free chlorine via the reduction of hypochlorite on gold or platinum working electrodes,[50, 97-99] but a few investigations reported anodic

detection[100-102] by utilizing, for instance, boron doped diamond electrodes.[101] In general, these sensors showed good linearity for hypochlorite concentrations down to 0.3 ppm,[97] but as with all amperometric measurements, calibration curves are required for analyte concentration determination.[50, 97-99]

A common issue faced by electrochemical sensors that operate under reducing conditions to detect analytes in aqueous environments is possible interference due to oxygen reduction. Fortunately, earlier amperometric studies have shown that hypochlorite can be successfully reduced on gold electrodes without the interference of oxygen reduction[50] by a two electron transfer process:[51]

$$OCl^- + H_2O + 2e^- \rightleftharpoons Cl^- + 2OH^- \qquad E^0 = +0.89V \quad (5.3)$$

In the previous chapter, we reported the development of a coulometric cell that can be employed for exhaustive coulometry applications without the necessity for calibration. Although the first generation cell had limitations controlling analyte diffusion coming from the inlet/outlet, we should nevertheless be able to detect hypochlorite using this coulometric system. In principle, when performing exhaustive coulometry, absolute quantitation of hypochlorite should be possible; and preliminary results of this approach, along with challenges encountered, are described here.

5.2. Experimental:

5.2.1. Reagents

Potassium phosphate monobasic, sodium phosphate dibasic, potassium chloride, and soluble starch were purchased from Fisher Scientific (Pittsburg, PA) and potassium iodide, sodium hypochlorite (10-15% available chlorine) were obtained from Sigma-

Aldrich (Milwaukee, WI) and sulfuric acid from VWR International (Batavia, IL) at the highest purity and were used without further purification. All solutions were always freshly prepared using deionized (DI) water. Analyte solutions contained 100 mM KCl and 50 mM PBS (pH 7.5, 8 and 9) and had to be prepared daily due to the instability of hypochlorite. After preparations, solutions were used within a 15 – 20 minute time frame. The concentration of hypochlorite stock solutions was verified via iodometric titrations on a weekly basis.[103]

5.2.2. Instrumentation

Electrochemical experiments were carried out by using a BASi epsilon potentiostat (Bioanalytical Systems, West Lafayette, IN). For bulk solution experiments a 2 mm diameter standard gold disk working, Ag/AgCl (3 M NaCl) reference and Pt wire counter electrode were used unless stated otherwise. Voltammetric and amperometric experiments conducted in the custom flow cell were always performed by employing a three electrode configuration with Au working, Ag/AgCl pseudo-reference and Au wire counter electrode. Solutions for the electrolysis were introduced to the electrolysis and counter compartment of the custom flow cell via a syringe. For exhaustive electrolysis applications the same cell configuration and a two electrode microchip (Design A) was always utilized and had been already described in Chapter IV section 4.2.2.1. and 4.2.2.2..

5.3. Results and Discussion:

When utilizing sensors for remote sensing, many variables such as changes in temperature, pH and ionic strength, the presence of interfering species, electrode fouling, and reference electrode drift cannot be easily controlled. Thus, many sensors that function well under ideal laboratory conditions often fail to perform acceptably in environmental settings, and therefore require frequent calibrations. As discussed in Chapter IV, exhaustive coulometry shows promise for remote sensing to minimize frequent maintenance and calibration. Hence, in this Chapter, we will apply the Chapter IV approach to the practical problem of free chlorine determination in drinking water.

5.3.1. Cyclic Voltammetry

Prior to amperometric/coulometric experiments, cyclic voltammetry was employed to determine the approximate potential to reduce OCl^- effectively. While performing CV, two cycles were always recorded using a three-electrode cell configuration, with a standard Au disk working, a Ag/AgCl (3 M NaCl) reference, and a Pt wire counter electrode. To correctly assign the peak origins, a non-dearated blank solution containing 50 mM PBS (pH 8), 0.1M KCl was used. The blank solution had one reduction wave with E_p of -290 mV. This is assigned to the reduction of O_2 because the wave disappeared after 15 minutes solution dearation. CVs of the analyte solution (0.5 mM hypochlorite in 50 mM PBS (pH 8), 0.1M KCl) showed clearly two reduction waves at 310 mV and at -290 mV(displayed in Figure 5.1). The irreversible reduction peak at 310 mV is ascribed to the reduction of OCl^-. Furthermore, the reduction potential for OCl^- at 310 mV matched the values reported earlier by Switzer et al.[51] This suggested that hypochlorite

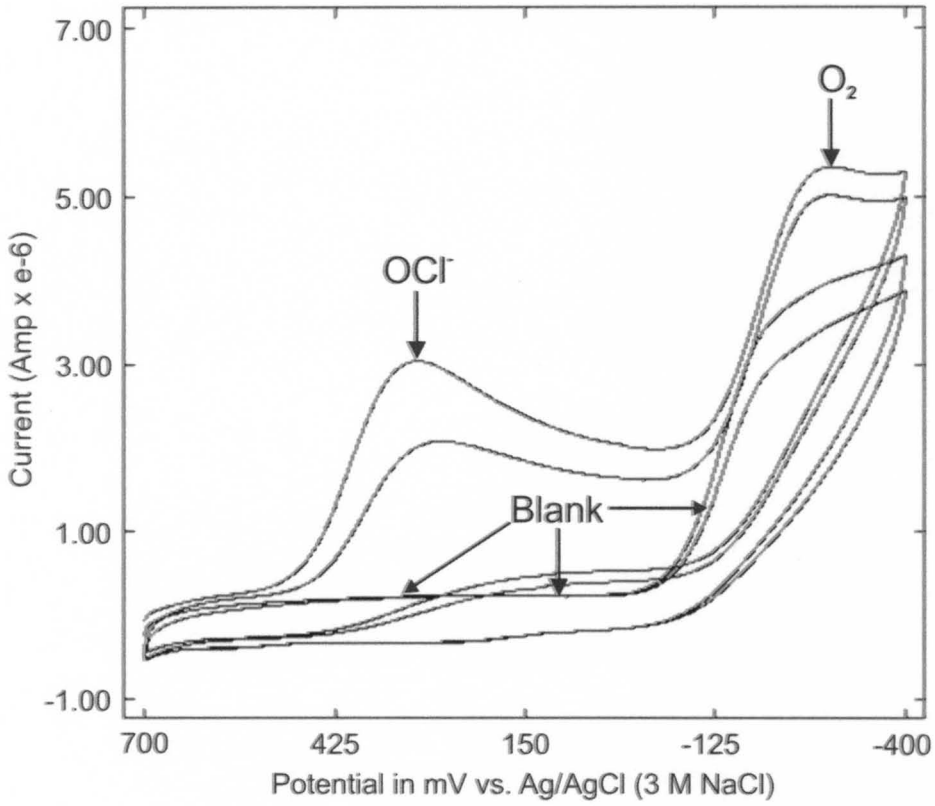

Figure 5.1 Cyclic voltammograms of 0.5 mM hypochlorite in 50 mM PBS (pH 8), 0.1M KCl at a Au disk electrode vs. Ag/AgCl (3 M NaCl) at a scan rate of 50 mV/s.

electrolysis in the coulometric system could be accomplished by using -150 mV vs a Ag/AgCl pseudo-reference electrode.

5.3.2. Amperometry/Coulometry

Initial amperometric hypochlorite experiments were performed in the same manner as described in Chapter IV. The first potential (pre-electrolysis potential) was applied for 10 seconds, and the experiment was initiated by stepping to the second potential (electrolysis potential) for 60 seconds. When using the microfabricated coulometric sensor system, all voltammetric and amperometric experiments were performed by utilizing a Ag/AgCl pseudo-reference. Using a Ag/AgCl pseudo-reference electrode in place of a standard Ag/AgCl (3 M NaCl) reference electrode shifts the potential window approximately 200 mV in the negative direction. Hence, the potentials necessary for the experiment were found to be 500 mV (pre-electrolysis potential) and -150 mV (electrolysis potential). Solutions containing OCl^- concentrations ranging from 1 ppm – 10 ppm (19.4 -194 μM) in 0.05M PBS (pH=8) were prepared and used immediately for the exhaustive coulometry experiment. Charges obtained by integrating the current over 60 sec tracked the hypochlorite concentration closely over the 1 ppm – 10 ppm range. But a closer analysis revealed that the expected/calculated charge of the hypochlorite reduction, considering a two electron reduction process, did not match the charge expected for the given concentration. In fact, in these initial experiments, the electrolysis only yielded approximately one tenth of the total charge. Therefore, more investigations were necessary in order to explain the low charge results.

OCl^-/HOCl containing solutions tend to disproportionate over time, depending on conditions such as temperature, pH, nature of the buffer system, the presence or absence of salts, and exposure to light.[95] The disproportionation of the sodium hypochlorite stock solution was taken into account by determining the hypochlorite concentration via iodometric titration prior to usage.[103] These titrations indicated that in fact the concentration of the originally 4M NaOCl stock solution had decreased to 1.43M over the 1.5 year storage time of this solution.

$$3OCl^- = 2Cl^- + ClO_3^- \qquad (5.4)$$

This also suggests that the hypochlorite solution may also contain chlorate and chloride ions. Given its standard potential, chlorate should also be reducible at a more negative potential compared to hypochlorite.[104]

$$ClO_3^- + 3H_2O + 6e^- = Cl^- + 6OH^- \qquad E^0 = +0.63 \qquad (5.5)$$

However, CV also showed no evidence of an addition reduction peak at the potentials utilized for our electrolysis.

Another possible source for the low total charge was that the OCl^- diffuses freely across the membrane, thereby diluting the concentration in the electrolysis compartment. Experiments to examine this possibility included voltammetric and amperometric detections of hypochlorite in the electrolysis compartment after filling the counter compartment with high OCl^- concentrations (up to 10 mM). The time to allow hypochlorite to diffuse through the membrane was systematically increased up to 1.5 hours after which both voltammetry and amperometry were carried out in working electrode chamber. However these experiments showed no evidence that hypochlorite was able to diffuse across the membrane, even at such high concentrations.

Further coulometric investigations showed that the length of the pre-electrolysis potential (first applied potential) influenced the amount of total charge obtained. This had not been the case for the ferri/ferrocyanide (Chapter IV) while the length of the pre-electrolysis time had no effect on the total charge obtained. But for reduction of OCl^-, the trend clearly was that, as the length of time before application of the electrolysis potential increased (1 → 10 sec), the charges seen for OCl^- reduction decreased dramatically (39.3 μC to 9.99 μC). Unfortunately, decreasing the pre-electrolysis time below one second was not possible with the BASi epsilon potentiostat. However, this should certainly be examined in future studies using the home-build potentiostat.

In light of the previous observation, it became apparent that the use of free floating working electrodes (no potential applied) during the loading stage of the electrolysis cell was not suitable for hypochlorite reductions. With this in mind, an additional potential of 500 mV (loading potential) was applied during the entire sample loading time. Applying a loading potential resulted in leaving the electrolysis cell turned on during the entire experiment time. Subsequent experiments, in which the 500 mV potential was applied during loading, increased the total amount of charge obtained substantially as shown in Table 5.1. However, even with this experimental change, the cumulative charge still remained at about 50% for that calculated system.

Current-time curves obtained under the above conditions displayed qualitative better results. When amperometric experiments were performed with solutions of different OCl^- concentrations (2, 4, and 10 ppm), the amplitude of the current spikes was seen to track directly with these concentrations, as shown in Figure 5.2 (A), and all the chronoamperometric observations were consistent with the reduction of OCl^- in a

	1sec	3sec	10sec	Calculated charge
Loading potential applied	44.9 μC	38.8 μC	26.8 μC	82.4 μC

Table 5.1. Background corrected total charges for 60 seconds of electrolysis at a concentration of 10 ppm of OCl^- in 0.05M PBS (pH=8).

thin-layer cell. Furthermore, the time frame of the current spikes following the potential step matched reasonably well the behavior seen for the ferri/ferrocyanide system described in Chapter IV. When, the i-t data shown in Figure 5.2(A) for different OCl^- concentrations were subsequently integrated to produce the corresponding q-t results shown in Figure 5.2(B), the results obtained were again qualitatively as expected, with RSDs of ca. 5% (n=3). The initial rapid increase in charge (corresponding to the electrolysis of the primary sample) was largely completed, and the cumulative charge leveled off, within 10-20 s. Further, the charge tracked the OCl^- concentration closely over the 2 – 10 ppm (38.8 -194 μM) in this set of experiments. The corresponding calibration curve is displayed in Figure 5.2(C).

So far, our microfabricated coulometric system has been shown to be able to effectively reduce hypochlorite in the target range of 1 – 10 ppm and to generate reproducible total charges at the 10 ppm level over several days. The main problem that remained was that the total charge obtained via complete electrolysis was still well below the calculated value. Two possibilities remained to be investigated: AuO_x formation and pH effect. Experiments related to each of these considerations are described in the following section.

5.3.3. Oxide formation

Hypochlorite is known to be a strong oxidizing agent, and studies have reported electrode passivation with platinum electrodes during prolonged hypochlorite exposure.[99] Therefore, the possibility that hypochlorite might oxidize the Au working electrode surface prior the electrolysis might explain the low amount of total charge obtained for

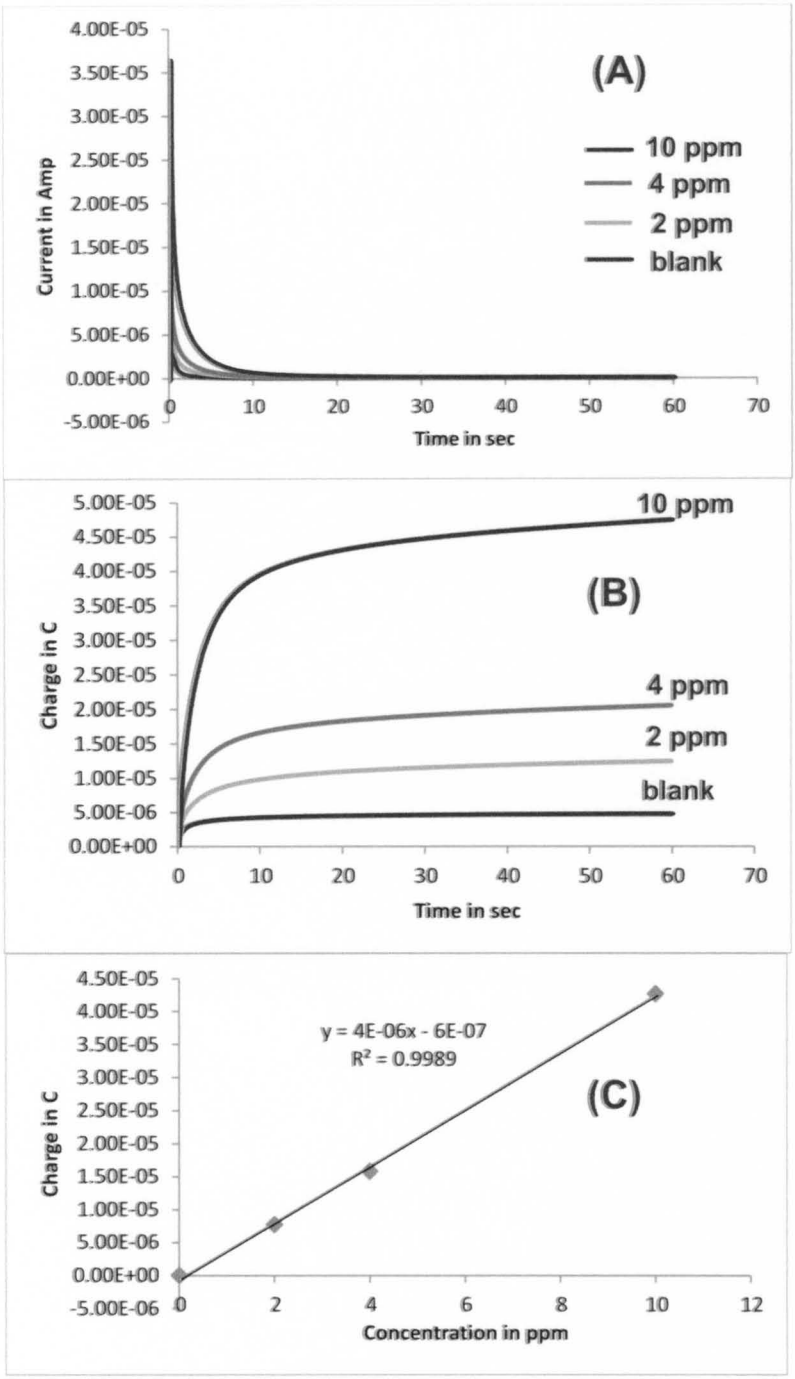

Figure 5.2. Current time curves (A) for the blank, 2 ppm, 4ppm and 10 ppm of OCl^- in 0.05M PBS (pH=8). The corresponding charge time curves are displayed in (B) along the calibration curve.

the coulometric system. In order to explore the possibility of AuO_x formation, cyclic voltammetry was employed; and experiments were conducted in an electrochemical cell using a gold disk electrode, a standard Ag/AgCl (3 M NaCl) reference electrode, and a Pt counter wire. During this study, the gold disk electrode was immersed for 30 minutes into a hypochlorite containing PBS (pH 8) solution, thereby permitting enough time for AuO_x formation at the electrode surface. Subsequently, the electrode was rinsed off with DI water, and a CV was performed in fresh PBS (pH 8) solution. The resulting CV clearly showed a reduction peak at 430 mV (Figure 5.3 peak b) in the first cycle only, suggesting the formation and the reduction of AuO_x. This wave was not present in subsequent cycles unless the electrode was again exposed to OCl^-. To show that this peak corresponds to the reduction of AuO_x, electrochemically induced AuO_x formation/reduction was carried out by cycling a clean Au electrode in PBS solution out to 1200 mV. This CV also exhibited a AuO_x reduction peak (peak a) offset only slightly in potential from the AuO_x reduction peak formed by hypochlorite exposure. In the same Figure, the dark blue trace containing peak c was overlaid to show the hypochlorite reduction potential under equivalent solution conditions. This verified that oxide and hypochlorite reduction occur at different potentials. Thereafter, time dependent CV studies showed that reduction peaks of AuO_x are apparent after 10 min of 0.5 mM OCl^- exposure time. While CV is not the most sensitive detection method, it clearly showed here that signal loss due to oxidation of Au is certainly a possibility.

Furthermore, to avoid losing hypochlorite by the oxidation of the electrode surface prior to the electrolysis a 700 mV potential was applied to the electrode during the entire hypochlorite exposure time. This strategy was tested in order to see if the applied

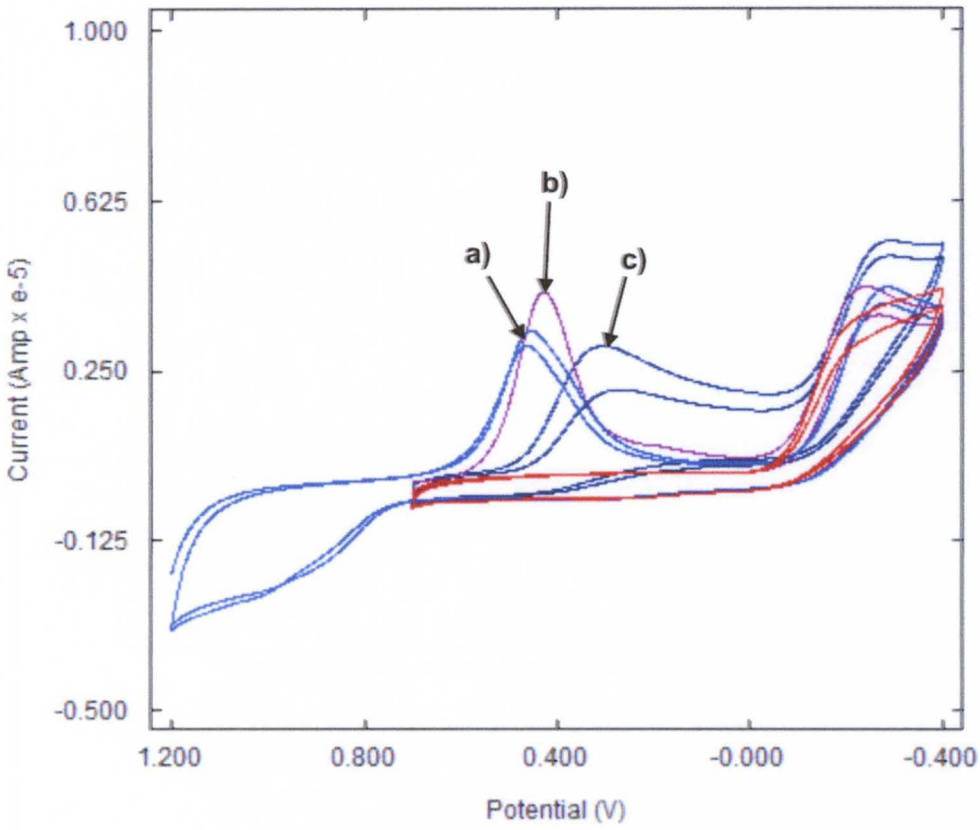

Figure 5.3 Cyclic voltammetry of electrochemical induced AuO_x reduction (peak a), AuO_x reduction formed by hypochlorite exposure (peak b), reduction of 0.5 mM OCl^- (peak c) in 0.05M PBS (pH=8) and the 0.05M PBS (pH=8) blank (red trace)

potential could eliminate AuO_x formation. Subsequent CVs in fresh PBS solutions did not reveal AuO_x reduction peaks. This observation indicated that gold oxide formation was not possible when applying a 700 mV potential during hypochlorite exposure.

5.3.4. pH effects

It is also relevant to investigate the effect of pH on the electrolysis behavior of OCl^-. The concentration ratio OCl^-/HOCl present in solution depends on the actual pH. When using pH 7.5 solutions, equal amounts of OCl^-/HOCl are present since the reported pK_a value is 7.5.[50] A depletion of OCl^-, based on Le Chatelier's principle, should shift the equilibrium in favor of OCl^-, and essentially a quantitative determination of free chlorine should be possible. Further, the reduction potential itself is also dependent on pH utilized and corresponding potential reduction shifts are expected. Therefore, pH 7.5, 8, and 9 PBS solutions containing 20 ppm free chlorine were used for both CV (Figure 5.4 (A)) and coulometric experiments (Figure 5.4 (B)). CVs were performed in the coulometric cell, in order to determine optimum reduction potentials for the OCl^- electrolysis at different pH. The corresponding OCl^- peak potentials observed for pH 7.5, 8, and 9 were 158 mV, 72 mV and -100 mV respectively; pre-electrolysis and electrolysis potentials were set for pH 7.5 and 8 for 500 mV and -150 mV, respectively. For the pH 9 solution, the electrolysis potential of -250 mV was applied to ensure sufficient overpotential. The charge (t = 60 seconds) was seen to increase with increasing pH which is also reflect by the corresponding peak current increase of the CVs. A closer look at the corresponding charge-time curves for pH 7.5 and 8 reveals the same curve shapes (electrolysis behavior) opposed to the charge curve of pH 9. The difference in the coulometric

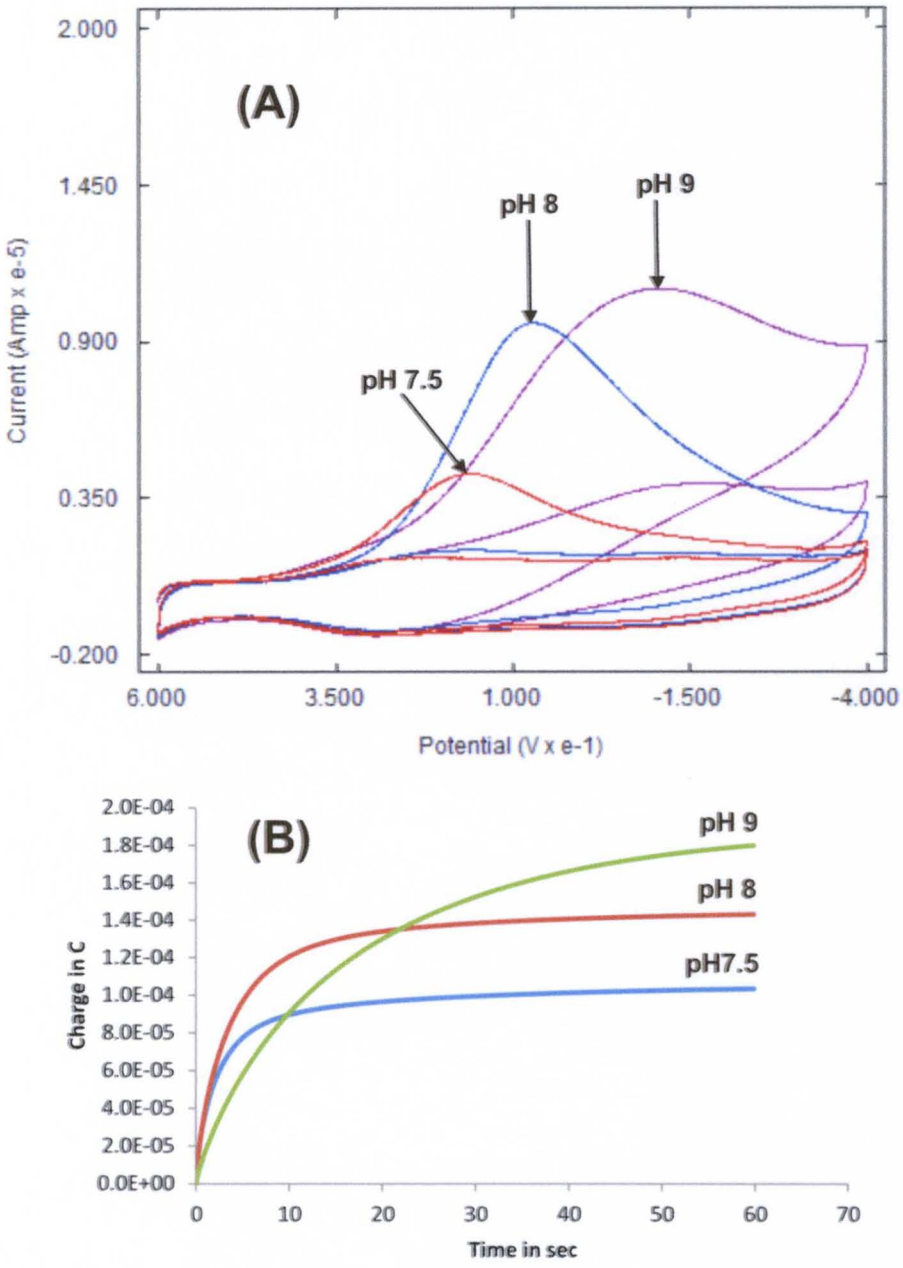

Figure 5.4 Depicting CVs (A) of 20 ppm hypochlorite in 50 mM PBS at pH 7.5, 8, and 9 utilizing the microfabricated coulometric sensor system. The corresponding charge time curves are displayed in (B).

responses could possibly be attributed to the fact that not enough overpotential was utilized for sufficient reduction of the analyte. The drawback of applying more negative potentials is the significant increase in the background current for the reduction at pH 9, probably due to the reduction of oxygen. A more detailed investigation for optimizing the reduction potential at this pH is advised in order to draw any further conclusions.

5.3.5. Drinking water

The ultimate test for the coulometric system is to conduct hypochlorite detection in actual drinking water in the 1 – 4 ppm range. Therefore, a fresh sample of drinking water from the Hardin County Water District # 2 was obtained and at the facility, the free chlorine concentration for this sample was reported as 2.45 ppm using a Hach CL-17 chlorine analyzer. The freshly obtained water sample was then brought to our laboratory and electrolyzed with the microfabricated coulometric system. Despite the problems we face with the OCl^- detection, we were able to obtain current-time and charge-time curves shown in Figure 5.5 (A) and (B) respectively. But a trickier question was background subtraction, since preparing blanks containing the same ionic strength and compositions of true unknowns is not possible. Therefore, backgrounds were collected after the OCl^- electrolysis, assuming that all of the OCl^- has been electrolyzed in the 60 second time frame. Unfortunately, this experiment was only performed once, and higher RSDs (RSD of 7.41% and 15.1% for the blank and tap water sample respectively with n=3), were obtained. However, this set of experiment clearly indicates the possibility of determining OCl^- in drinking water. Although the system at present is still not functioning to the

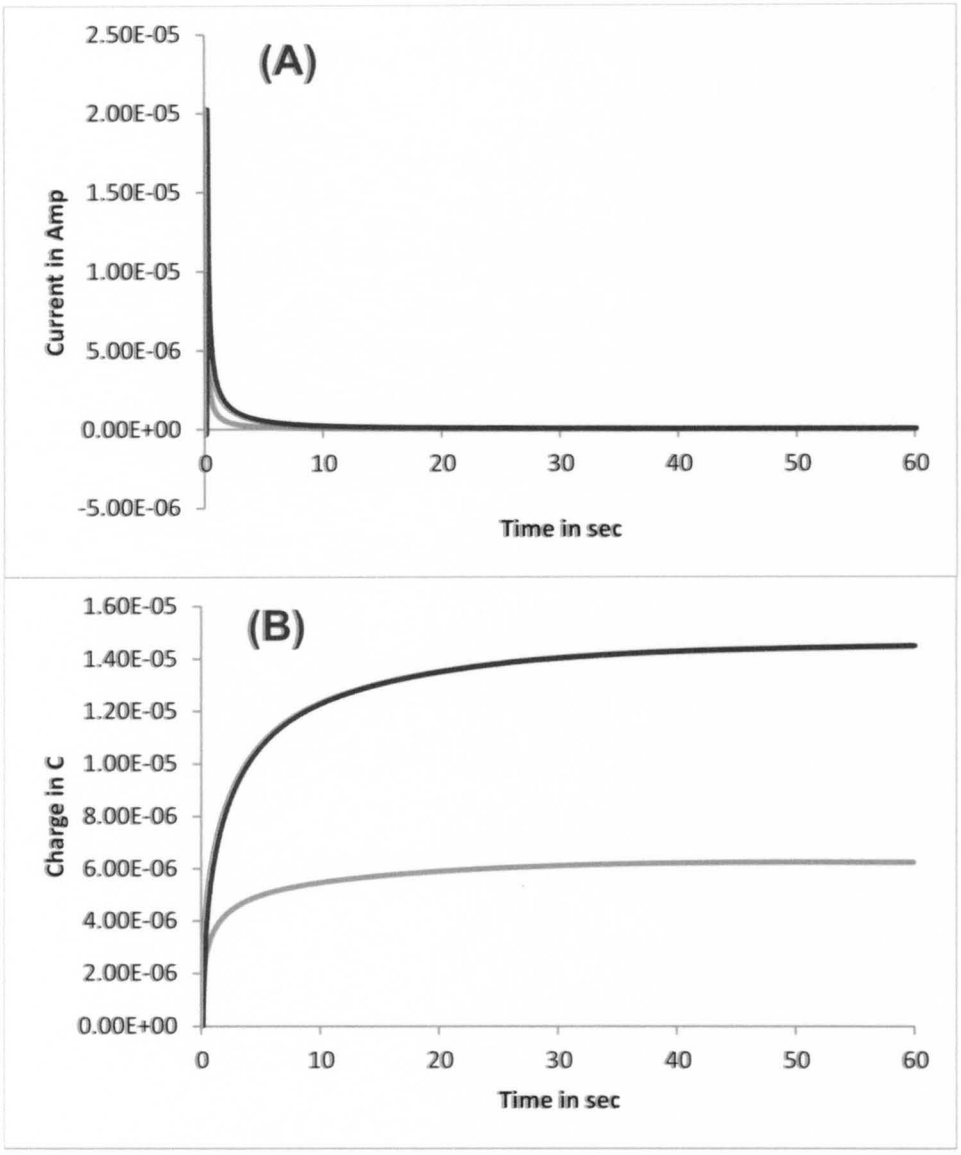

Figure 5.5 Current-time curves (A) and charge-time curves (B) for the electrolysis of free chlorine in Hardin County tap water. In both figures, the black trace represents the tape water, whereas the grey trace displays the background.

extent of providing the correct amount of expected charges, it still shows promise that we could be able to effectively use this system to determine free chlorine in drinking water.

5.4. Conclusion:

Although the present coulometric system still needs to be optimized in terms of applying the appropriate loading potentials to eliminate the formation of AuO_x at the electrode surface, preliminary experiments have already demonstrated that this system might be useful for the detection of hypochlorite in drinking water systems. Further investigations on the effect of pH, as well as a complete study utilizing a wider range of concentrations at different pH, are advised. Despite the pH effect, if the AuO_x formation on the electrode cannot be eliminated, then other electrode materials (e.g., boron doped diamond) should be considered as well. Another avenue of opportunity is the detection of monochloramine. This particular disinfectant is used in the Louisville metropolitan drinking water system. Monochloramine has less oxidizing strength and hence may aid in the problem of AuO_x formation at the electrode surface. This compound is also electroactive and its reduction possibility has been already demonstrated.[105]

CHAPTER VI

CONCLUSIONS

In Chapter II we have demonstrated that simplification of microfabrication techniques by the "stamp and stick" approach is advantageous in terms of increasing the success rate in glass microchip production to near 100%. Not only did this UV adhesive bonding technique allowed us to bond glass CE microchips effectively under room temperature conditions, it also offered other numerous practical advantages compared to the conventional thermal bonding approach. In particular, we were able to complete the entire bonding process in only 30 minutes, as opposed to several hours for the thermally bonded chips. Due to the usage of the mask aligner, alignment control of the top and bottom substrate was provided during the bonding process, resulting in perfect placement of the working electrodes at the end of the CE channel. Furthermore, the new process is more tolerable of surface imperfection and therefore does not require ultraflat glass and extensive pretreatment of the glass with sulfuric acid or piranha solution. This process also allowed recycling of the bottom and top substrates if non-uniform or faulty placement of the UV adhesive was observed prior to bonding or even after bonding. For the former case, both substrates could be easily separated by hand and cleaned with acetone before reusing them. But a long-term soak (one day) in concentrated NaOH solution was necessary for already bonded chips in order to dissolve the cross-linked adhesive. Of course, this approach is compatible with the presence of temperature-

sensitive materials or structures on the bonded substrates (although this feature was not highlighted in this study). Overall, while realizing all the advantages offered by the UV adhesive bonding approach, the analytical performance of devices prepared by this process was essentially the same as that seen for conventional thermally bonded chips.

More important, we also have made substantial progress toward the development of smart sensing device for remote monitoring applications. The specific goal of our work was to investigate simple ways in which the microfabrication approach could be used to make electrochemical sensors behave "more intelligently" and thereby improve upon device performances for long-term remote monitoring applications. Important features that were investigated to enhance a sensor's capabilities and therefore make the sensor smarter were:

1) the inclusion of redundant sensing electrodes to function either as a back up when one sensor fails or as a way of verifying questionable results,
2) the development of in situ electrode regeneration and calibration procedures,
3) the construction and utilization of a coulometric system for absolute quantitative analysis, and
4) the integration of reference and auxiliary electrodes onto the sensor platform.

In Chapter III we investigated a simple strategy, made possible by microfabrication methodologies, for improving sensor performance for on-site unattended operation. Specifically in the case of pH measurement, arrays of microfabricated Au electrodes coated with IrO_x films were shown to perform effectively for drinking water samples from municipal treatment facilities. Perhaps most important, a simple potentiostatic calibration procedure, requiring no external buffer solutions, was

shown to be highly effective both for standardizing the absolute potential response of all the individual electrodes in the array and for restoring the potential response of a single electrode over an extended period of time. This IrO_x array represented an example illustrating a simple way in which microfabrication can be employed to allow instrumentation to operate at a more "intelligent" and independent level.

In Chapter IV a microfabricated coulometric system to determine absolute analyte quantities was designed, fabricated and evaluated by using ferri/ferrocyanide as a model analyte. This study demonstrated many of the potential advantages of developing microfabricated coulometric devices for remote monitoring applications. By use of low-volume thin-layer cells, exhaustive electrolysis can be carried out on the time scale of a minute or less and can be repeated for weeks with highly reproducible results. Most important, reliable quantitative results can be obtained over a very wide concentration range in a calibration-free manner that offers the possibility of long-term unattended operation. A second-generation device that allows the cell volume to be defined absolutely and, in particular, minimizes analyte entry from the inlet and outlet channels still needs to be developed. This can be achieved by using microfabrication to define the cell height and channel dimensions using either SU-8 or polyimide as the "gasket" material. The cell height and channel dimensions can then be precisely measured using profilometry.

Chapter V applied the coulometry system, which was characterized in Chapter IV, to a more practical application by determining the hypochlorite concentration in drinking water. Although as yet unsolved challenges were encountered, preliminary experiments show promise that this system may be utilized to determine the free chlorine content in

drinking water. Even if the problems of the gold oxide formation prior electrolysis can't be resolved, other electrode materials could be considered as an alternative. Additionally, the recent trend for water companies to use monochloramine instead of hypochlorite as the disinfectant agent offers the possibility to adapt the system to this new analyte. More important, monochloramine has lower oxidizing strength and hence may minimize AuO_x formation at the electrode surface. This compound is also electroactive, and its reduction electroactivity has been already demonstrated.[105]

Although automated monitoring of pH and concentration determination via coulometry alone may be important for some applications, integration of additional sensing functions would be necessary in order to achieve a practical device suitable for general surveillance of drinking water quality. For example, inclusion of sensors for other parameters such as conductivity, redox potential, and temperature would certainly increase the available analytical information to a very useful level. Interestingly, not only do electrochemical approaches appear to be well suited for the design of sensors for all of these parameters, but also their actual construction and miniaturization seem highly amenable to conventional microfabrication techniques. Therefore, we expect that there will be rapid progress in the development of smart microfabricated sensors for routine monitoring of water quality. In addition, in view of the innumerable practical applications of electroanalysis that are already well-known, it seems likely that the approach can be extended to very many important measurement situations.

REFERENCES

1. Schwarz, M. A.; Hauser, P. C., *Lab Chip* **2001,** *1*, 1-6.
2. Tanyanyiwa, J.; Leuthardt, S.; Hauser, P. C., *Electrophoresis* **2002,** *23*, 3659-3666.
3. Sun, T.; Green, N. G.; Gawad, S.; Morgan, H., *Iet Nanobiotechnology* **2007,** *1*, 69-79.
4. Yu, J.; Liu, C.-C., *Sensors-Basel* **2010,** *10*, 5845-5858.
5. Buttry, D. A.; Ward, M. D., *Chem Rev* **1992,** *92*, 1355-1379.
6. Carroll, S.; Baldwin, R. P., *Anal Chem* **2010,** *82*, 878-85.
7. Dittrich, P. S.; Tachikawa, K.; Manz, A., *Anal Chem* **2006,** *78*, 3887-908.
8. West, J.; Becker, M.; Tombrink, S.; Manz, A., *Anal Chem* **2008,** *80*, 4403-19.
9. Arora, A.; Simone, G.; Salieb-Beugelaar, G. B.; Kim, J. T.; Manz, A., *Anal Chem* **2010,** *82*, 4830-4847.
10. Baldwin, R. P.; Roussel, T. J., Jr.; Crain, M. M.; Bathlagunda, V.; Jackson, D. J.; Gullapalli, J.; Conklin, J. A.; Pai, R.; Naber, J. F.; Walsh, K. M.; Keynton, R. S., *Anal Chem* **2002,** *74*, 3690-7.
11. Jackson, D. J.; Naber, J. F.; Roussel, T. J., Jr.; Crain, M. M.; Walsh, K. M.; Keynton, R. S.; Baldwin, R. P., *Anal Chem* **2003,** *75*, 3643-9.
12. Keynton, R. S.; Roussel, T. J.; Crain, M. M.; Jackson, D. J.; Franco, D. B.; Naber, J. F.; Walsh, K. M.; Baldwin, R. P., *Anal Chim Acta* **2004,** *507*, 95-105.

13. Sztaberek, L. Microfabricated electrochemical sensors for field analysis: Anodic stripping voltammetry of Pb and As in drinking water. Louisville, 2009.

14. Crain, M. M.; Keynton, R. S.; Walsh, K. M.; Roussel, T. J., Jr.; Baldwin, R. P.; Naber, J. F.; Jackson, D. J., *Methods Mol Biol* **2006,** *339*, 13-26.

15. Geschke, O.; Klank, H.; Tellemann, P., *Microsystem engineering of lab-on-a-chip devices*. Wiley-VCH ;: Weinheim, 2004; p xi, 258 p.

16. Iles, A.; Oki, A.; Pamme, N., *Microfluid Nanofluid* **2007,** *3*, 119-122.

17. Jia, Z. J.; Fang, Q.; Fang, Z. L., *Anal Chem* **2004,** *76*, 5597-5602.

18. Howlader, M. M. R.; Suehara, S.; Suga, T., *Sensor Actuat a-Phys* **2006,** *127*, 31-36.

19. Mukhopadhyay, R., *Anal Chem* **2007,** *79*, 3248-53.

20. Feng, W.; Patel, S. H.; Young, M. Y.; Zunino, J. L., III; Xanthos, M., *Advances in Polymer Technology* **2007,** *26*, 1-13.

21. Pasparakis, G.; Vamvakaki, M., *Polymer Chemistry* **2011,** *2*, 1234-1248.

22. Lei, M.; Baldi, A.; Nuxoll, E.; Siegel, R. A.; Ziaie, B., *Biomed Microdevices* **2009,** *11*, 529-538.

23. Shim, B. S.; Chen, W.; Doty, C.; Xu, C.; Kotov, N. A., *Nano Lett* **2008,** *8*, 4151-4157.

24. Hrudey, S. E.; Leiss, W., *Environ Health Persp* **2003,** *111*, 1577-1581.

25. Hrudey, S. E.; Rizak, S., *J Am Water Works Ass* **2004,** *96*, 110-113.

26. Quinton, D.; Girard, A.; Kim, L. T. T.; Raimbault, V.; Griscom, L.; Razan, F.; Griveau, S.; Bedioui, F., *Lab Chip* **2011,** *11*, 1342-1350.

27. Ritter, C.; Heike, F.; Herbert, K.; Josef, K. F.; Susanne, L.; Christian, N.; Helmut, O.; Gabriele, P.; Bernhard, S.; Marieluise, S.; Wolfgang, S.; Gregor, S., *Sensor Actuat B-Chem* **2001,** *76*, 220-225.

28. Vonau, W.; Gerlach, F.; Herrmann, S., *Microchim Acta* **2010,** *171*, 451-456.

29. Storey, M. V.; van der Gaag, B.; Burns, B. P., *Water Res* **2011,** *45*, 741-747.

30. Johnson, K. S.; Needoba, J. A.; Riser, S. C.; Showers, W. J., *Chem Rev* **2007,** *107*, 623-640.

31. Cheremisinoff, N. P., *Handbook of water and wastewater treatment technologies*. Butterworth-Heinemann: Boston, 2002; p xii, 636 p.

32. www.whitehouse.gov/news/release/2004/02/20040203-2.html.

33. Hall, J.; Zaffiro, A. D.; Marx, R. B.; Kefauver, P. C.; Krishnan, E. R.; Herrmann, J. G., *J Am Water Works Ass* **2007,** *99*, 66-77.

34. www.epa.gov/safewater.

35. http://www.epa.gov/safewater/watersecurity/pubs/fs_watersecurity_security

36. http://water.epa.gov/infrastructure/watersecurity/lawsregs/initiative.cfm.

37. http://www.epa.gov/safewater/watersecurity/pubs/rpt_post_imp_system_status

38. Vonau, W.; Guth, U., *J Solid State Electr* **2006,** *10*, 746-752.

39. Yao, S.; Wang, M.; Madou, M., *J Electrochem Soc* **2001,** *148*, H29-H36.

40. Chou, J. C.; Liao, Y. H., *Sensor Actuat B-Chem* **2008,** *128*, 603-612.

41. Glab, S.; Hulanicki, A.; Edwall, G.; Ingman, F., *Crit Rev Anal Chem* **1989,** *21*, 29-47.

42. Vonau, W.; Enseleit, U.; Gerlach, F.; Herrmann, S., *Electrochim Acta* **2004,** *49*, 3745-3750.

43. Marzouk, S. A. M., *Anal Chem* **2003,** *75*, 1258-1266.

44. Marzouk, S. A. M.; Ufer, S.; Buck, R. P.; Johnson, T. A.; Dunlap, L. A.; Cascio, W. E., *Anal Chem* **1998,** *70*, 5054-5061.

45. Wang, M.; Yao, S.; Madou, M., *Sensor Actuat B-Chem* **2002,** *81*, 313-315.

46. Wipf, D. O.; El-Giar, E. E. D. M., *J Electroanal Chem* **2007,** *609*, 147-154.

47. Hitchman, M. L.; Ramanathan, S., *Talanta* **1992,** *39*, 137-144.

48. Lee, K. H.; Ishikawa, T.; Sasaki, S.; Arikawa, Y.; Karube, I., *Electroanal* **1999,** *11*, 1172-1179.

49. Fukuda, J.; Tsujimura, S.; Kano, K., *Electrochim Acta* **2008,** *54*, 328-333.

50. Del Campo, F. J.; Ordeig, O.; Munoz, F. J., *Anal Chim Acta* **2005,** *554*, 98-104.

51. Switzer, J. A.; Rajasekharan, V. V.; Clark, B. N.; Boonsalee, S., *Environ Sci Technol* **2007,** *41*, 4252-4257.

52. Niklaus, F.; Stemme, G.; Lu, J. Q.; Gutmann, R. J., *J Appl Phys* **2006,** *99*.

53. Velten, T.; Ruf, H. H.; Barrow, D.; Aspragathos, N.; Lazarou, P.; Jung, E.; Malek, C. K.; Richter, M.; Kruckow, J., *Ieee T Adv Packaging* **2005,** *28*, 533-546.

54. Chiem, N.; Lockyear-Shultz, L.; Andersson, P.; Skinner, C.; Harrison, D. J., *Sensor Actuat B-Chem* **2000,** *63*, 147-152.

55. Chen, L.; Luo, G.; Liu, K.; Ma, J.; Yao, B.; Yan, Y.; Wang, Y., *Sensor Actuat B-Chem* **2006,** *119*, 335-344.

56. Huang, Z. L.; Sanders, J. C.; Dunsmor, C.; Ahmadzadeh, H.; Landers, J. P., *Electrophoresis* **2001,** *22*, 3924-3929.

57. Zhuang, G.; Jin, Q.; Liu, J.; Cong, H.; Liu, K.; Zhao, J.; Yang, M.; Wang, H., *Biomed Microdevices* **2006,** *8*, 255-61.

58. Schlautmann, S.; Besselink, G. A. J.; Prabhu, R.; Schasfoort, R. B. M., *J Micromech Microeng* **2003,** *13*, S81-S84.

59. Satyanarayana, S.; Karnik, R. N.; Majumdar, A., *J Microelectromech S* **2005,** *14*, 392-399.

60. Ymeti, A.; Kanger, J. S.; Greve, J.; Besselink, G. A. J.; Lambeck, P. V.; Wijn, R.; Heideman, R. G., *Biosens Bioelectron* **2005,** *20*, 1417-1421.

61. Stachowiak, J. C.; Yue, M.; Castelino, K.; Chakraborty, A.; Majumdar, A., *Langmuir* **2006,** *22*, 263-268.

62. Papautsky, I.; Jing, G. S.; Polaczyk, A.; Oerther, D. B., *Sensor Actuat B-Chem* **2007,** *123*, 614-621.

63. Zhu, J. J.; Wang, W.; Zhao, L.; Zhang, J. R.; Wang, X. M.; Chen, H. Y., *Journal of Chromatography A* **2006,** *1136*, 111-117.

64. Castano-Alvarez, M.; Fernandez-Abedul, M. T.; Costa-Garcia, A., *Journal of Chromatography A* **2006,** *1109*, 291-299.

65. Culbertson, C. T.; Jacobson, S. C.; Ramsey, J. M., *Anal Chem* **2000,** *72*, 5814-5819.

66. Matysik, F. M., *Electrochem Commun* **2006,** *8*, 1011-1015.

67. http://www.norlandprod.com/techrpts/chemresit.html.

68. Einerhand, R. E. F.; Visscher, W. H. M.; Barendrecht, E., *Electrochim Acta* **1989,** *34*, 345-353.

69. Ives, D. J. G. J., G. J., *Reference Electrodes; Academic Press: New York* **1961.**

70. Liu, C. C.; Bocchicchio, B. C.; Overmyer, P. A.; Neuman, M. R., *Science* **1980,** *207*, 188-189.

71. Baudenbacher, F. J.; Ges, I. A.; Ivanov, B. L.; Werdich, A. A., *Biosens Bioelectron* **2007,** *22*, 1303-1310.

72. Bezbaruah, A. N.; Zhang, T. C., *Anal Chem* **2002,** *74*, 5726-5733.

73. Chen, Y. J.; Taylor, P. L.; Scherson, D., *J Electrochem Soc* **2009,** *156*, F14-F21.

74. Elsen, H. A.; Monson, C. F.; Majda, M., *J Electrochem Soc* **2009,** *156*, F1-F6.

75. Ges, I. A.; Ivanov, B. L.; Schaffer, D. K.; Lima, E. A.; Werdich, A. A.; Baudenbacher, F. J., *Biosens Bioelectron* **2005,** *21*, 248-256.

76. Meyer, R. D.; Cogan, S. E.; Nguyen, T. H.; Rauh, R. D., *Ieee T Neur Sys Reh* **2001,** *9*, 2-11.

77. Petit, M. A.; Plichon, V., *J Electroanal Chem* **1998,** *444*, 247-252.

78. Yamanaka, K., *Jpn. J. Appl. Phys., Part 1* **1989,** *28*, 632–637.

79. Zhang, J. M.; Lin, C. J.; Feng, Z. D.; Tian, Z. W., *J Electroanal Chem* **1998,** *452*, 235-240.

80. Fog, A.; Buck, R. P., *Sensor Actuator* **1984,** *5*, 137-146.

81. Diamond, D.; Coyle, S.; Scarmagnani, S.; Hayes, J., *Chem Rev* **2008,** *108*, 652-679.

82. Namour, P.; Lepot, M.; Jaffrezic-Renault, N., *Sensors-Basel* **2010,** *10*, 7947-7978.

83. Heller, A.; Feldman, B., *Chem Rev* **2008,** *108*, 2482-2505.

84. Bard, A. J.; Faulkner, L. R., *Electrochemical methods : fundamentals and applications*. 2nd ed.; John Wiley: New York, 2001; p xxi, 833 p.

85. Vaireanu, D. I.; Ruck, N.; Fielden, P. R., *Anal Chim Acta* **1995,** *306*, 115-122.

86. Dzyadevych, S. V.; Arkhypova, V. N.; Soldatkin, A. P.; El'skaya, A. V.; Martelet, C.; Jaffrezic-Renault, N., *Irbm* **2008,** *29*, 171-180.

87. Ronkainen, N. J.; Halsall, H. B.; Heineman, W. R., *Chem Soc Rev* **2010,** *39*, 1747-1763.

88. Huang, X. J.; Aldous, L.; O'Mahony, A. M.; del Campo, F. J.; Compton, R. G., *Anal Chem* **2010,** *82*, 5238-5245.

89. Tsujimura, S.; Nishina, A.; Kamitaka, Y.; Kano, K., *Anal Chem* **2009,** *81*, 9383-9387.

90. Bakker, E.; Bhakthavatsalam, V.; Gemene, K. L., *Talanta* **2008,** *75*, 629-635.

91. Bhakthavatsalam, V.; Shvarev, A.; Bakker, E., *Analyst* **2006,** *131*, 895-900.

92. Grygolowicz-Pawlak, E.; Bakker, E., *Electrochem Commun* **2010,** *12*, 1195-1198.

93. Shanthi, C.; Barathan, S.; Jaiswal, R.; Arunachalam, R. M.; Mohan, S., *Mater Lett* **2008,** *62*, 4519-4521.

94. Condit, D. A.; Herrera, M. E.; Stankovich, M. T.; Curran, D. J., *Anal Chem* **1984,** *56*, 2909-2914.

95. Greenwood, N. N.; Earnshaw, A., *Chemistry of the elements*. 1st ed.; Pergamon Press: Oxford Oxfordshire ; New York, 1984; p xxi, 1542 p.

96. http://www.hach.com/cl17-free-chlorine-analyzer/product-details?id=7640295880.

97. Mehta, A.; Shekhar, H.; Hyun, S. H.; Hong, S.; Cho, H. J., *Water Sci Technol* **2006,** *53*, 403-410.

98. Olive-Monllau, R.; Orozco, J.; Fernandez-Sanchez, C.; Baeza, M.; Bartroli, J.; Jimenez-Jorquera, C.; Cespedes, F., *Talanta* **2009,** *77*, 1739-1744.

99. Ordeig, O.; Mas, R.; Gonzalo, J.; Del Campo, F. J.; Munoz, F. J.; de Haro, C., *Electroanal* **2005,** *17*, 1641-1648.

100. Kodera, F.; Umeda, M.; Yamada, A., *Anal Chim Acta* **2005,** *537*, 293-298.

101. Murata, M.; Ivandini, T. A.; Shibata, M.; Nomura, S.; Fujishima, A.; Einaga, Y., *J Electroanal Chem* **2008,** *612*, 29-36.

102. Kishioka, S. Y.; Kosugi, T.; Yamada, A., *Electroanal* **2005,** *17*, 724-726.

103. Nollet, L. M. L., *Handbook of water analysis*. 2nd ed.; CRC Press: Boca Raton, 2007; p xiv, 769 p.

104. Cotton, F. A., *Advanced inorganic chemistry*. 6th ed.; Wiley: New York, 1999; p xv, 1355 p.

105. Rajasekharan, V. V.; Clark, B. N.; Boonsalee, S.; Switzer, J. A., *Environ Sci Technol* **2007,** *41*, 4252-4257.

APPENDIX

All devices were fabricated in the cleanroom facility in the University of Louisville Center for Micro/Nano Technology.

Table A.1. Microfabrication procedure steps for the top substrate of the CE device

Procedure Steps	Conditions
Pattern transfer	Use the ABM mask aligner to transfer the pattern from the mask to the glass substrate - expose for 6.5 seconds
Substrate development	Place substrate into MF 319 for 25 sec - rinse with DI water - dry with N_2
Chrome etch	Place substrate into CR-100 Chromium Etchant (2 - 3 min) until area becomes clear - rinse with DI water - dry with N_2
Preparation for hole drilling and dicing	Protect substrate with photoresist - spin 1813 onto substrate (*spread*: 0 *spin*: 2000 rpm, 10 sec) - bake at 115°C for 3 min
Channel etching	Submerse substrate for 1 min in agated BOE solution - rinse with DI water - dry with N_2 Submerse device for 10 sec in Nanostrip - rinse with DI water - dry with N_2 - inspect under microscope Submerse substrate again in BOE solution for 3 min - repeat the steps of cleaning/drying/nanostrip and inspection Increase the BOE time to 5, 9 and 15 min and repeat the cleaning/drying/nanostrip and inspection
Chrome etch	Place substrate into CR-100 Chromium Etchant (2 - 3 min) until the chrome is completely removed

	- rinse with DI water - dry with N_2
Cleaning	take resist of with acetone - rinse with DI water - rinse with methanol - repeat the DI water/methanol rinse at least twice - dry with N_2 - inspect under microscope for impurities (if impurities persist use nanostrip bath)

Table A.2. Microfabrication procedure steps for the bottom substrate

Procedure Steps	Conditions
Pattern transfer	Use the ABM mask aligner to transfer the pattern from the mask to the glass substrate - expose for 6.5 seconds
Substrate development	Place substrate into MF 319 for 25 sec - rinse with DI water - dry with N_2
Chrome etch	Place substrate into CR-100 Chromium Etchant (2 - 3 min) until area becomes clear - rinse with DI water - dry with N_2
Electrode recess etching	Submerse substrate for 45 sec in agated BOE solution - rinse with DI water - dry with N_2
Metal deposition	Use the Sputtering Machine Technics 4604 Sputterer - plasma etch for 2 min - deposit Ti (adhesion layer): RF, 250 W for 2 min at 19 mT - deposit Pt: DC, 100 W for 2 min at 19-22 mT
Lift off	Place bottom substrate into lift off bath (acetone) for at least 20 min - rinse with DI water - dry with N_2 - use cotton swap with acetone to wipe off persisting metal specs - repeat lift off bath/DI water/cotton swaps until the lift off process is completed

	- inspect under microscope
Chrome etch	Place substrate into CR-100 Chromium Etchant (2 - 3 min) until the chrome is completely removed - rinse with DI water - dry with N_2
Preparation for dicing	Protect substrate with photoresist - spin 1813 onto substrate (*spread*: 0 *spin*: 2000 rpm, 10 sec) - bake at 115°C for 3 min
Cleaning	take resist of with acetone - rinse with DI water - rinse with methanol - repeat the DI water/methanol rinse at least twice - dry with N_2 - inspect under microscope for impurities (if impurities persist use nanostrip bath)

Table A.3. Microfabrication procedure steps for the bonding process

Procedure Steps	Conditions
Evaporation bake	Place top and bottom substrate and an transfer wafer onto hotplate at 150 °C for 10min
Top substrate placement	Use big clear glass plate - place water drop on glass plate - place top substrate (channels facing away) on glass plate - remove excess water with paper towel - dry with N_2 for better adhesion between both glass surfaces - position glass plate with top substrate into the the AB-M mask aligner frame
Initial alignment/planarization	Use a 2nd wafer and place it on the bottom cuck - move wafer up for initial contact alignment - remove wafer
Norland coating	Spin Norland NOA 61onto transfer wafer (*spread*: 500 rpm, 5.5 sec and *spin*: 7000 rpm, 20 sec
Stamping process	Place transfer wafer on bottom chuck

	- make contact with top substrate and wafer (carefully) - look at monitor for even channel wall coating - push occasionally the alignment button - inspect entire substrate - remove transfer wafer
Sticking process	Use alignment wafer - place water drop on wafer - place bottom substrate (electrodes facing away) on wafer - remove excess water with paper towel - dry with N_2 for better adhesion between both surfaces - position wafer with bottom substrate onto the bottom chuck - make stamping contact - ensure EC electrode alignment at the detection reservoir - ensure complete wall coverage
Adhesive curing	Expose to UV-light for 3 min - remove chip and inspect under microscope

Table B.1. Microfabrication procedure steps for the coulometric sensor

Procedure Steps	Conditions
Clean SiO_2 wafer	Place wafer into nanostrip for 5 min - rinse with DI water - dry with N_2
Measure the O_2 thickness	Use the Filmetrics Thin Film Measurement System
Evaporation bake	Place wafer onto hotplate at 200°C for 5 min or 150 °C for 10 min
Resist coating	Spin LOR 3A onto wafer (*spread*: 500 rpm, 1 sec and *spin*: 3000 rpm, 10 sec) - bake at 150°C for 5 min - let wafer cool to room temperature Spin 1813 onto wafer (*spread*: 500 rpm, 1sec and *spin*: 4000 rpm, 10 sec) - bake at 115 °C for 2 min

Pattern transfer	Use the Suss Mask Aligner to transfer pattern from the mask to the wafer - expose for 12 sec - post bake for 2 min at 115 °C
Pattern development	Place wafer in MF-319 for at least 85 sec - rinse DI - dry N_2 - inspect pattern development under microscope
Recess electrode area	Place wafer into BOE for 3 min - rinse with DI water - dry with N_2
Metal deposition	Use the Sputtering Machine Technics 4604 Sputterer - plasma etch for 2 min - deposit Ta (adhesion layer): RF, 250 W for 3 min at 19 mT - deposit Au: DC, 100 W for 2 min at 19-22 mT
Lift off	Place wafer into lift off bath (acetone) for 10 min (takes of resist) - rinse with DI water - dry with N_2 Place wafer into MF 319 (takes of LOR) - rinse with DI water - dry with N_2 Sonicate at low power in acetone - rinse with DI water - dry with N_2 repeat the MF 319 and sonication steps until a clean product appears at the inspection
Preparation for dicing	Protect wafer with photoresist - spin 1813 onto wafer (*spread*: 500 rpm, 1 sec and *spin*: 4000 rpm, 10 sec) - bake at 115°C for 2 min
Cleaning	take resist of with acetone - rinse with DI water - dry with N_2

Table B.2. Area dimensions for the coulometric sensors

Design	Electrode 1 Area in cm^2	Electrode 2 Area in cm^2	Electrode 3 Area in cm^2	Electrode 4 Area in cm^2	Electrode 5 Area in cm^2	Electrode 6 Area in cm^2
1	.228	.00714				
2	.442	.00819				
3	.0451	.0523				
4	.0173	.0184	.0195	.0205	.0215	.0249
5	.00864	.00920	.00976	.0103	.0107	.0126
6	.0324	.0359	.0382	.0399	.0415	.0431

COPYRIGHT PERMISSIONS

RightsLink®

Home | Create Account | Help

Title:	Self-Calibrating Microfabricated Iridium Ox pH Electrode Array for Ren Monitoring
Author:	Susan Carroll et al.
Publication:	Analytical Chemistry
Publisher:	American Chemical Society
Date:	Feb 1, 2010
Copyright © 2010, American Chemical Society	

User ID

Password

Enable Auto Login

LOGIN

Forgot Password/User ID?

If you're a copyright.com user, you can login to Rightslink using your copyright.com credentials.

Already a Rightslink user or want to learn more?

Quick Price Estimate

Permission for this particular request is granted for print and electronic formats at no charge. Appropriate credit should be given. Please print this page for your records and provide a copy to your publisher. Requests for up to 4 figures require only this record. Five or more figures will generate a printout of additional terms and conditions. Appropriate credit should read: "Reprinted with permsision from {COMPLETE REFERENCE CITATION}. Copyright {YEAR} American Chemical Society." Insert appropriate information in place of the capitalized words.

I would like to... reuse in a Thesis/Dissertation

Requestor Author (original w ork)

This service provides permission for reuse only. If you do not

Type	
Portion	Full article
Format	Print
Will you be translating?	No
Select your currency	USD - $
Quick Price	Click Quick Price

QUICK PRICE CONTINUE

have a copy of the article you are using, you may copy and paste the content and reuse according to the terms of your agreement. Please be advised that obtaining the content you license is a separate transaction not involving Rightslink.

To request permission for a type of use not listed, please contact the publisher directly.

Copyright Clearance Center RightsLink®

Home | Create Account | Help

ACS Publications High quality. High impact.

Title:	Self-Calibrating Microfabricated Iridium Ox pH Electrode Array for Ren Monitoring
Author:	Susan Carroll et al.
Publication:	Analytical Chemistry
Publisher:	American Chemical Society
Date:	Feb 1, 2010
Copyright © 2010, American Chemical Society	

User ID

Password

Enable Auto Login

LOGIN

Forgot Password/User ID?

If you're a copyright.com user, you can login to Rightslink using your copyright.com

credentials.
Already a Rightslink user or want to learn more?

No charge permission and attribution

Permission for this particular request is granted for print and electronic formats at no charge. Appropriate credit should be given. Please print this page for your records and provide a copy to your publisher. Requests for up to 4 figures require only this record. Five or more figures will generate a printout of additional terms and conditions. Appropriate credit should read: "Reprinted with permission from {COMPLETE REFERENCE CITATION}. Copyright {YEAR} American Chemical Society." Insert appropriate information in place of the capitalized words.

BACK CLOSE WINDOW

COPYRIGHT PERMISSIONS

Author Deposition

The following apply only to authors signing one of the non-Open Science Licence to Publish. For authors who have signed one of the Open Science Licence to Publish, or are thinking of signing one of the Open Science Licence to Publish, please click on the relevant link below.

Deposition of any form of the article is allowed in non-commercial repositories only.

Deposition by the RSC

The RSC shall:

- Deposit the accepted version of the submitted article in non-commercial repository(ies) as deemed appropriate, including but not limited to the author(s)' funding agency repository(ies). There shall be an embargo of making the above

deposited material available to the public of 12 months from the date of acceptance.

Allowed Deposition by the author(s)

When the author accepts the exclusive Licence to Publish for a journal article, he/she retains certain rights concerning the deposition of the whole article. He/she may:

- Deposit the accepted version of the submitted article in their institutional repository(ies). There shall be an embargo of making the above deposited material available to the public of 12 months from the date of acceptance. There shall be a link from this article to the PDF of the final published article on the RSC's website once this final version is available.
- Make available the accepted version of the submitted article via the personal website(s) of the author(s) or via the Intranet(s) of the organisation(s) where the author(s) work(s). No embargo period applies.
- Make available the PDF of the final published article via the personal website(s) of the author(s) or via the Intranet(s) of the organisation(s) where the author(s) work(s). No embargo period applies.
- Republish the PDF of the final published article in theses of the author(s) in printed form and may make available this PDF in this theses of author(s) via any website(s) that the university(ies) of the author(s) may have for the deposition of theses. No embargo period applies.

Excluded deposition of any version of the article by any person or organisation

- No deposited article, whether in an Institutional Repository, Funding Body Repository or personal website, may be forwarded to any website collection of research articles without prior agreement from the RSC.
- Deposition of the article on any website acting as a collection of personal articles from multiple scientists is explicitly prohibited. This does not apply to Institutional and Funding Body Repositories.

CURRICULUM VITAE
Susan Carroll

Personal Details

Nationality:	German	**Phone:**	(270) 245 0042
Citizenship:	Permanent Resident	**E-mail:**	s0carr02@louisville.edu
Address:	University of Louisville 2320 S. Brook St. Louisville, KY 40292		

Education

Aug., 2011: **Doctor of Philosophy in Chemistry** anticipated
Dissertation Title: Application of Microfabrication in Electrochemical Sensing

Dec., 2009: **Master of Science in Chemistry**
University of Louisville, Louisville, Kentucky
(Research Advisor: Dr. R.P. Baldwin)

May, 2004: **Bachelor of Science in Chemical Science**
Kansas State University, Manhattan, Kansas

Sept., 1999: **National Preclinical Examination**
(Attended Medical School from June 1995 - February 2000)
Friedrich-Alexander-University, Erlangen-Nuernberg, Germany

Professional Experience

August, 2005 - present:
Graduate Teaching Assistant, Department of Chemistry, University of Louisville
General Chemistry Recitations, Analytical Chemistry Laboratories

February, 2004 - May, 2004:
Chemistry Tutor, Educational Services, Kansas State University
Assessed student's need and developed lesson plan. Identified student's thought process and responded with applicable teaching techniques. Assisted students with study tasks and provided students with study objectives.

June, 2003 - May, 2004:

Undergraduate Research Assistant, Department of Chemistry, Kansas State University

Advisor: Dr. C.T. Culbertson

Worked in the field of analytical chemistry, manufactured LOC devices and performed separations with laser induced fluorescence detection on microchips.

October, 1998 - March, 2000

Internal Medicine Intern

Administered medications; performed IV infusion therapies; performed minor medical procedures ordered and supervised by physicians; reported vital signs, blood sugar levels, urine balances; provided special care for patients; filed and oversaw lab results; prepared and handled documents for specific procedures per physician's orders.

Publications

Carroll, S; Marei, M.; Roussel, T.J.;Keynton, R.S.; Baldwin, R.P.Microfabricated Electrochemical Sensors for Exhaustive Coulometry Applications. *Sensors and Actuators B: Chemical* manuscript submitted.

Carroll, S.; Baldwin, R.P.Self-Calibrating Microfabricated Iridium Oxide pH Electrode Array for Remote Monitoring. *Anal. Chem.*, **2010,** 82, 878-885.

Carroll, S.; Crain, M.M.; Naber, J.F.; Keynton, R.S.; Walsh, K.M.; Baldwin, R.P. Room temperature UV adhesive bonding of CE devices. *Lab on a Chip,* **2008**, 8,1564-1569.

Roman, G.T.; Carroll, S.; McDaniel, K.; Culbertson, C.T. Micellarelectrokinetic chromatography of fluorescently labeled proteins on poly(dimethylsiloxane)-based microchips. *Electrophoresis*, **2006**, 27, 2933-2939.

Presentations

Roussel, T.J.; Carroll, S.; Marei, M.; Keynton, R.S.; Baldwin, R.P. **(November 2010)** A Calibration Free Coulometric Detection System for Remote Monitoring. Poster presentation at the 9th Annual IEEE Conference on Sensors, Waikoloa, HI (Poster Presentation)

Carroll, S.; Roussel, T.J.; Keynton, R.S.; Baldwin, R.P. **(March 2010)** Towards a Smart Sensing Platform for Water Quality Determination. Oral presentation at Pittcon Conference, Orlando, FL (Oral Presentation)

Carroll, S.; Baldwin, R.P. **(August 2009)** Progress Toward a Smart Sensing Device for Water Quality Detection. Poster presentation at the 238thAmerican Chemical Society National Meeting, Washington, DC (Poster Presentation)

Baldwin, R.P.; Carroll, S.; Sztaberek, L. **(August 2009)** Progress Toward a Smart Electrochemical Sensing Device for Water Quality Detection. Oral presentation at the 12th International Symposium on Electroanalytical Chemistry, Changchun, China (Oral Presentation)

Carroll, S.; Crain, M.M.; Naber, J.F.; Keynton, R.S.; Walsh, K.M.; Baldwin, R.P. **(July 2008)** Low Temperature Adhesive Bonding of CE Devices. Poster presentation at the 17th Biennial IEEE UGIM (University Government Industry Micro/nano) Symposium, Louisville, KY(Poster presentation)

Carroll, S.; Crain, M.M.; Walsh, K.M.; Baldwin, R.P. **(April 2008)** Room temperature UV adhesive bonding of CE devices. Oral presentation at the 235th American Chemical Society National Meeting, New Orleans, LA (Oral Presentation)

Franco, D.B.; Carroll, S.; Baldwin, R.P.; Walsh, K.M.; Keynton, R.S.; Naber, J.F. **(February 2007)** Lab-on-a-Chip with Integrated Carbon Microelectrodes. Oral Presentation at Pittcon Conference, Chicago, IL (Oral Presentation)

Scholarships and Travel Grants

University of Louisville Student Government Travel Grant (2007; 2008; 2009; 2010)

Chemistry Department, Kansas State University Hawks Scholarship (fall semester 2003 and spring semester 2004)

Barton County Community College Dean's List (2001; 2002)

Extra-Curricular Activities

August, 2008 – August, 2010: Vice president of the Chemistry Graduate Student Association

Research Skills

Experiences in microchip design, fabrication and utilization for chemical analysis methods for glass, PDMS and silicon based microchips/sensors.

Electrochemistry including potentiometry, coulometry, various voltammetric methods, electrochemical depositions and modifications.

Spectroscopic analysis and interpretation, including: UV/visible spectroscopy, capillary electrophoresis with laser induced fluorescence detection and/or electrochemical detection, spectro-electrochemistry, gas chromatography, atomic absorption spectroscopy.

Clean room experiences including photolithography processes, etching, sputtering, e-beam, metrology, chip bonding techniques.

Microsoft Office program suite, Corell Draw, L-Edit, AutoCAD, Lab-view IGOR and Endnote programs.

Professional Memberships

American Chemical Society (ACS)